

Modeling of Multicomponent Gas-Solid Reactions

by

AlHaji Ibrahim Abba

A Thesis Presented to the

FACULTY OF THE COLLEGE OF GRADUATE STUDIES

KING FAHD UNIVERSITY OF PETROLEUM & MINERALS

DHAHRAN, SAUDI ARABIA

In Partial Fulfillment of the
Requirements for the Degree of

MASTER OF SCIENCE

In

CHEMICAL ENGINEERING

April, 1995

INFORMATION TO USERS

This manuscript has been reproduced from the microfilm master. UMI films the text directly from the original or copy submitted. Thus, some thesis and dissertation copies are in typewriter face, while others may be from any type of computer printer.

The quality of this reproduction is dependent upon the quality of the copy submitted. Broken or indistinct print, colored or poor quality illustrations and photographs, print bleedthrough, substandard margins, and improper alignment can adversely affect reproduction.

In the unlikely event that the author did not send UMI a complete manuscript and there are missing pages, these will be noted. Also, if unauthorized copyright material had to be removed, a note will indicate the deletion.

Oversize materials (e.g., maps, drawings, charts) are reproduced by sectioning the original, beginning at the upper left-hand corner and continuing from left to right in equal sections with small overlaps. Each original is also photographed in one exposure and is included in reduced form at the back of the book.

Photographs included in the original manuscript have been reproduced xerographically in this copy. Higher quality 6" x 9" black and white photographic prints are available for any photographs or illustrations appearing in this copy for an additional charge. Contact UMI directly to order.

UMI

A Bell & Howell Information Company
300 North Zeeb Road, Ann Arbor, MI 48106-1346 USA
313/761-4700 800/521-0600



**MODELING OF MULTICOMPONENT
GAS-SOLID REACTIONS**

BY

ALHAJI IBRAHIM ABBA

A Thesis Presented to the
FACULTY OF THE COLLEGE OF GRADUATE STUDIES
KING FAHD UNIVERSITY OF PETROLEUM & MINERALS
DHAHRAN, SAUDI ARABIA

In Partial Fulfillment of the
Requirements for the Degree of

MASTER OF SCIENCE
In
CHEMICAL ENGINEERING

April, 1995

UMI Number: 1375125

UMI Microform 1375125

Copyright 1995, by UMI Company. All rights reserved.

**This microform edition is protected against unauthorized
copying under Title 17, United States Code.**

UMI

**300 North Zeeb Road
Ann Arbor, MI 48103**

**KING FAHD UNIVERSITY OF PETROLEUM AND MINERALS
DHAHRAN, SAUDI ARABIA**

COLLEGE OF GRADUATE STUDIES

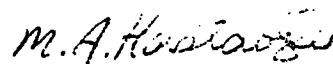
This thesis, written by

ALHAJI IBRAHIM ABBA

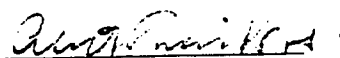
under the direction of his thesis committee, and approved by all the members, has been presented and accepted by the Dean, College of Graduate Studies, in partial fulfillment of the requirements for the degree of

MASTER OF SCIENCE IN CHEMICAL ENGINEERING

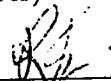
Thesis committee



Dr. Mehmet A. Hastaoglu
(Chairman)



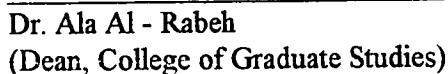
Dr. Abdullah A. Shaikh
(Member)



Dr. Ramazan Kahraman
(Member)



Dr. Dulaihan Al - Harbi
(Department Chairman)



Dr. Ala Al - Rabeh
(Dean, College of Graduate Studies)

Date: 



This work is wholly dedicated to the cause of justice

ACKNOWLEDGMENT

My unqualified gratitude is to Allah, the Almighty who guided me in every facet of this work in his infinite wisdom and bounties.

I am sincerely grateful to Dr. Mehmet A. Hastaoglu, my thesis committee chairman, who not only made himself available for consultation at all times, but also served as a source of continuing inspiration throughout the course of this work.

My sincere thanks and appreciation is also due to the other members of the committee, Dr. Abdullah A. Shaikh and Dr. Ramazan Kahraman for their invaluable support, suggestions and constructive criticisms that enormously facilitated this work.

I would like to acknowledge the King Fahd University of Petroleum and Minerals (KFUPM) for providing the financial support and especially for making available all the facilities. I would also like to thank the chemical engineering department and especially the faculty members for their invaluable contributions, and assistance in several ways throughout the course of my graduate program.

I owe a deep sense of indebtedness to my numerous friends and colleagues whose presence and moral support greatly made the research task easier. I sincerely thank them all.

Finally, my deep thanks go to my family for their love, support and encouragement for the entire length of my stay here.

TABLE OF CONTENTS

	Page
DEDICATION	ii
ACKNOWLEDGMENT	iii
TABLE OF CONTENTS	iv
LIST OF TABLES	viii
LIST OF FIGURES	ix
ABSTRACT (English)	xiv
ABSTRACT (Arabic)	xv
CHAPTER 1 INTRODUCTION	1
1.1 Motivation	1
1.2 Objectives of this study	2
1.3 Organization of Thesis	4
CHAPTER 2 BACKGROUND AND REVIEW OF LITERATURE	5
2.1 Fluid - Solid Reaction Studies	5
2.2 Classification of Gas - Solid Reaction Schemes	6
2.3 Model Studies	7
2.3.1 Sharp Interface Model	7
2.3.2 Volume Reaction Mode	9
2.3.3 Pore Model	12
2.3.4 The Network Model	16
2.3.5 Particle - Pellet Model	18

2.3.6	Miscellaneous Models	22
2.4	Complex Reaction Systems	23
2.5	Flux Relations for Gas Transport	25
2.5.1	Flux Model	25
2.5.2	The Dusty Gas Concept	26
 CHAPTER 3 DEVELOPMENT OF THE MATHEMATICAL		
MODELS		30
3.1	Problem Formulation	30
3.1.1	Reaction Scheme	32
3.1.2	Factors Controlling the Rate of Reactions	34
3.1.3	Assumptions	35
3.2	Model Equations	36
3.2.1	Continuity Equations	36
3.2.2	Energy Balance Equations	39
3.2.3	Thermophysical and Transport Parameters	40
3.2.3.1	Thermophysical Parameters	40
3.2.3.2	Flux and Transport Equations	42
3.2.4	Structural Changes and Conversion	45
3.2.4.1	Structural Changes due to Reaction	45
3.2.4.2	Local Conversion	47
3.2.4.3	Global Conversion for Solid B_k	48
3.2.4.4	Overall Pellet Conversion	48
3.2.5	Heat and Mass Transfer Equations	49
 CHAPTER 4 NUMERICAL FORMULATION		50
4.1	Discretization of Model Equations	50

4.2 Solution Technique

57

CHAPTER 5 BINARY SIMULATION : MODEL VALIDATION

	61
5.1 Introduction	61
5.2 Case Studies	62
5.2.1 Carbon Gasification Reaction	62
5.2.2 Nickel Oxide / Hematite Mixture Reduction	69
5.3 Observation and Conclusion	76

CHAPTER 6 MULTICOMPONENT SIMULATION

	77
6.1 Introduction	77
6.2 Concentration and Thermal Gradients Inside the Pellet	79
6.2.1 Diffusion and Reaction Effects	79
6.2.2 Thermal Gradient	92
6.2.3 System Stability	98
6.2.4 Conclusion	99
6.3 Parametric Study	99
6.3.1 Effect of Bulk temperature	99
6.3.2 Effect of Bulk Pressure	106
6.3.3 Effect of Inert Gas in the Bulk Stream	114
6.3.4 Effect of Pellet Porosity	119
6.3.5 Effect of Inert Solid Inside Pellet	125

CHAPTER 7 CONCLUSIONS AND RECOMMENDATIONS

	132
7.1 Conclusions	132
7.2 Recommendations	133

NOMENCLATURE	135
BIBLIOGRAPHY	140
APPENDICES	152
A : MAIN COMPUTER CODING	153
B : COMPLETE DATA FILES	165
B1 : Input Data to the Main Computer Coding for the Carbon Gasification Reaction	165
B2 : Input Data to the Main Computer Coding for the Reduction of NiO / Fe ₂ O ₃ Mixture	167
B3 : Input Data to the Main Computer Coding for the Multiple Reaction	169

LIST OF TABLES

Table	Page
2.1 Examples of Some Complex Gas - Solid Reactions	24
4.1 Discretization of Flux and Thermal Diffusion Terms in the Continuity and Energy Balance Equations {flat plate ($F_p = 1$); cylinder ($F_p = 2$); sphere ($F_p = 3$)}	55
5.1 Experimental Data for Carbon Gasification Reaction	64
5.2 Data used in the Modelling Work for Carbon Gasification Reaction	64
5.3 Comparison Between Model and Experimental Values for Carbon Conversion at Various Bulk Gas Temperatures.	68
5.4 Experimental Data for NiO / Fe ₂ O ₃ Reduction	71
5.5 Comparison Between Model and Experimental Values for NiO / Hematite Mixture Conversion at Bulk Gas Temperatures of 581 and 608 K.	75
B1 Input Data to the Main Computer Coding for the Carbon Gasification Reaction	165
B2 Input Data to the Main Computer Coding for the Reduction of NiO / Fe ₂ O ₃ Mixture	167
B3 Input Data to the Main Computer Coding for the Multiple Reaction	169

LIST OF FIGURES

Figure	Page
2.1 Schematic representation of the sharp interface model	8
2.2 The three stages of the zone model	11
2.3 Schematic representation of the single pore model	13
2.4 Random pore intersections of the RPM	15
2.5 Development of reaction surface according to the random pore model	15
2.6 Bethe lattice with coordination number, $Z = 3$.	17
2.7 Schematic representation of the PPM	20
2.8 Diffusion in capillaries: (a) Knudsen regime; (b) molecular regime; (c) transition regime	27
2.9 The dusty gas concept: (a) The dusty gas; (b) Schematic ways of visualizing the dusty gas model for transport in porous media	28
3.1 Schematics of pellet and grain structures	31
4.1 Numerical solution algorithm	60
5.1 Schematic diagram of the TGA experimental set - up	66
5.2 Comparison of transient model prediction with experimental data for carbon gasification reaction at various bulk gas temperatures	67

5.3	Comparison of transient model prediction with experimental data for NiO / Fe ₂ O ₃ reduction at T _b = 581 K and d _p = 0.89 mm for 50% NiO and 50% Fe ₂ O ₃	73
5.4	Comparison of transient model prediction with experimental data for NiO / Fe ₂ O ₃ reduction at T _b = 608 K and d _p = 0.89mm for 50% NiO and 50% Fe ₂ O ₃	74
6.1	The radial concentration profile at: t = 1 s, GXT = 1.95 x 10 ⁻⁵ , T _b = 1173 K, P _b = 101.3 kPa and R _p = 3.28 x 10 ⁻⁴ m.	80
6.2	The radial concentration profile at: t = 1 s, GXT = 1.95 x 10 ⁻⁵ , T _b = 1173 K, P _b = 101.3 kPa , C _b = 1.04 mol/m ³ and R _p = 3.28 x 10 ⁻⁴ m.	81
6.3	The radial concentration profile at: t = 60 s, GXT = 0.012, T _b = 1173 K, P _b = 101.3 kPa and R _p = 3.28 x 10 ⁻⁴ m.	82
6.4	The radial concentration profile at: t = 60 s, GXT = 0.0123, T _b = 1173 K, P _b = 101.3 kPa , C _b = 1.04 mol/m ³ and R _p = 3.28 x 10 ⁻⁴ m.	83
6.5	The radial concentration profile at: t = 480 s, GXT = 0.093, T _b = 1173 K, P _b = 101.3 kPa , and R _p = 3.28 x 10 ⁻⁴ m.	84
6.6	The radial concentration profile at: t = 480 s, GXT = 0.093, T _b = 1173 K, P _b = 101.3 kPa , C _b = 1.04 mol/m ³ and R _p = 3.28 x 10 ⁻⁴ m.	85
6.7	The transient concentration profile at: R/R _p = 0.5, T _b = 1173 K, P _b = 101.3 kPa , and R _p = 3.28 x 10 ⁻⁴ m.	88
6.8	The transient concentration profile at: R/R _p = 0.5, T _b = 1173 K, P _b = 101.3 kPa , and R _p = 3.28 x 10 ⁻² m.	89
6.9	Local conversion along radius of pellet at: t = 480 s, GXT = 0.093, T _b = 1173 K, P _b = 101.3 kPa, C _b = 1.04 mol/m ³ and R _p = 3.28 x 10 ⁻⁴ m.	91

6.10	The radial temperature distribution: $t = 1$ s, $GXT = 1.95 \times 10^{-5}$, $T_b = 1173$ K, $P_b = 101.3$ kPa, and $R_p = 3.28 \times 10^{-4}$ m.	94
6.11	The dimensionless radial temperature profile at: $t = 1$ s, $GXT = 1.95 \times 10^{-5}$, $T_b = 1173$ K, $P_b = 101.3$ kPa, and $R_p = 3.28 \times 10^{-4}$ m.	95
6.12	The temperature history in pellet at: $T_b = 1173$ K, $P_b = 101.3$ kPa and $R_p = 3.28 \times 10^{-4}$ m.	96
6.13	The temperature history in pellet at: $T_b = 1173$ K, $P_b = 101.3$ kPa and $R_p = 3.28 \times 10^{-2}$ m.	97
6.14	Effect of bulk temperature on conversion at: $T_b = 873$ K, and $P_b = 101.3$ kPa.	100
6.15	Effect of bulk temperature on conversion at: $T_b = 973$ K, and $P_b = 101.3$ kPa.	101
6.16	Effect of bulk temperature on conversion at: $T_b = 1173$ K, and $P_b = 101.3$ kPa.	102
6.17	Effect of bulk temperature on conversion at: $T_b = 1273$ K, and $P_b = 101.3$ kPa.	103
6.18	Effect of bulk temperature on conversion at: $T_b = 1373$ K, and $P_b = 101.3$ kPa.	104
6.19	Effect of bulk temperature on the overall solid conversion at $P_b = 101.3$ kPa.	105
6.20	Effect of bulk pressure on conversion at $T_b = 1173$ K and $P_b = 101.3$ kPa.	107
6.21	Effect of bulk pressure on conversion at $T_b = 1173$ K and $P_b = 202.6$ kPa.	108
6.22	Effect of bulk pressure on conversion at $T_b = 1173$ K and $P_b = 506.5$ kPa.	109

6.23	Effect of bulk pressure on conversion at $T_b = 1173$ K and $P_b = 701.9$ kPa.	110
6.24	Effect of bulk pressure on conversion at $T_b = 1173$ K and $P_b = 1013$ kPa.	111
6.25	Effect of bulk pressure on overall solid conversion at $T_b = 1173$ K.	112
6.26	The radial pressure distribution at : $t = 480$ s, $GXT = 0.093$, $T_b = 1173$ K $P_b = 101.3$ kPa. and $R_p = 3.28 \times 10^{-4}$ m.	113
6.27	Effect of inert gas (N_2) in the bulk stream on conversion at: $T_b = 1173$ K $P_b = 101.3$ kPa. and $X_{bi} = 20\%$.	115
6.28	Effect of inert gas (N_2) in the bulk stream on conversion at: $T_b = 1173$ K $P_b = 101.3$ kPa. and $X_{bi} = 30\%$.	116
6.29	Effect of inert gas (N_2) in the bulk stream on conversion at: $T_b = 1173$ K $P_b = 101.3$ kPa. and $X_{bi} = 50\%$.	117
6.30	Effect of inert gas (N_2) in the bulk stream on overall solid conversion at: $T_b = 1173$ K, $P_b = 101.3$ kPa.	118
6.31	Effect of pellet porosity on conversion at: $T_b = 1173$ K, $P_b = 101.3$ kPa. and $\varepsilon = 0.1$	120
6.32	Effect of pellet porosity on conversion at: $T_b = 1173$ K, $P_b = 101.3$ kPa. and $\varepsilon = 0.2$	121
6.33	Effect of pellet porosity on conversion at: $T_b = 1173$ K, $P_b = 101.3$ kPa. and $\varepsilon = 0.556$	122
6.34	Effect of pellet porosity on conversion at: $T_b = 1173$ K, $P_b = 101.3$ kPa. and $\varepsilon = 0.8$	123
6.35	Effect of pellet porosity on overall solid conversion at $T_b = 1173$ K, $P_b = 101.3$ kPa.	124

6.36	Effect of inert solid (Si) inside solid matrix on conversion at: $T_b = 1173$ K, $P_b = 101.3$ kPa. and $W_f = 5\%$.	127
6.37	Effect of inert solid (Si) inside solid matrix on conversion at: $T_b = 1173$ K, $P_b = 101.3$ kPa. and $W_f = 10\%$.	128
6.38	Effect of inert solid (Si) inside solid matrix on conversion at: $T_b = 1173$ K, $P_b = 101.3$ kPa. and $W_f = 30\%$.	129
6.39	Effect of inert solid (Si) inside solid matrix on conversion at: $T_b = 1173$ K, $P_b = 101.3$ kPa. and $W_f = 50\%$.	130
6.40	Effect of inert solid (Si) inside solid matrix on overall conversion at: $T_b = 1173$ K, $P_b = 101.3$ kPa.	131

THESIS ABSTRACT

NAME OF STUDENT : ALHAJI IBRAHIM ABBA
TITLE OF STUDY : **Modeling of Multicomponent Gas -Solid Reactions**
MAJOR FIELD : **Chemical Engineering**
DATE OF DEGREE : **April, 1995**

A generalized multicomponent gas - solid reaction model is developed based on the particle - pellet model that considers the transient nature of the system, inter and intra particle heat and mass transfer and the variation of structural parameters with reaction. The principal significance of such model is in its integration in the design and simulation of a number of commercially important operations. This model can be used in the modeling of both catalytic and non catalytic gas - solid reactions. The computer coding developed is implemented following Newton's method. The Gauss - Jordan complete elimination method with maximum pivot strategy is employed in solving the set of linearized equations that resulted from the principal model equations. The model is validated by comparing simulation results with experimental data for carbon gasification reaction over the temperature range of 900°C - 1100°C and reduction of NiO / Fe₂O₃ mixture at 581 K and 608 K respectively. The match between model and experiment was found to be satisfactory in general.

Multicomponent simulation results are also presented herein, that resulted from a scenario in which four sequential reactions (carbon gasification, reduction of nickel oxide / hematite mixture and water gas shift reaction) are considered to be taking place simultaneously. From the analysis of the effects of external and internal mass and heat transfer, it was found that, the reactions studied are both diffusion and kinetic controlled, i.e., intermediate regime, in which the magnitude of each varies with the individual reactions. It is established that, the external mass and heat transfer effects are negligible for the pellet size studied. A detailed parametric study is carried out, in which the effects of bulk temperature, bulk pressure, inert gas in the bulk stream, pellet porosity and inert solid inside pellet matrix are clearly demonstrated. The established effects are found to be consistent with theoretical observations.

The model developed can, therefore, be integrated in the design and simulation of Fluidized Bed Reactors, Packed Towers and for control purposes among others.

MASTER OF SCIENCE DEGREE
KING FAHD UNIVERSITY OF PETROLEUM AND MINERALS
DHAHRAN, SAUDI ARABIA
APRIL, 1995

ملخص الرسالة

اسم الطالب : الحاج ابراهيم أبا

عنوان الرسالة : نمذجة التفاعلات الكيماكية بين الصلب لعدة عناصر

مجال التخصص : الهندسة الكيماكية

تاريخ الدرجة : ١٩٩٥م

لقد طور نموذج للتفاعلات الكيماكية بين الغاز الصلب لعدة عناصر متفاعلة بناءً على نموذج الجزئ والحبة الذي يراعي الطبيعة المتغيرة للنظام وانتقال الحرارة والمادة الداخلي والخارجي وكذلك التغير في حدود الشكل البنائي التفاعل . تكمن أهمية النموذج الرئيسية في شموله على تصميم ومحاكاة عدد من العمليات الصناعية المهمة . يمكن استخدام هذا النموذج في نمذجة تفاعلات الغار الصلب المحفز وغير المحفز

لقد استخدمت طريقة نيوتن في ترميز بنامج الكمبيوتر . استخدمت طريقة قاوس جوردان لاختصار الكلي مع استراتيجية أكبر محور في حل مجموعة المعادلات الخطية الناتجة من معادلات النموذج الأصلي .

لقد أثبتت صلاحية النموذج بالمقارنة بين نتائج المحاكاة مع نتائج التجارب للتفاعل تغويز الكربون في مجال درجة حرارة ٩٠٠ م - ١١٠٠ م وكذلك تفاعل الاختزال الخليط Fe_2O_3 / NiO في مجال درجة حراره ٥٨١ ك - ٦٠٨ ك لقد كان التقارب في النموذج والتجارب مرضي بشكل عام .

لقد عرضت الرسالة نتائج محاكاة العناصر المتعدده لأربع تفاعلات متتاليه (تغويز الكربون ، واختزال أكسيد ، النيكل الهيماتان ، وتفاعل تحول الغاز) . من تحليل نتائج التأثيرات الخارجية والداخلية لانتقال المادة والحراره ، وجد أن التفاعلات المدروسة متحكممة بالادماص والكيماكية ، وكان مقدار كل منها متغيراً من تفاعل الآخر لقد استنتج أن الانتقال الخارجي للماده والحراره غير مهم لمقاس الحبه المدروسة . لقد أجريت دراسة محموريه مفصله لتأثير الحراره الرئيسي والضغط الرئيسي والغاز الحامل في الوسط الرئيسي ومساميه الحبه والصلب الحامل داخل الحبه . الظواهر المستنتجه كانت موافقه للملاحظات النظرية .

من أجل ذلك يمكن تكامل هذا النموذج المطور في تصميم ومحاكاة المفاعلات المانع والأعمده المحشيه وفي أغراض التحكم الأخرى .

درجة الماجستير في العلوم

جامعة الملك فهد للبترول والمعادن

الظهران - المملكة العربية السعودية

أبريل - ١٩٩٥م

CHAPTER 1

INTRODUCTION

1.1 Motivation

Gas-solid reactions are frequently encountered in the Chemical Process Industries, encompassing a broad range of operations such as extractive metallurgy, combustion of solid fuels, energy generation, environmental control, petroleum refinery operations, chemical production and catalyst manufacture and regeneration. These reactions are classified as catalytic and non-catalytic reactions. Some specific examples of non catalytic gas-solid reactions include coal gasification, roasting of pyrites, and pyrolysis. Such reactions also find wide applications in some auxiliary operations in the Petrochemical Industry. Examples include regeneration of coked catalyst by means of oxygen containing gases, reduction or re - oxidation of nickel (reforming) or iron (ammonia-synthesis) catalysts prior to or after their use in the actual production.

Non catalytic gas-solid reactions have several aspects in common with reactions catalyzed by porous solids, the essential difference being that, the solid matrix inside the particle does not change its chemical composition with time in the latter. Consequently, catalyzed heterogeneous reactions of gaseous species are a class of gas-solid reactions with reduced difficulty in the solution algorithm leading to complete description of the system. Examples of such reactions include synthesis of NH_3 and SO_3 .

Rigorous mathematical modeling of these systems is, therefore, very crucial in the interpretation of experimental data for system identification and especially in reactor design. Also in actual operation of reactors, this type of modeling forms the basis for predictive and control simulation. Because of the widely evolving nature of the modeling of gas-solid reactions, considerable work has been done and the existing ones are being refined. From the Heterogeneous Shrinking Core Model through the Grain Model to the Pore Network Model, a lot of workers have come up with different approaches. However, efforts are being continuously expended in refining these models and developing new ones. The grain model explicitly accounts for the structure of the solid and compares favorably with the more complex models that have more recently been considered such as fractals; especially with the assumption that structure modification resulting from the reaction does allow the access of the reacting gas to the originally closed pores. The explanation to this lies in the tortuosity factor concept (Froment and Bischoff, 1990).

The principal significance of the single pellet model is in its integration in the design and simulation of a number of commercially important systems such as pyrolysis of wood in circulating fluidized bed (Hastaoglu and Hassam, 1995), sulfur capture in fluidized bed combustors in power plants, modeling of packed tower (Hastaoglu, M. A., 1995), hydrodesulfurization in fixed bed, and enzyme production in solid matrix (Behie et al., 1984) among others.

1.2 Objectives of this study

In all the studies carried out thus far, model equations are explicitly formulated and solved for specific reactions. The breadth and diversity of systems encountered in gas-solid reactions suggest a need for the formulation

of a versatile and comprehensive model for the simulation of multicomponent - multireaction schemes. Such a model when evolved to encompass multicomponent with multiple reactions could greatly contribute to the studies in this area. This thesis is, therefore, aimed at formulating a rigorous gas-solid reaction model that will consider the transient nature of the system, inter- and intrapellet heat and mass transfer, and the variation of structural parameters with reaction. Consequently, the specific objectives of this study are:

- i) Formulation of comprehensive transient model equations for a scheme of N_r reactions of heterogeneous/homogeneous nature with N_g gaseous components and N_s solid components. This is done through the development of continuity and energy balance equations for the multicomponent, multireaction system along with the appropriate initial and boundary conditions.
- ii) Development of equations describing the structural changes in the pellet and evaluation schemes for the multicomponent thermophysical and transport properties. Appropriate approximation techniques would be utilized in the evaluation of the properties. These properties include heat and mass transfer coefficients, diffusivities, viscosities, and thermal conductivities of mixture and other thermophysical properties of the system.
- iii) Development of a solution technique and implementation of numerical solution schemes developed to computer coding.

- iv) Validation of the model for selected cases. Asymptotic cases with established reaction schemes are considered in checking the validity of the model. Examples include carbon gasification, nickel oxide / hematite reduction and radon diffusion in concrete.
- v) Rendering the model into a robust and easily accessible form.

1.3 Organization of Thesis

The review of literature relevant to gas-solid reactions with particular emphasis on complex reactions is presented in Chapter 2. The problem formulation and mathematical modeling are discussed in Chapter 3. Chapter 4 is devoted to the discretization of the complex equations that result from the formulation. Model comparison with experiment is carried out for selected asymptotic reaction schemes in Chapters 5 and 6. The thesis is concluded in Chapter 7 with a presentation of the summary of this work, observations and recommendations for future work.

CHAPTER 2

BACKGROUND AND REVIEW OF LITERATURE

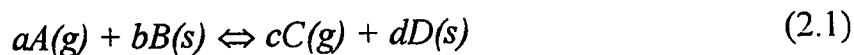
2.1 Fluid - Solid Reaction Studies

The study of fluid-solid reactions is very diverse. However, various investigators have reported enriching advances in this area. A critical survey of these works revealed that, the choice of the model and especially the consideration of structural changes determine to a great extent the accuracy and reliability of the formulation. Owing to the bewildering complexities that accompany gas - solid reactions and the diversity of the already existing models and approaches, the need for gaining further insight into the behavior of these systems cannot be over stressed. Excellent reviews have been provided by Szekely et al. (1976), Ramachandran and Doraiswamy (1982b) and Doraiswamy and Kulkarni (1987).

In most gas - solid systems, the morphology of the solid changes due to the presence of reaction, temperature gradient, etc. Typical changes that may accompany a reaction include pore shrinkage or closure, swelling, softening, or cracking of the particles. Sintering that results from temperature effects causes increase in density of the particles. These influences suggest that the effective diffusivity as applied to noncatalytic gas - solid reactions (as distinct from their catalytic counterparts) needs careful attention and to be modified continuously with the progress of reaction in a realistic manner.

2.2 Classification of Gas - Solid Reaction Schemes

A general type of heterogeneous reaction can be represented by



where A and C are gaseous and B and D are solid components respectively. Further, one of the reactants or products may not be present at all. Some important types of single gas - solid reactions are the following (Doraiswamy and Sharma, 1984):

i) Reduction and roasting of ores:

Fluid and solid reactants \rightarrow Fluid and solid products

ii) Decomposition reactions:

Solid reactants \rightarrow Fluid and solid products

iii) Oxidation and chlorination of ores:

Fluid and solid reactants \rightarrow Fluid products

iv) Gasification reactions:

Solid reactants \rightarrow Fluid products

In view of the generality of the first category of reactions and their importance in industrial practice, most studies reported in the literature put emphasis on this class of reaction.

2.3 Model Studies

Owing to the complexity of modeling gas - solid reactions, it is extremely difficult for a single model to incorporate all the features of these reactions. Consequently, different models have been postulated and used to describe these systems. In this section, the basic models (Sharp Interface Model, Volume Reaction Model, Particle - Pellet Model), Network Model and other miscellaneous models will be reviewed briefly. For a more complete review, the reader is referred to Ramachandran and Doraiswamy (1982b).

2.3.1 Sharp Interface Model

The Sharp Interface Model (SIM) otherwise referred to as the Shrinking Core Model or Topochemical Model is one of the earliest models used. An important assumption in the use of this model is that, the solid reactants are considered to be highly nonporous and, thus, it is assumed that the reaction takes place at a sharp interface that divides the exhausted outer shell (ash layer) and the unreacted core of the solid. A schematic representation of the model is shown in Figure 2.1.

Detailed formulations of the model accounting for a number of effects have been reported in the literature. Sohn and Sohn (1980) studied the effects of bulk flow for the case where diffusion in the product layer is rate controlling. The influence of pressure gradient has been examined by Deb Roy and Abraham (1974) and Turkdogan et al. (1973). For non linear systems the conversion - time relations have to be examined by numerical integration as described by Sohn and Szekely (1972a) for power law kinetics, by Ramachandran (1982a) for Langmuir - Hinshelwood kinetics

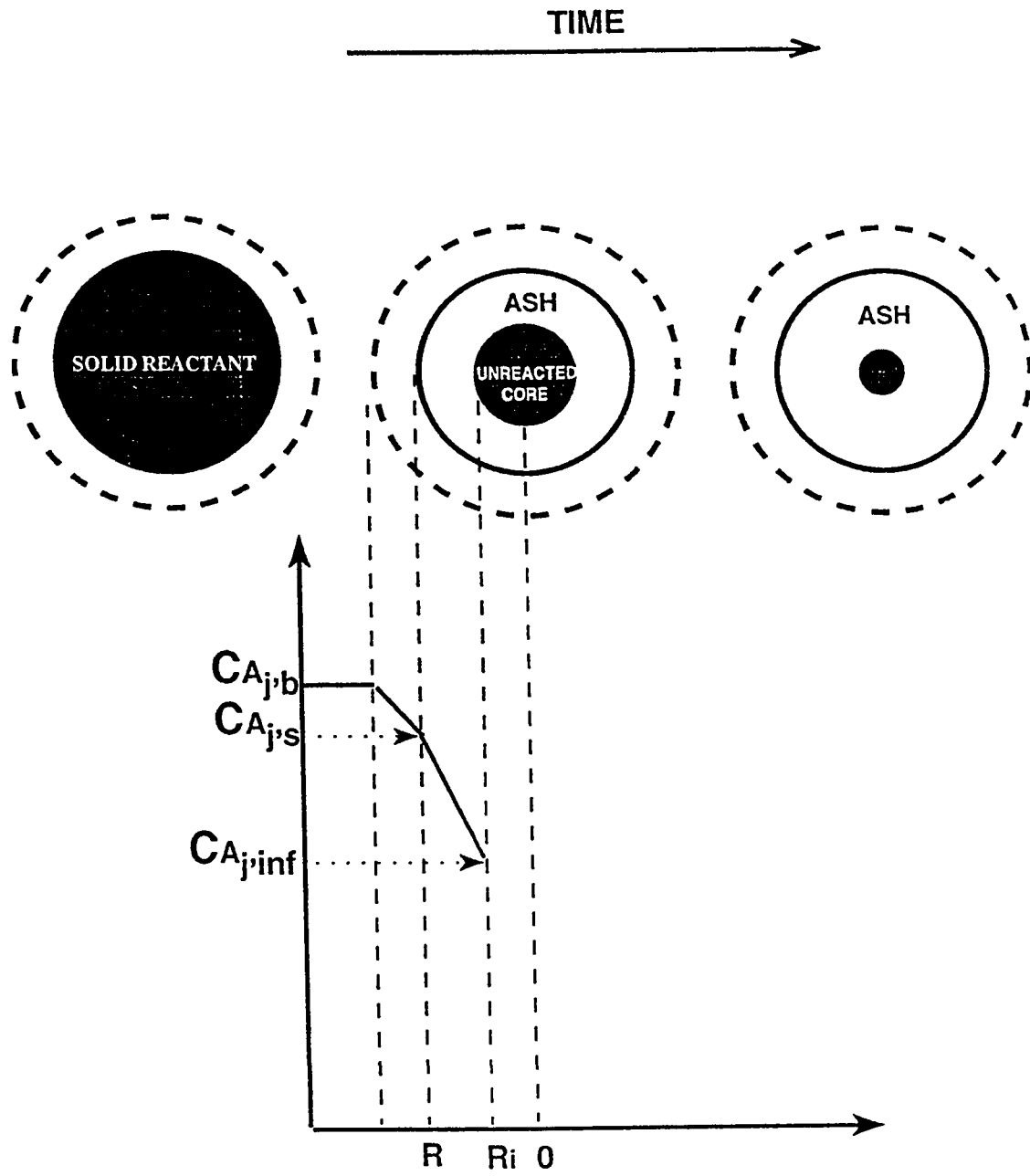


Figure 2.1. Schematic Representation of the Sharp Interface Model

and an interesting case of zero - order reactions by Simonsson (1979).

The prediction of temperature profiles in the pellet may be the key problem in some situations. Typical examples are in catalyst manufacture by reduction of metal salts or in the oxidation of coke from spent catalysts, where the temperature rise in the pellet has to be restricted below a permissible maximum in order to prevent catalyst deactivation. Equations for predicting the complete transient temperature profile in the pellet have been derived by Luss and Amundson (1969). More recently, Cao et al. (1993) developed approximate analytical solutions for non - linear gas - solid reactions following the SIM, without any assumptions about possible rate controlling regimes. They treated the case of Langmuir - Hinshelwood kinetics and concluded that the relative error with respect to the true solution for reaction completion time is about 5%. It should be noted here that, SIM (the sharp interface model) has the advantage of mathematical simplicity. However, its applicability is limited to non - porous solids and this is one of the short comings of this model.

2.3.2 Volume Reaction Model

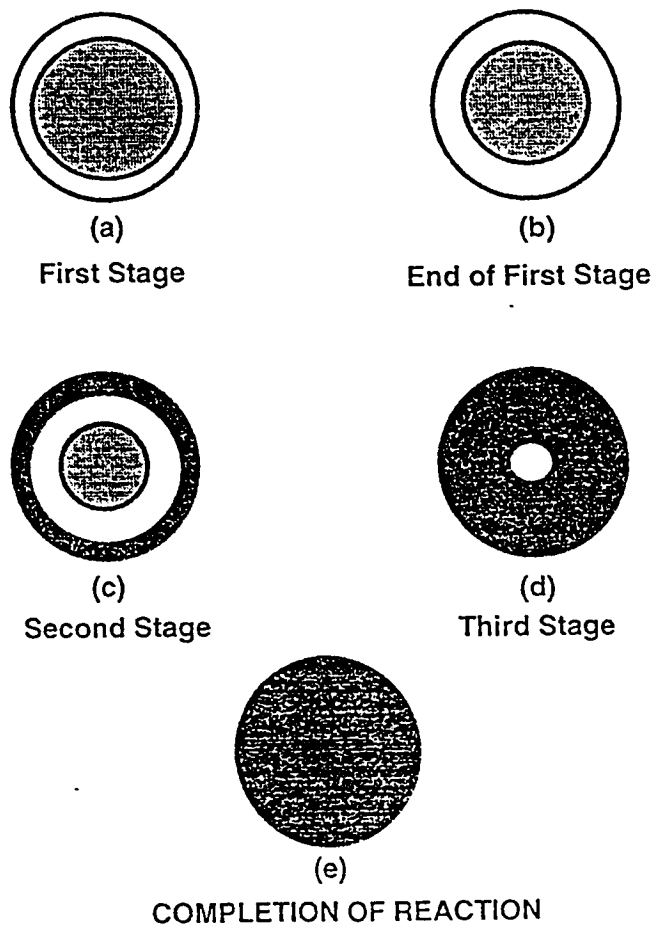
The volume reaction model (VRM) otherwise referred to as the homogeneous model addresses porous solids. When the solid is porous and the rate of diffusion of the reactant gas is rapid, the gas will penetrate everywhere into the solid and the reaction will take place throughout the pellet.

Ausman and Watson (1962) and Ishida and Wen (1968) analyzed the case of first order kinetics using the VRM. The latter proposed the two zone

model in which the total reaction time is divided into constant rate and falling rate periods. In the two zone model, when the rate of reaction is very rapid, the concentration of the gaseous species drops very sharply in the reaction zone. The reaction zone can further be subdivided into zones comprising the actual reaction zone where the bulk of the reaction occurs and a core of completely unreacted solid. This has led to the development of the so called "zone models" (Boweng and Chang, 1969; Mantri et al., 1976). Reaction in the two zone model as it contrasts with the sharp interface model (where also two zones exist) is not restricted to the interface between the zones.

Mantri et al. (1976) postulated the three - zone model that has the merit of being general and reducible to simpler situations. The three - zones that develop in a pellet are: i) a zone of the product or exhausted solid ash layer near the outer surface of the pellet, ii) a zone of finite thickness where reaction occurs and iii) a zone of unreacted solid towards the center of the pellet. These are shown schematically in Figure 2.2. It may be noted that at a certain point during the reaction when the core completely disappears, the model reduces to that of Ishida and Wen (1968) described earlier.

Ramachandran and Doraiswamy (1982a) considered the case where the reaction is zero - order with respect to both gaseous and solid reactant species. They observed an interesting phenomenon of jumping reaction zones and termed this the "jumping zone model". In this model, once the zone is formed, the reaction progresses within this zone until the solid there gets completely exhausted. The reaction then jumps to another zone, where the phenomenon continues.



KEY

 REACTION ZONE

 UNREACTED CORE

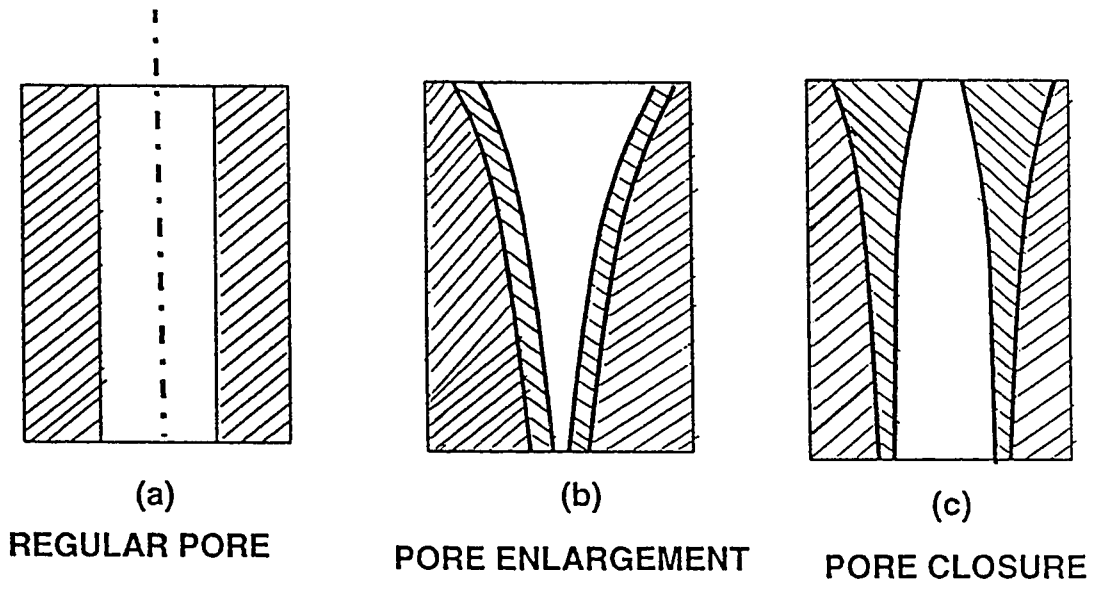
 EXHAUSTED SOLID

Figure 2.2 The Three Stages of the Zone Model

2.3.3 Pore Model

A class of models incorporating structural features such as pore size distribution have also evolved. Since Petersen (1957) first proposed the model, several workers have considered various extensions. The simplest of such models is the single - pore model of Ramachandran and Smith (1977a) and Chrostowski and Georgakis (1978). They matched their model predictions with experimental results of sulfation of calcium oxide satisfactorily. A schematic of the single pore model is given in Figure 2.3. The single pore is assumed to be cylindrical with the concentric ring of solid B_k associated with it. Figures 2.3(b) and 2.3(c) show the effects of structural changes that lead to the pore opening and closure phenomena respectively.

The model of Christman and Edgar (1980) assumes the applicability of a single pore model at a local point r in the pellet. The mass balance equation is supplemented by an equation describing the evolution of pore size distribution with the progress of reaction. They modelled this process using a population balance approach. The key feature of this model is that it gives the variation of pore size distribution with time and position - a remarkable improvement over the conventional single pore model. The model of Simons and Rawlins (1980) assumes that each pore within the solid ends up at the surface of the pellet, where a distribution of pore radii can exist. An extension of the single pore model to account for the effect of bulk flow and reversibility of the reaction has been proposed by Ulrichson and Mahoney (1980). Their model predicted the experimental results of chlorination of MgO fairly adequately.




$t = 0$

$t > 0$

KEY

 PORE

 SOLID Bk ASSOCIATED WITH THE PORE

 SOLID PRODUCT

Figure 2.3. Schematic Representation of the Single Pore Model (Doraiswamy and Kulkarni, 1987)

The single pore model has two disadvantages. Firstly, it does not take into account the intersections of the reaction surfaces as the various pores present in the pellet react. And secondly, the model does not take into account the pore size distribution which normally exists.

A more realistic model is the Random Pore Model (RPM). The RPM is similar to the single pore model but takes into account the effect of pore size distribution. Some of the more recent RPMs are those proposed by Bhatia and Perlmutter (1980) and by Gavalas (1980). Bhatia and Perlmutter considered the pore structure to consist of cylindrical pores parallel to each other. The overlapping of these pores was taken into account by correlating them to the non-overlapped pore model following the approach of Avrami (1940). Figure 2.4 illustrates the random pore intersections of the RPM. The encircled detail shows structural changes. A schematic of the RPM is shown in Figure 2.5 which depicts the product layer surrounding the pores at different stages of the reaction. The dotted area represents the product layer: (a) early stage showing product layer around each pore; (b) intermediate stage showing some overlapping reaction surfaces and (c) later stages showing full development of product layer and reaction surface for the particular view.

Detailed description of pore growth and pore combination have been realized by population balance techniques (Hashimoto and Silveston, 1973; Zygourakis et al., 1982; Christman and Edgar, 1983). Models based on the population balance techniques assume that there is no net fractional increase in the number of pores by "birth" or "death" mechanisms, that is, it assumes that the total number of pores are conserved. This fundamental assumption used in the formulation of the population balance approach limits its applicability, since in gasification systems, "birth" mechanisms may be

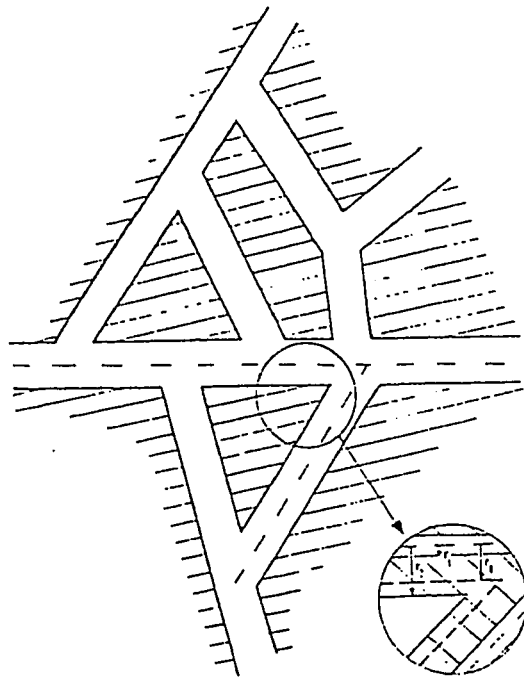


Figure 2.4 Random Pore intersections of the RPM (Petersen, 1957).

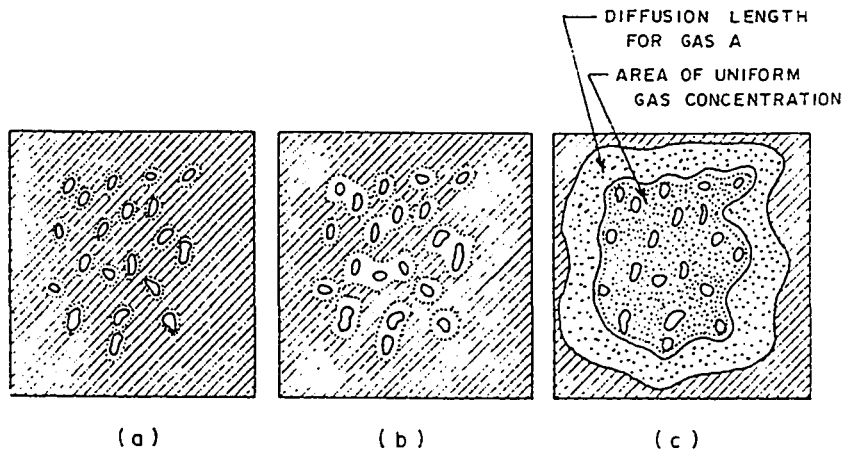


Figure 2.5 Development of Reaction Surface according to the Random Pore Model (Bhatia and Perlmutter, 1981a).

present. Likewise, in a sintering solid matrix, "death" mechanisms exist as well. Further, models based on the population balance techniques usually contain a number of adjustable parameters that cannot be determined from direct measurement of porous solid properties (Reyes and Jensen, 1987).

More recently, RPMs for solids with a pore size distribution with or without pore closure were presented for use under reaction conditions controlled by intrinsic kinetics and diffusion in the product layer (Sotirchos and Yu, 1985 and Bhatia, 1985). These models can be used for any type of pore size distribution and take into account the effects of pore overlap on the diffusion flux in the product layer and on the evolution of the reaction and pore surfaces.

2.3.4 The Network Model

The Network Model (NM) is a structural model based on a network representation of the pore space called Bethe Lattice or Bethe Network. Reyes and Jensen (1985) developed and conveniently used this model to simulate the essential geometrical and topological properties of porous structures. A Bethe Network is a regular branching tree which has Z bonds connected to each site. Z is the coordination number of the Bethe Network, which can be implied from mercury porosimetry experiments, effective diffusivity measurements or microscopy studies. A random removal of a fraction of bonds $(1-\epsilon)$ generates a related network that closely resembles topological features of porous structures (Reyes and Jensen, 1987). An illustration of the Bethe lattice with coordination number 3 is shown in Figure 2.6.

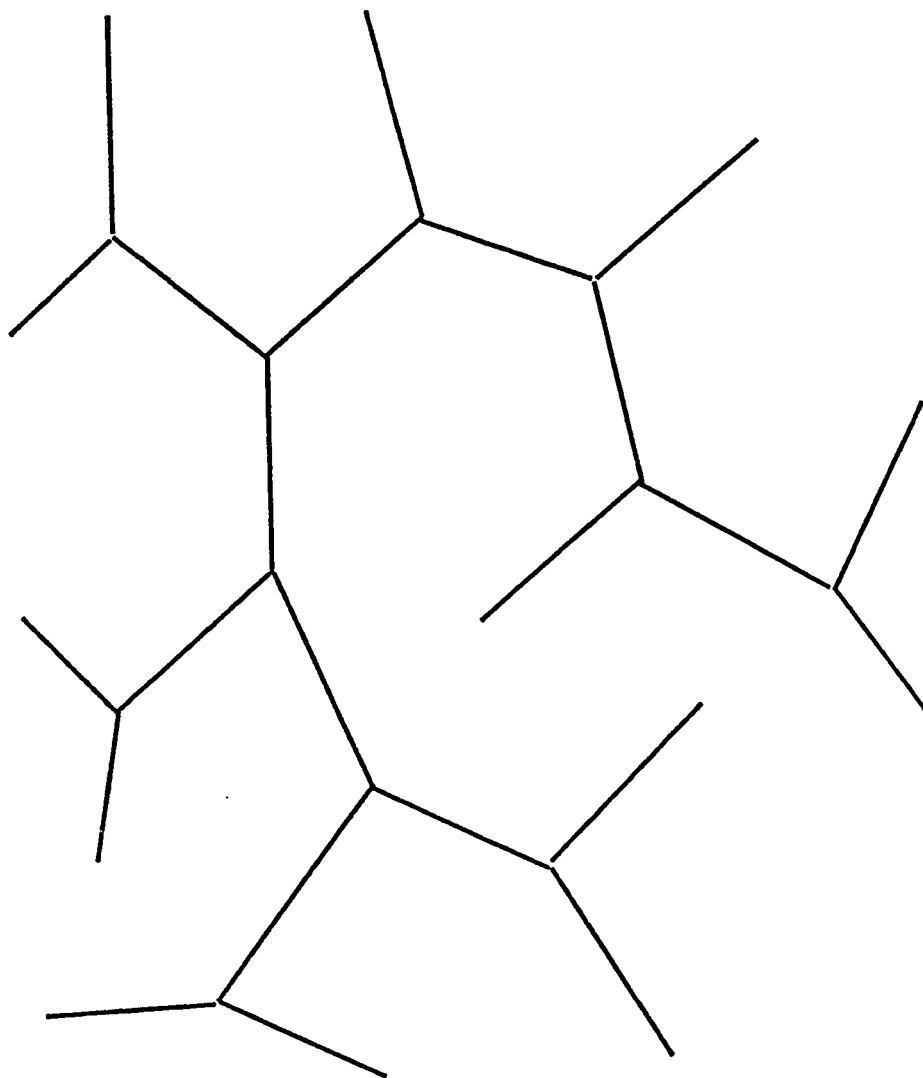


Figure 2.6 Bethe Lattice with coordination number, $Z = 3$.

Percolation concepts have been used to develop comprehensive model for reaction and transport in changing pore structures with particular emphasis on char gasification (Reyes and Jensen, 1986a & b). Reyes and Jensen (1987) extended this model to describe pore plugging reactions which explicitly incorporates the role of pore space topology on the isolation of partially reacted pores. This aspect is not accounted for in the RPM. A major advantage of this model structure is that, its topological properties can be determined in closed form. Reyes and Jensen applied the model to sulfation of calcium limestone and observed a good agreement between the model predictions and the experimental observations. They attributed this to the consistent and detailed picture of the pore space given by the use of the Bethe Network.

Yortsos and Sharma (1984) described the formation of inaccessible pore volume by employing percolation theory concepts. Yu and Sotirchos (1987) extended Yortsos and Sharma's work to investigate the adsorption of sulfur dioxide by calcined limestone. They placed particular emphasis on the combined effects of pore closure and formation of inaccessible volume on the evolution of the reactivity of the solid and of its sorptive capacity for SO_2 removal. In general, their model predicted the experimentally measured data well and they concluded that the broader the pore size distribution of the solid, the larger the inaccessible pore volume formed in the interior.

2.3.5 Particle - Pellet Model

The Particle - Pellet Model (PPM), also referred to as the grain model proposed by Szekely and Evans (1970), visualizes the solid as consisting of a number of closely packed arrangement of small non - porous particles or

grains. In this model, it is assumed that, the grains are of a regular shape with uniform size and that each grain reacts according to the sharp interface model. It is further assumed that the grain does not change with reaction, thereby implying no change in the voidage of the pellet. A product layer will form with time in the outer regions of each grain and this will, in turn, offer some additional resistance to diffusion. The basic features of the model are shown in Figure 2.7 for a non - isothermal situation. This model is considered to be realistic especially in describing physical systems where the solid pellets are agglomerates of grains.

The mathematical formulation of the model requires consideration of the rate processes within an individual grain, and the overall mass balance for the gaseous reactants in the pellet and its stoichiometric relationship with the extent of solid consumed. A mathematical analysis of the PPM has been presented by Calvelo and Smith (1970) and Szekely and Evans (1971a,b) for a simple isothermal first order reaction.

A number of simplifying assumptions inherent in the early models include restriction of the reaction kinetics to first order in gas concentration, pseudo - steady state describing the concentration of gas in the pellet, uniform grain size, absence of bulk flow and absence of pore structure variation in the pellet. Considerable effort has been expended in improving the grain model through relaxation of these simplifying assumptions. Szekely and Evans (1971c) considered the effects of grain size, porosity and temperature on the porous pellets. A general formulation which assumes various grain shapes such as spheres, long cylinders and slabs has been presented by Sohn and Szekely (1972b, 1974). The constant grain size model has been generalized by Szekely and Propster (1975) to include grain size distribution.

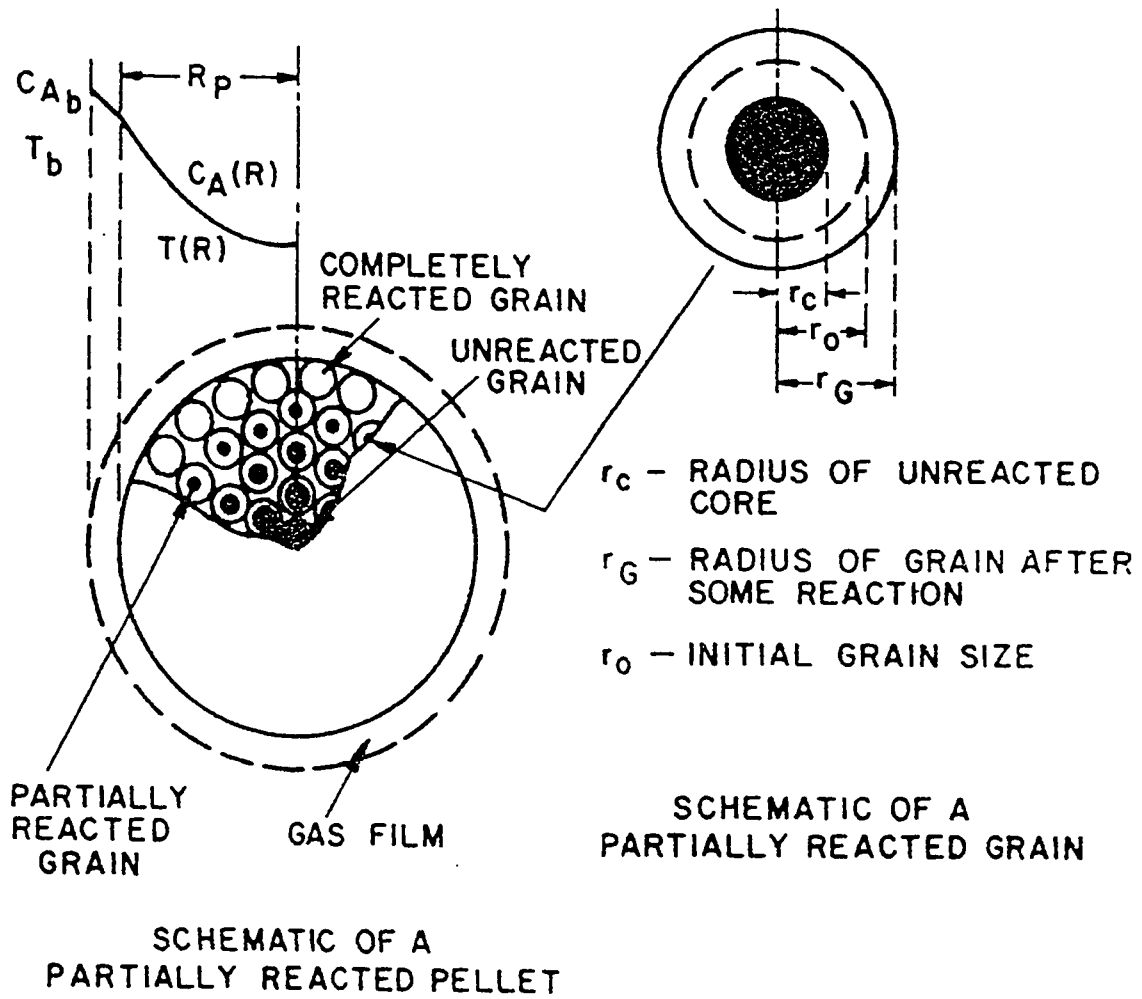


Figure 2.7. Schematic Representation of the PPM (Hassam, 1987).

The case of non - linear kinetics has been proposed by Sohn and Szekeley (1973a, b) for reactions following the Langmuir - Hinshelwood rate law.

A complete transient analysis was carried out employing the orthogonal collocation technique by Sampath et al. (1975a, b). They compared the temperature profiles obtained by the pseudo steady state model and the transient model. They also integrated the single particle model in the simulation of a packed bed reactor.

The structural changes that occur in the solid during reaction have been studied very extensively. There are certain special behavior patterns which have been observed experimentally such as leveling - off of conversion - time data far below complete conversion; existence of maxima in the rate - time data, especially, for gasification reactions and strong dependence of the reactivity of the solid on the pore size distribution that cannot be accounted for with the assumption of constant pore structure properties. The main structural changes are due to chemical reaction and sintering. Sintering becomes significant at higher temperatures in many systems. The changes due to reaction are mainly caused by the differences in the molal volumes of the reactant and the product solids. This causes a change in the porosity of the solid and in the effective diffusivity. A comparison of some models incorporating the effects of structural changes is presented by Linder and Simonsson (1981).

The grain model has been applied to a number of systems. Gibson and Harrison (1980) have applied this model to the reaction of hydrogen sulfide with zinc oxide. Sulfur profiles were measured using electron probe microanalysis and were found to agree quite closely with the grain model predictions in the low temperature range. The modified grain model (incorporating the effects of structural changes) has been used in the

interpretation of experimental data on hydrofluorination of UO_2 (Ramachandran and Smith, 1977b) and sulfation of limestone (Georgakis et al., 1979). Both systems were observed to exhibit phenomenon of pore closure. More recently, Hastaoglu and Karmann (1987) have applied the modified grain model to catalytic carbon gasification for an isothermal system. The catalytic effect of nickel has been assessed quantitatively through the model and predicted the experimental conversion satisfactorily. Hastaoglu and Hassam (1988) further extended the model to incorporate temperature and pressure variations in the pellet. The model predictions matched conversion trends for carbon gasification over a temperature range of 800 to 1000 °C investigated experimentally. A similar transient model have been used to predict conversion trend in the pyrolysis of wood (Hastaoglu and Berruti, 1989).

From the foregoing discussion, it can be observed that, while no single model perfectly describes all situations, perhaps the most successful model is the particle - pellet model. The generalized multicomponent formulation in the present study is based on the PPM. The choice of this model is based, in part, on the success of the model in predicting a myriad of conversion trends, and in part, on the important consideration that the number of parameters that need to be determined independently are fewer than the ones needed for the more complex models.

2.3.6 Miscellaneous Models

Several other models have been described separately. For example; Park and Levenspiel (1975) proposed the so - called Crackling Core Model to account for the sigmoidal behavior of conversion versus time plots in some

observed systems. This model is only an approximation and does not consider the basic mechanisms responsible for the sigmoidal behavior. One such reason could be the nucleation effect. Sohn (1978) and Rao (1979) have discussed some aspects of the nucleation. Formation and growth of nuclei in the H₂ reduction of wustite has been observed by El-Rahaiby and Rao (1979). Tadafumi et al. (1987) investigated the dynamic change in gasification rate of chars using the overlapped grain model. Sotirchos and Yu (1988) developed a generalized model for single gas - solid reactions with solid product based on the overlapping grain concepts. A single pellet - moment technique has been presented for evaluating reaction rate constants, effective diffusivities and adsorption equilibrium constants for gas - solid non - catalytic reactions (Dogu et al., 1986).

2.4 Complex Reaction Systems

Many of the industrially important reactions follow complex reaction schemes and modeling of these systems is correspondingly difficult. Thus far, no generalized approach has been reported in the literature. The models discussed in the earlier sections primarily addressed simple gas - solid reaction schemes.

A complex reaction scheme could be consecutive gas - solid reactions, reactions of more than one gas with same solid, reaction of more than one solid with same gas or reaction of more than one gas and solid components. Representative types of complex gas - solid systems with some examples are presented in Table 2.1.

Fahim et al (1978) presented a grain - cell model for complex reactions. They considered one of the solid reactants to be comprised of porous grains

Table 2.1 Examples of Some Complex Reactions

<i>Classification</i>	<i>Examples</i>	<i>References</i>
1. Reaction of two or more gases with the same solid	<ol style="list-style-type: none"> 1. Reduction of iron ore with a mixture of CO and H₂ 2. Decay and diffusion of gases in the subsurface 	<p>Tsay et al. (1976)</p> <p>Abu-El-Shar (1993)</p>
2. Reaction of two solids with the same gas	<ol style="list-style-type: none"> 1. Regeneration of coked catalysts 2. Reduction of a mixture of iron oxide and nickel oxide 	Ramachandran et al. (1975) Szekely and Hastaoglu (1976)
3. Gaseous product of first reaction reacting with a second solid	<ol style="list-style-type: none"> 1. Reduction of Cobalt sulfide in the presence of CaO 	Fahim and Ford (1978)
4. Homogeneous / Heterogeneous reactions	<ol style="list-style-type: none"> 1. Reduction of metal chlorides with hydrogen 	Rao (1981)

consisting of non - porous subgrains. This is an extension of the basic particle - pellet model. Fahim and Ford (1978) presented results of an experimental program to test the applicability of the grain - cell model to complex gas - solid reactions. They studied the reduction of cobalt sulfide in the presence of calcium oxide and reported good agreement between experimental results and model. Sohn and Braun (1980) presented a general model describing simultaneous independent reactions between one solid reactant and two fluid reactants. They applied the law of additive reaction times previously developed by Sohn (1978). In a later communication, they also described reactions between one fluid and two solid reactants (Sohn and Braun, 1984).

The studies reported thus far on complex gas - solid reactions are limited owing to the complexities involved in modeling such systems.

2.5 Flux Relations for Gas Transport

2.5.1 Flux Model

The modeling of gas transport in porous media have been developed distinctly via three approaches: i) The momentum transfer approach (Knudsen, 1909), ii) the dusty gas approach - Dusty Gas Model (Mason and Malinauskas, 1983) and iii) the volume averaging approach (Whitaker, 1987).

Customarily, the laws of molecular diffusion are invoked in the presence of pore diffusion effects and an assumption is made of their applicability to porous media with an effective diffusive parameter. This equivalence is, at best, an approximation, and the total flux balance should include the contributions from the pressure gradient (Hite and Jackson, 1977), the viscous flow (Evans, 1972 and Haynes, 1978) and bulk flow due to

diffusion. Consequently, these contributions are neglected and perhaps justifiably so in some cases. However, in certain instances such as when "multicomponent diffusion" is involved, they should be taken into account. Studies on diffusion in porous media have established the significance of the flux mechanisms in the molecular regimes (see Figure 2.8). It is therefore essential in this study that, the flux relations adopted should be capable of describing the behavior of the system in these regimes. The simplest flux relations with these properties are associated with the "Dusty Gas Model" (DGM). Therefore, the DGM which represents a framework for the rigorous treatment of multicomponent diffusional processes in porous media is employed in this study. The concept of the dusty gas is briefly reviewed.

2.5.2 The Dusty Gas Concept

The DGM is composed of a set of constitutive equations derived from momentum balance relations of the Chapman - Enskog kinetic theory. In this model, the porous medium is viewed as a collection of spherical particles of uniform distribution. These solid grains or "dust" particles are treated as one component of the gas mixture, consisting of giant molecules fixed in space to which the highly developed kinetic theory of gases is applied. A configurational representation of the dusty gas and illustration of a schematic way of visualizing the dusty gas model are shown in Figure 2.9. Jackson (1977) described the diffusing mixture as composed of "n" gaseous species supplemented by an (n+1)th "dummy" species (pseudo gas) of very massive molecules known as the "dust" constrained by unspecified external forces to have zero drift velocity at all times. Interaction of the gas molecules with the

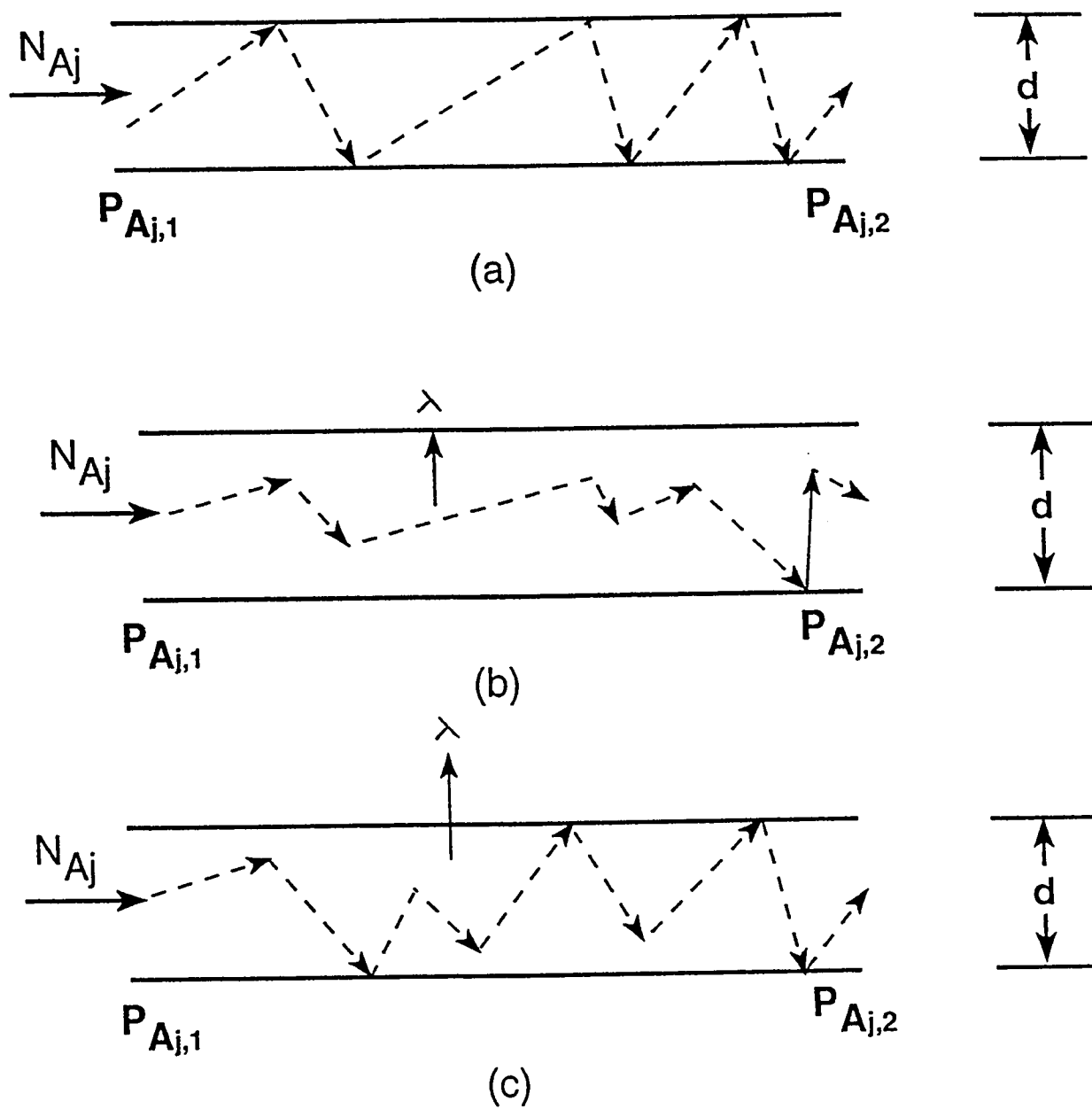
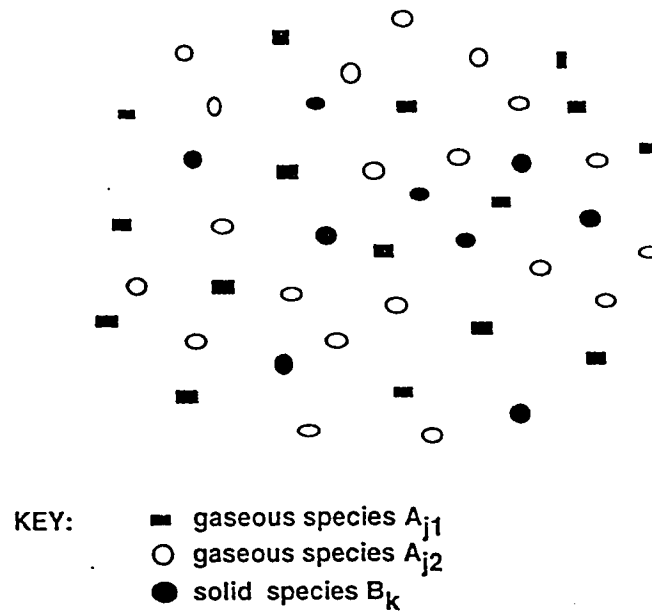
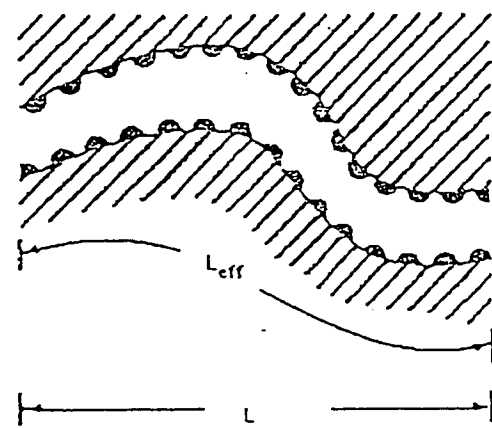
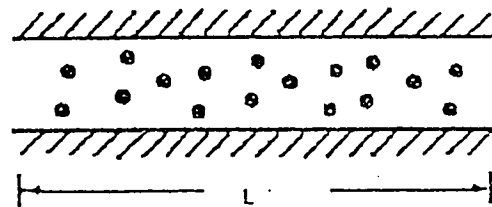


Figure 2.8. Diffusion in Capillaries: (a) Knudsen regime; (b) Molecular regime; (c) Transition regime. λ = Mean Free Path.



(a)



(b)

Figure 2.9. The dusty gas concept: (a) The dusty gas; (b) Schematic ways of visualizing the dusty gas model for transport in porous media (Mason and Malinauskas, 1983).

dust molecules simulates their interaction with the immobile solid matrix of a porous medium which is dispersed throughout, as if constituting its representative dust.

CHAPTER 3

DEVELOPMENT OF THE MATHEMATICAL MODEL

3.1 Problem Formulation

In this study, the reaction environment envisaged is one complex multireaction system in which a number of gaseous and solid species participate. The model formulation and equation development are therefore focused on such schemes. It should be noted that the resulting equations can describe single reaction scenarios equally well.

The equations to be presented below are based on the PPM of Szekely et al. (1970), in which the pellet is considered to comprise of compaction of initially non - porous grains. In this formulation, an additional consideration is made of different solid species of possibly different sizes constituting the agglomeration of grains inside the pellet. A schematic representation of this is given in Figure 3.1. The reactant gases are considered to diffuse through the interstices between the grains and react with individual grains according to the sharp interface model as previously described in section 2.3.1. Allowances are made for the accommodation of all geometries (flat plate, cylindrical and spherical) in the shapes of the grains and the pellet. For disc (flat plate) shaped pellets, R_p is the pellet half thickness; for cylindrical or spherically shaped pellets, it is the pellet radius.

Complex porous structures can also be accommodated in this approach by finding equivalent grain diameter to represent the porous area

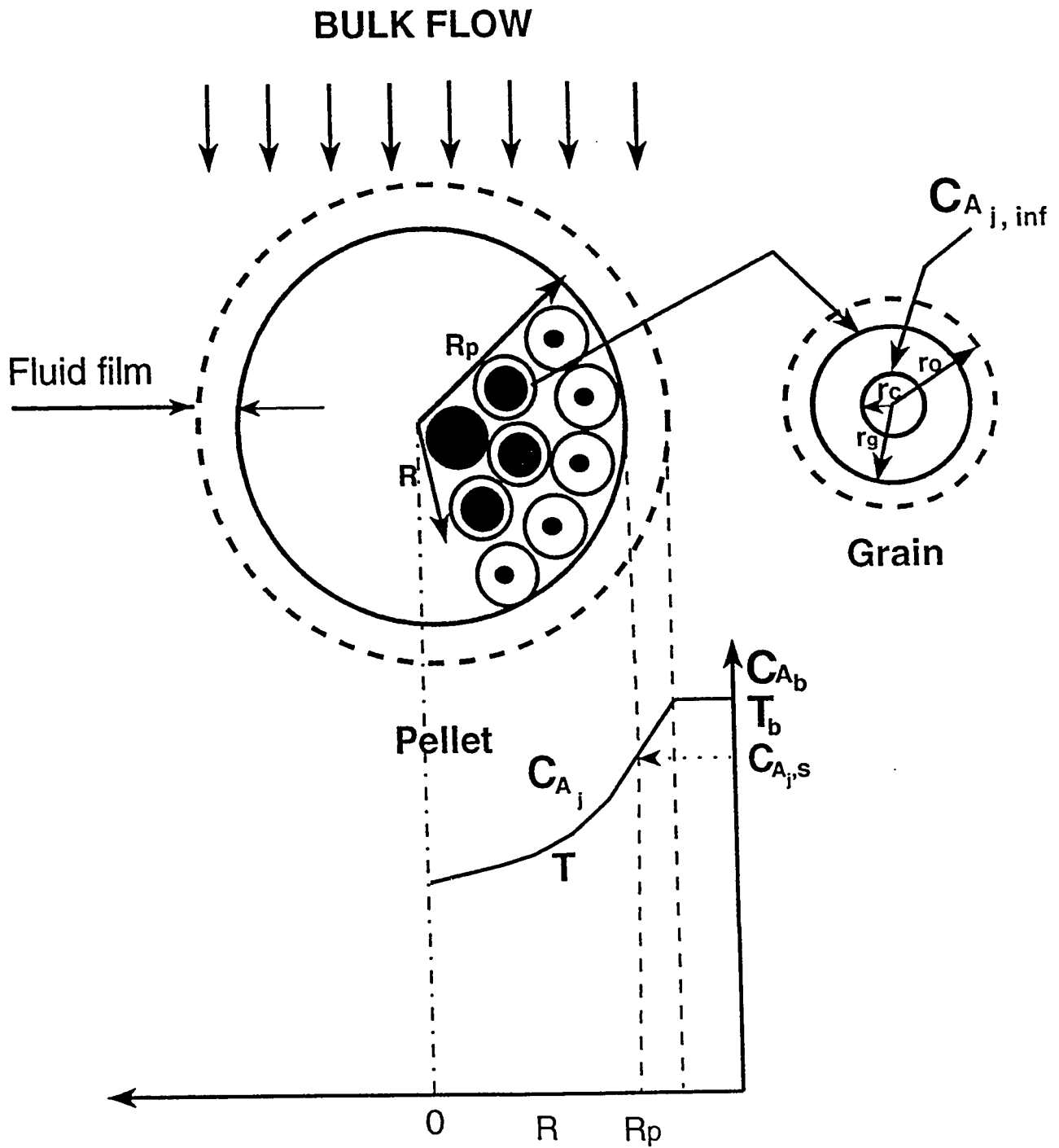


Figure 3.1. Schematics of Pellet and Grain Structures.

$$\sum_{j=1}^{N_g} a_{ij} A_j + \sum_{k=1}^{N_s} b_{ik} B_k = 0 \quad i = 1, \dots, N_r \quad (3.4)$$

where

A_j = gaseous component j as reactant or product

B_k = solid component k as reactant or product

a_{ij}, b_{ik} = coefficients of gas A_j and solid B_k respectively in reaction i

The rate expression for reaction i is thus

$$(\text{Specific rate of reaction } i) = f_i(\vec{A}) \quad (3.5)$$

for a base gas or solid component (pivot component).

The net rate of consumption of component A_j and B_k can be written as

$$(\text{Rate of net consumption of } A_j) = \sum_{i=1}^{N_r} a_{ij} f_i(\vec{A}) \quad (3.6)$$

$$(\text{Rate of net consumption of } B_k) = \sum_{i=1}^{N_r} b_{ik} f_i(\vec{A}) \quad (3.7)$$

Equations (3.5) - (3.7) are utilized for the rate terms in the continuity and energy balance equations respectively.

For a non-reacting (inert) gaseous or solid component, the stoichiometric coefficients a_{ij} and b_{ij} for all reactions are zero. A typical example is N_2 in air where only O_2 reacts during combustion. This consideration has enormous effect on the thermophysical and transport property calculations.

3.1.2 Factors Controlling the Rate of Reactions

There are several factors controlling the rate of gas - solid reactions. The following factors have been outlined for single reaction systems which are also applicable to the multireaction scheme considered:

- i) External mass transfer of the gaseous reactants across the gas film from the bulk gas stream to the pellet surface
- ii) Diffusion of the gaseous reactants into the pellet through the porous space between the grains and through the product layer surrounding individual grains.
- iii) Reaction of the gaseous and solid reactants, as controlled by the intrinsic reaction kinetics.
- iv) Diffusion of the gaseous products out of the pellet through the pores between the grains.
- v) External mass transfer from the pellet surface to the bulk gas through a gas film surrounding the particle.

It should be noted that, validity of the smooth field approximation is assumed in the formulation of the conservation equations for the intrapellet mass transfer, implying that the concentration of a particular species is constant at a given radial coordinate. Physically, this approximation will be valid, if the degree of pore interconnectivity is large and agglomeration does not occur. Adsorption, surface diffusion, chemical reaction and desorption steps are considered together in the form of an intrinsic reaction rate.

3.1.3 Assumptions

Any mathematical model designed to represent a physical system takes into consideration certain simplifying assumptions to prevent solution difficulties. The following assumptions are made for the present study.

- i) The grains are considered to retain their original shape during the reaction.
- ii) Temperature and pressure are constant in the grains. Though the pellets are large enough to permit both concentration and temperature gradients to exist, the grains are considered to be sufficiently small so that internal temperature gradients may be neglected.
- iii) Sintering does not occur to a significant degree. Sintering can be significant in some systems and especially at high temperatures and can cause considerable reduction in the effective diffusivity due to removal of pore interconnectivity. Although this assumption can be relaxed, it is assumed that both the solid reactants and products do not sinter appreciably.
- iv) The transport of gas species is characterized to be via a convective mass transfer coefficient.
- v) Porosity of the product layer is taken to be constant within the grain.
- vi) The solid - solid reaction and solid diffusion mechanism are ignored.

3.2 Model Equations

3.2.1 Continuity Equations

The conservation equation of reactant A_j is

$$\frac{\partial(\varepsilon C_{A_j})}{\partial t} = -\nabla N_{A_j} - \sum a_{ij} (Ar)_i \times f_i(\vec{A}) \quad (3.8)$$

where

N_{A_j} = flux of component A_j

$(Ar)_i$ = specific reaction area per unit volume of gross reaction space

$f_i(\vec{A})$ = the intrinsic reaction rate term per unit surface area for reaction i based on a pivot component. It can describe any reaction kinetics desired

ε = pellet porosity at any time t .

In equation (3.8), the term in the left hand side is the accumulation term; the first term in the right hand side represents the flux gradient of component A_j in the pellet; and the second term accounts for the generation or consumption in reaction i . The specific reaction area per unit volume of gross reaction space is given by

$$(Ar)_i = F_g (1 - \varepsilon_o) \frac{r_{cBk}^{F_g - 1}}{r_{oBk}^{F_g}} \quad (3.9)$$

where r_{cBk} is the reaction front radius and r_{oBk} is the initial radius of grain B_k . ε_o is the initial pellet porosity.

The initial and boundary conditions are

$$\text{at } t=0 \quad C_{A_j} = C_{A_{j0}} \quad 0 \leq R \leq R_p \quad (3.10)$$

$$\text{at } R=0 \quad N_{A_j} = 0 \quad (\text{symmetry at pellet center}) \quad (3.11)$$

$$\text{at } R=R_p \quad N_{A_j} = k_c (C_{A_{jN}} - C_{A_{jb}}) \quad (3.12)$$

where the subscripts N and b stand for pellet surface and bulk gas conditions respectively. $C_{A_{jb}}$ in equation (3.12) is the bulk concentration of A_j and is assumed constant, consistent with the assumption number five.

The concentration of all gaseous species (reactants and products) at the reaction fronts in the grains (interface concentrations) are determined from the combination of the component fluxes through the product layer surrounding the individual grains. Thus, for a spherical grains as example, a material balance on component A_j yields;

$$\sum_k^{N_s} 4\pi r_{gBk} r_{cBk} N_{A_j}^P + \sum_k^{N_s} 4\pi r_{cBk}^2 \times \sum_i^{N_r} a_{ij} f_i(\vec{A}) = 0 \quad (3.13)$$

where $N_{A_j}^P$ is the flux through the product layer of component A_j . An assumption implicit in equation (3.13) is that, the diffusion through the product layer within the grain is a steady state process. Thus, only the fluxes through the product layer and the rate of generation (or consumption) by reaction at the interface are considered. The flux through the product layer is approximated with the simple Fickian expression as:

$$N_{A_j}^P = -D_{A_j}^P \frac{dC_{A_j}}{dr} \quad (3.14)$$

Eq. (3.14) can be approximated for grains under consideration as;

$$N_{A_j}^P = -D_{A_j}^P \frac{C_{A_j} - C_{A_j,inf}}{r_{gBk} - r_{cBk}} \quad (3.15)$$

where $D_{A_j}^P$ represents the effective diffusivity of component A_j through the product layer surrounding type B_k grains. $C_{A_j,inf}$ is the interface concentration of component A_j . Substituting eq. (3.15) into eq. (3.13) results in:

$$\frac{dn_{A_j}}{dt} = -\sum_k^{N_s} 4\pi r_{gBk} r_{cBk} D_{A_j}^P \frac{C_{A_j} - C_{A_j,inf}}{r_{gBk} - r_{cBk}} = -\sum_k^{N_s} 4\pi r_{cBk}^2 \times \sum_i^{N_r} a_{ij} f_i(\vec{A}) \quad (3.16)$$

The conservation equations for solid reactant B_k can be written based on stoichiometry as follows:

$$\frac{dn_{B_k}}{dt} = \frac{b_k}{a_j} \frac{dn_{A_j}}{dt} \quad (3.17)$$

where n_{A_j} and n_{B_k} are number of moles of components A_j and B_k respectively. The number of moles of reactant B_k per grain can be written as:

$$n_{Bk} = \frac{4}{3} \pi r_{cBk}^3 \frac{\rho_{Bk}}{M_{Bk}} \quad (3.18)$$

Combination of equations (3.16) through (3.18) and simplification yields:

$$\frac{dn_{Bk}}{dt} = 4\pi r_{cBk}^2 \frac{\rho_{Bk}}{M_{Bk}} \frac{dr_{cBk}}{dt} \quad (3.19)$$

Therefore the equation governing the movement of the reaction front is:

$$\frac{dr_{cBk}}{dt} = -\frac{\rho_{Bk}}{M_{Bk}} \sum_i^{N_r} b_{ik} a_{ij} f(\vec{A})_i \quad (3.20)$$

The initial condition necessary to completely define eq. (3.20) throughout the pellet, which is a non - linear ordinary differential equation is:

$$\text{at } t=0 \quad r_{cBk} = r_{oBk} \quad 0 \leq R \leq R_p \quad (3.21)$$

where r_{oBk} is the initial radius of reactant grain B_k .

3.2.2 Energy Balance Equations

The generalized heat balance for the pellet may be written as:

$$C_p^e \frac{\partial T}{\partial t} = \nabla \cdot k^e \nabla T - \sum_j^{N_g} (N_{Aj} C_{p,N}) \nabla T - \sum_i^{N_r} (Ar)_i a_{ij} \times f_i(\vec{A}) \times \Delta H_i \quad (3.22)$$

where

C_p^e = effective heat capacity

k^e = effective thermal conductivity

ΔH_i = heat of reaction i

In equation (3.22), the left hand side shows the accumulation term; the first term in the right hand side represents heat transfer by conduction (the effective thermal conductivity k^e is considered to vary with position); the

second term accounts for the heat transfer by convection over the entire gaseous species and the last term is the heat of reaction(s). It should be noted that, because of the multireaction consideration, allowances are made to incorporate the heat contributions from all the reactions in the system. The limiting case is a one reaction scenario.

The heat transport from the surrounding to the outer surface is considered to be described by convection and radiation in addition to the conduction term. The effect of radiation becomes pronounced especially at elevated temperatures. The initial and boundary conditions are, therefore:

$$\text{at } t=0 \quad T = T_b \quad 0 \leq R \leq R_p \quad (3.23)$$

$$\text{at } R=0 \quad \nabla T = 0 \quad (\text{symmetry at pellet center}) \quad (3.24)$$

$$\text{at } R=R_p \quad -k^e \nabla T = h_c (T_N - T_b) + \sigma \theta (T_N^4 - T_b^4) \quad (3.25)$$

3.2.3 Thermophysical and Transport Parameters

3.2.3.1 Thermophysical Parameters

The thermophysical parameters that appear in the energy balance equation are approximated by the following equations (Sotirchos and Amundson, 1984):

$$k^e = (1 - \varepsilon)^2 k_s + \varepsilon^2 k_m \quad (3.26)$$

$$C_p^e = (1 - \varepsilon) \rho_s C_{p_s} + \varepsilon C_i C_{p_g} \quad (3.27)$$

The heat of reaction can also be written as:

$$-\Delta H_i = \Delta H_i^r - \sum_j \nu_{Aj} C_{P,Aj} (T - T^r), \quad \text{for reaction } i \quad (3.28)$$

Equations (3.26) and (3.27) are modified for the multicomponent scheme as follows:

$$k^e = \sum_k y_{Bk} (1 - \varepsilon)^2 k_{Bk} + \varepsilon^2 k_m \quad (3.29)$$

$$C_p^e = \sum_k y_{Bk} (1 - \varepsilon) \rho_{Bk} C_{P,Bk} + \varepsilon C_i C_{Pg} \quad (3.30)$$

where k^e is the effective thermal conductivity of the gas permeated solid; C_p^e is the effective heat capacity of the porous solid per unit particle volume. y_{Bk} is the weight fraction of solid B_k . The thermal conductivity of a gas mixture k_m is not usually a linear function of mole fraction. The Wassiljewa equation, often used for low pressure, non - polar gas mixtures is (Reid et al., 1987):

$$k_m = \sum_i \frac{x_i k_i}{\sum_i x_i A_{ij}} \quad (3.31)$$

$$A_{ij} = \frac{[1 + (\mu_i / \mu_j)^{1/2} (M_j / M_i)^{1/4}]^2}{[8(1 + M_i / M_j)]^{1/2}} \quad (3.32)$$

with $A_{ii} = 1.0$. k_i and μ_i are the thermal conductivity and viscosity of pure component i .

The average specific heat capacity of the gas mixture is obtained as follows:

$$C_{Pg} = \sum_i x_i C_{Pi} \quad (3.33)$$

The heat capacity is considered to be a temperature dependent polynomial function as follows (Reid et al., 1987):

$$C_{Pi} = A + BT + CT^2 + DT^3 \quad (3.34)$$

The coefficients A, B, C, and D are constants to calculate the isobaric heat capacity of the ideal gas, with C_p in $J/(mol.K)$ and T in Kelvins.

3.2.3.2 Flux and Transport Equations

The "dusty gas" flux relations for a multicomponent mixture comprising of the total diffusive and viscous components, neglecting thermal and gravitational effects, is developed. For component i in a mixture of j diffusing species, this can be written as (Jackson, 1977):

$$\frac{N_i}{D_{i,k}^e} + \sum_{\substack{j=1 \\ j \neq i}}^{N_g} \frac{x_i N_j - x_j N_i}{D_{ij}^e} = -\frac{P}{R_g T} \nabla x_i - \frac{x_i}{R_g T} \left(1 + \frac{B_o P}{\mu_m D_{i,k}^e} \right) \nabla P, \quad i=1, \dots, N_g \quad (3.35)$$

In equation (3.35), the last term in the right hand side represents the viscous flow term which accounts for the slip flow that is caused by pressure variations. It may be noted that, the DGM describes the composition of the gas in the pores by a smooth function of position in the medium, but cannot

describe the real pore geometry (i.e. "through" pores, with two open ends, and "dead end" pores with only one). As noted in Section 2.5, the DGM avoids this situation by dispersing the solid medium (see Figure 2.9a). However, this situation is not important as long as chemical reactions do not take place at the pore walls. With chemical reaction in porous systems, the influence of the "dead end" pores on the transport is substantial. In spite of these difficulties, the DGM provides the simplest and most effective method presently available for representing flow and diffusion throughout the intermediate region between the extremes of Knudsen streaming and bulk diffusion with viscous flow.

D_{ij}^e and $D_{i,k}^e$ are the effective binary and Knudsen diffusion coefficients. B_0 is a factor characteristic of the scale and geometry of the pore structure, known as the permeability of the medium. Jackson (1977) reported approximate relations for the parameters in equation (3.35):

$$D_{i,k}^e = P_1 \left(\frac{8R_g T}{\pi M_i} \right)^{1/2} \quad (3.36)$$

$$D_{ij}^e = P_0 D_{ij} \quad (3.37)$$

$$B_0 = \frac{d_p^2}{8} \quad (3.38)$$

$$P_1 = \frac{2\epsilon d_p}{3\tau} \quad (3.39)$$

$$P_0 = \frac{\epsilon}{\tau} \quad (3.40)$$

where P_1 is a constant characteristic of the scale and geometry of the porous medium and P_0 is a factor determined by the geometry of the pore structure only. ε is the porosity and τ , the tortuosity factor, while d_p is the mean pore diameter, determined by approximating the interstices between the grains with a cubical shape. Therefore, for a closely packed spherical grains, d_p can be expressed as:

$$d_p^3 = \sum_k y_{Bk} \left[(2r_{Obk})^3 - \frac{4}{3} \pi r_{gbk}^3 \right] \quad (3.41)$$

where y_{Bk} is the weight fraction of grain B_k .

The binary diffusivity D_{ij}^e , is determined from the Chapman Enskog kinetic theory (Bird et al., 1960) as:

$$D_{ij} = 1.858 \times 10^{-3} \frac{\left[T^3 \left(\frac{1}{M_i} + \frac{1}{M_j} \right) \right]^{1/2}}{\rho \sigma_{ij}^2 \omega_{ij}}, \text{ cm}^2 / \text{ s} \quad (3.42)$$

where σ_{ij} is a constant in the Leonard - Jones 12-6 potential function and ω_{ij} is the collision integral as a function of kT / ε_{ij} . These may be calculated from:

$$\sigma_{ij} = 0.5(\sigma_i + \sigma_j) \quad (3.43)$$

$$\frac{\varepsilon_{ij}}{k} = \left(\frac{\varepsilon_i}{k} \cdot \frac{\varepsilon_j}{k} \right)^{1/2} \quad (3.44)$$

In a multicomponent system, the dynamic viscosity μ_m which appears in the flux equation [eq. (3.35)] will have a compositional dependence. One

semi-empirical formula usually adopted for non polar gas mixtures is the Wilkes approximation (Reid et al., 1987):

$$\mu_m = \frac{\sum_i x_i \mu_i}{\sum_i x_i \Phi_{ij}} \quad (3.45)$$

where

$$\Phi_{ij} = \frac{[1 + (\mu_i/\mu_j)^{1/2} (M_j/M_i)^{1/4}]^2}{[8(1 + M_i/M_j)]^{1/2}} \quad (3.46)$$

The viscosity of the individual gas components and the bulk gas stream are determined via the method of Thodos (Reid and Sherwood, 1977):

$$\mu\alpha = 4.61T_r^{0.618} - 2.04 \exp(-0.449T_r) + 1.94 \exp(-4.058T_r) + 0.1 \quad (3.47)$$

where

$$\alpha = T_C^{1/6} M^{-1/2} P_C^{-2/3} \quad (3.48)$$

The viscosity μ is in micro poise, T_C ($^{\circ}\text{C}$) and P_C (atm) are the critical properties of the gas stream and M is the molecular weight.

3.2.4 Structural Changes and Conversion

3.2.4.1 Structural Changes due to Reaction

In the grain model, it is considered that the radius of the pellet changes as the reaction progresses due to differences in the molal volume of the

products and reactants. The change in radius can be expressed by a mass balance on the product layer:

$$\sum_{b_{ik} < 0} \frac{1}{b_{ik}} (\text{moles of solid products formed}) = \sum_{b_{ik} > 0} \frac{1}{b_{ik}} (\text{moles of solid reactants reacted})$$

Negative b_{ik} represents products. For spherical grains B_k , this becomes

$$\frac{4}{3} \pi (r_{gt}^3 - r_{Ckt}^3) = Z_V \frac{4}{3} \pi (r_{Okt}^3 - r_{Ckt}^3) \quad (3.49)$$

or

$$r_{gt} = [r_{Ckt}^3 + Z_V (r_{Okt}^3 - r_{Ckt}^3)]^{1/3} \quad (3.50)$$

where r_{gt} is the grain size at time t , r_{Okt} is the initial grain size and Z_V is the ratio of the molal volume of the product to the reactant, defined as:

$$Z_V = \text{volume of product} / \text{volume of reactant}$$

i.e.

$$Z_V = \frac{\sum_k \frac{b_{ik} M_{Bk}}{\rho_{Bk} (1 - \varepsilon_{Bk})}}{\sum_k \frac{b_{ik} M_{Bk}}{\rho_{Bk}}} \quad (3.51)$$

where ε_{Bk} is the porosity of the product layer, assumed constant. The parameter Z_V determines the changes in particle (grain) dimension. If $Z_V > 1$, swelling occurs; for $Z_V = 1$, there is no change in particle size as reaction progresses and if $Z_V < 1$, the particle shrinks during reaction.

The porosity changes in the pellet can be related to changes in particle size by the following equation:

$$\frac{1-\varepsilon}{1-\varepsilon_0} = \sum_k n_{Bk} \frac{r_{gBk}}{r_{OBk}} (1 + \beta x_{Bk}) \quad (3.52)$$

or

$$\varepsilon = 1 - (1 - \varepsilon_0) \sum_k n_{Bk} \frac{r_{gBk}}{r_{OBk}} (1 + \beta x_{Bk}) \quad (3.53)$$

where β is the swelling / shrinkage factor and x_{Bk} is the local conversion of solid grain B_k . The pellet shrinkage or swelling considered to occur with the reduction or expansion of pore volume at any time, is evaluated from the following equation:

$$V_j = V_{0,j} \sum_k n_{Bk} (1 + \beta x_{Bk,j}) \quad (3.54)$$

where $V_{0,j}$ is the initial pore volume of the j th cell for a pellet of $(n-1)$ elements, n being the number of grid points.

3.2.4.2 Local Conversion

The local conversion of individual solid reactants, considered to be varying both temporally and spatially in the pellet is evaluated as a function of the volume change as follows (for a spherical grain):

$$x_{Bk}(R, t) = \frac{\frac{4}{3} \pi r_{OBk}^3 - \frac{4}{3} \pi r_{CBk}^3}{\frac{4}{3} \pi r_{OBk}^3} \quad (3.55)$$

or more generally

$$x_{Bk}(R, t) = 1 - \left[\frac{r_{CBk}}{r_{OBk}} \right]^{Fg} \quad (3.56)$$

where F_g is the grain shape factor. $F_g = 1, 2,$ or 3 stand for disk, cylindrical or spherical grains respectively.

3.2.4.3 Global Conversion for Solid B_k

Experimentally, the overall conversion is determined from the analysis of the weight change of the pellet. The model analogue is obtained by integrating the individual local conversion (for solid species B_k) over the entire pellet as following:

$$GX_{B_k}(t) = \frac{\int_0^{R_p} R^{F_p-1} x_{B_k}(R,t) dR}{\int_0^{R_p} R^{F_p-1} dR} \quad (3.57)$$

where F_p is the pellet shape factor. $F_p = 1, 2$ or 3 stand for disk, cylindrical or spherical pellets respectively.

3.2.4.4 Overall Pellet Conversion

The cumulative (overall) pellet conversion is found from the ratio of pellet weight loss at time t , to the total possible pellet weight loss:

$$GXT(t) = \frac{\text{(Pellet weight loss at time } t\text{)}}{\text{(Total possible pellet weight loss)}} \quad (3.58)$$

3.2.5 Heat and Mass Transfer Equations

The empirical relationships for heat and mass transfer were manipulated by Chilton and Colburn (1934) to obtain an analogy between these processes in terms of quantities designated as j factors. Several workers utilized this concept and presented a myriad of correlations for evaluating the transfer coefficients. Rowe and Claxton (1965) proposed the following correlation for flow through spherical pellets:

$$Sh = 2.0 + 0.69 Re^{0.5} Sc^{0.33} \quad (3.59)$$

(for $20 \leq Re \leq 2000$, $0.7 \leq Sc \leq 1500$)

For flow perpendicular to cylinders:

$$Sh = [0.35 + 0.34 Re^{0.5} + 0.15 Re^{0.58}] Sc^{0.33} \quad (3.60)$$

(for $0.1 \leq Re \leq 10^5$, $0.7 \leq Sc \leq 1500$)

For flow parallel to flat plates (Treybal, 1980):

$$Sh = 0.664 Re^{0.5} Sc^{0.33} \quad (3.61)$$

(for $Re \leq 50000$, $0.7 \leq Sc \leq 1500$)

Employing the Colburn's analogy of heat and mass transfer (Skelland, 1985), the heat transfer equivalents can be obtained by replacing Sh and Sc by Nu and Pr respectively.

CHAPTER 4

NUMERICAL FORMULATION

The set of partial differential equations (PDE) resulting from the continuity and energy balance equations is a class of parabolic PDEs. Analytical solution to these coupled sets of non linear equations is by no means possible. The complexity of the model equations, therefore, requires that a numerical solution be developed. Thus, this chapter is devoted to the formulation of the numerical solution to the system considered using the finite difference technique. The discretization of the model equations is outlined in Section 4.1 and Section 4.2 presents the solution technique adopted.

4.1 Discretization of Model Equations

In using finite - difference technique to solve PDEs (with associated boundary and initial conditions), a network of grid points is first established throughout the region of interest (the pellet) occupied by the independent variables. Consider a grid system that divides the pellet radius R_p into N grid points at regularly spaced intervals, $dr = R_p / (N-1)$. For a variable u at grid pint i , u_i , the finite difference formulae for the first and second order derivatives are therefore produced below for completeness;

$$\frac{\partial u}{\partial r} = \frac{u_{i+1} - u_i}{dr} + O(dr) \quad (\text{forward}) \quad (4.1)$$

$$\frac{\partial u}{\partial r} = \frac{u_i - u_{i-1}}{dr} + O(dr) \quad \text{(backward)} \quad (4.2)$$

$$\frac{\partial u}{\partial r} = \frac{u_{i+1} - u_{i-1}}{2dr} + O[(dr)^2] \quad \text{(central)} \quad (4.3)$$

$$\frac{\partial^2 u}{\partial r^2} = \frac{u_{i-1} - 2u_i + u_{i+1}}{2dr} + O[(dr)^2] \quad \text{(central)} \quad (4.4)$$

Equations (4.1) - (4.4) are known as the forward, backward and central difference forms respectively.

The main step in the approach is the simultaneous solution to the principal model equations (3.8) and (3.22) along with their initial and boundary conditions. These equations completely describe the changes taking place in the pellet both temporally and spatially. As noted, the pellet geometry could be flat plate, cylindrical or spherical in shape. Consequently, the equations are discretized considering each of these configurations.

Equation (3.8) can be reproduced thus

$$\frac{\partial(\varepsilon C_{A_j})}{\partial t} = -\nabla N_{A_j} - \sum_i \alpha_{ij} (Ar)_i \times f_i(\vec{A}) \quad (3.8)$$

The first term is discretized through explicit scheme (forward difference) in time as follows:

$$\frac{\partial(\varepsilon C_{A_j})}{\partial t} = \frac{(\varepsilon C_{A_j})^{n+1} - (\varepsilon C_{A_j})^n}{dt} \quad (4.5)$$

where dt is the time step and n is the time level. The second term changes in

form with geometry and thus, the laplacian operation is expanded and discretized accordingly.

i) For a flat plate ($F_p = 1$):

$$\nabla N_{A_j} = \frac{\partial N_{A_j}}{\partial R} = \frac{(N_{A_j})_{i+1} - (N_{A_j})_i}{dr} \quad (4.6)$$

ii) For a cylinder ($F_p = 2$):

$$\nabla N_{A_j} = \frac{1}{R} \frac{\partial (RN_{A_j})}{\partial R} = \frac{1}{R_i} \frac{(RN_{A_j})_{i+1} - (RN_{A_j})_i}{dr} \quad i = 2, N \quad (4.7)$$

Eq. (4.7) is undefined at the pellet center $R = 0$, corresponding to grid point $i = 1$. L' Hospital rule is applied to overcome the discontinuity as follows:

$$\lim_{R \rightarrow 0} \frac{1}{R} \frac{\partial (RN_{A_j})}{\partial R} = \lim_{R \rightarrow 0} \left(\frac{\partial N_{A_j}}{\partial R} + \frac{N_{A_j}}{R} \right) = 2 \frac{\partial N_{A_j}}{\partial R} \quad (4.8)$$

Therefore at the pellet center,

$$\nabla N_{A_j} = 2 \frac{\partial N_{A_j}}{\partial R} = 2 \frac{(N_{A_j})_{i+1} - (N_{A_j})_i}{dr} \quad (4.9)$$

iii) For a sphere ($F_p = 3$):

$$\nabla N_{A_i} = \frac{1}{R^2} \frac{\partial(R^2 N_{A_i})}{\partial R} = \frac{1}{R_i^2} \frac{[(R^2 N_{A_i})_{i+1} - (R^2 N_{A_i})_i]}{dr} \quad i = 2, N \quad (4.10)$$

Applying L' Hospital rule at the pellet center yields:

$$\nabla N_{A_i} = 3 \frac{\partial N_{A_i}}{\partial R} = 3 \frac{(N_{A_i})_{i+1} - (N_{A_i})_i}{dr} \quad (4.11)$$

A generalized expression in terms of the pellet shape factor, F_p , can be written for all geometries as follows:

$$\nabla N_{A_i} = \frac{1}{R_i^{F_p-1}} \frac{(R_i + dr)^{F_p-1} (N_{A_i})_{i+1} - R_i^{F_p-1} (N_{A_i})_i}{dr} \quad i = 2, N \quad (4.12)$$

at the pellet center ($i=1$):

$$\nabla N_{A_i} = F_p \frac{(N_{A_i})_{i+1} - (N_{A_i})_i}{dr} \quad (4.13)$$

the energy equation, eq. (3.22), is reproduced below:

$$C_p^e \frac{\partial T}{\partial t} = \nabla \cdot k^e \nabla T - \sum_j^{Ng} (N_{A_j} C_{pA_j}) \nabla T - \sum_i^{Nr} (Ar)_i a_{ij} \times f_i(\vec{A}) \times \Delta H_i \quad (3.22)$$

The second term in eq. (3.22) changes with geometry also. Following similar procedure outlined above, the Laplacian is expanded and discretized for the three geometries as shown below:

$$\nabla \cdot k^e \nabla T = \frac{\partial^2}{\partial R^2} (k^e T) \quad (\text{flat plate}) \quad (4.14)$$

$$\nabla \cdot k^e \nabla T = \frac{\partial^2}{\partial R^2} (k^e T) + \frac{1}{R} \frac{\partial}{\partial R} (k^e T) \quad (\text{cylinder}) \quad (4.15)$$

$$\nabla \cdot k^e \nabla T = \frac{\partial^2}{\partial R^2} (k^e T) + \frac{2}{R} \frac{\partial}{\partial R} (k^e T) \quad (\text{sphere}) \quad (4.16)$$

General discretized expressions in term of the pellet shape factor F_p can be written as follows:

$$\nabla \cdot k^e \nabla T = k_{i+1/2}^e \frac{T_{i+1} - T_i}{(dr)^2} - k_{i-1/2}^e \frac{T_i - T_{i-1}}{(dr)^2} + \frac{F_p - 1}{R_i} \frac{(k^e T)_{i+1} - (k^e T)_i}{dr} \quad (4.17)$$

and at the pellet center ($i=1$):

$$\nabla \cdot k^e \nabla T = F_p \left[k_{i+1/2}^e \frac{T_{i+1} - T_i}{(dr)^2} - k_{i-1/2}^e \frac{T_i - T_{i-1}}{(dr)^2} \right] \quad (4.18)$$

A summary of the discretized flux term ∇N_{A_j} and the conduction term $\nabla \cdot k^e \nabla T$ is given in Table 4.1 for all the geometries considered. The final forms of representative discretized continuity and energy balance equations, casted in residual form are shown below for a cylindrical pellet:

$$\frac{(\varepsilon C_{A_j})^{n+1} - (\varepsilon C_{A_j})^n}{dt} + \frac{1}{R_i} \frac{(RN_{A_j})_{i+1} - (RN_{A_j})_i}{dr} + \sum_i (Ar)_{ij} a_{ij} f_i(\vec{A}) = 0 \quad (4.19)$$

Table 4.1 Discretization of Flux and Thermal Diffusion terms in the Continuity and Energy Balance Equations
 {flat plate ($F_p = 1$); cylinder ($F_p = 2$); sphere ($F_p = 3$)}.

Position in pellet	Flux Term (∇N_A)	Thermal Diffusion Term ($\nabla \cdot k^e \nabla T$)
$i = 1$ (at pellet center)	$\nabla N_A = F_p \frac{(N_A)_{i+1} - (N_A)_i}{dr}$	$\nabla \cdot k^e \nabla T = F_p \left[k_{i+1/2}^e \frac{T_{i+1} - T_i}{(dr)^2} - k_{i-1/2}^e \frac{T_i - T_{i-1}}{(dr)^2} \right]$
$i = 2, N$	$\nabla N_A = \frac{1}{R_i^{F_p-1}} \frac{(R_i + dr)^{F_p-1} (N_A)_{i+1} - R_i^{F_p-1} (N_A)_i}{dr}$	$\nabla \cdot k^e \nabla T = k_{i+1/2}^e \frac{T_{i+1} - T_i}{(dr)^2} - k_{i-1/2}^e \frac{T_i - T_{i-1}}{(dr)^2} + \frac{F_p - 1}{R_i} \frac{(k^e T)_{i+1} - (k^e T)_i}{dr}$

$$\begin{aligned}
 C_{pi}^e \frac{T^{n+1} - T^n}{dt} = & k_{i+1/2}^e \frac{T_{i+1} - T_i}{(dr)^2} - k_{i-1/2}^e \frac{T_i - T_{i-1}}{(dr)^2} + \frac{1}{R_i} \frac{(k^e T)_{i+1} - (k^e T)_i}{dr} \\
 & + \sum_j (N_{Aj} C_{PN}) \frac{(T_{i+1} - T_i)}{2dr} + \sum_i (Ar)_i a_{ij} f_i(\vec{A}) \Delta H_i \quad (4.20)
 \end{aligned}$$

Equations (4.19) and (4.20) constitute a coupled set of $(N_g + 1)$ non - linear equations. N_g is the number of gaseous components A_j and 1 stands for the energy equation. The unknowns are respectively, C_{Aj} , $j = 1, N_g$ and T and these variables are unknown at N nodes.

The flux expression, eq. (3.35), can be written in an explicit form for a gaseous component i as:

$$N_i = \frac{-\frac{P}{RT} \nabla x_i - \frac{x_i}{RT} \left(1 + \frac{B_{OP}}{\mu_m D_{i,k}^e}\right) \nabla P + x_i \sum_{\substack{j=1 \\ j \neq i}}^{N_g} \frac{N_j}{D_{ij}^e}}{\frac{1}{D_{i,k}^e} + \sum_{\substack{j=1 \\ j \neq i}}^{N_g} \frac{x_j}{D_{ij}^e}}, \quad i=1, \dots, N_g \quad (4.21)$$

The differential terms, ∇x_i and ∇P in equation (4.21) are discretized using implicit first order finite difference scheme at grid point i as follows:

$$\nabla x_i = \frac{x_i - x_{i-1}}{dr} \quad (4.22)$$

$$\nabla P_i = \frac{P_i - P_{i-1}}{dr} \quad (4.23)$$

4.2 Solution Technique

Solution to the discretized sets of equations is attained via Newton - Raphson iterative technique for non linear systems with second order convergence. In the formulation leading to the solution via Newton's method, the following approach is adopted. Consider first an approximation of the solution vector

$$\vec{X} = [X(1), X(2), \dots, X(N), X(N+1), \dots, X(2N), \dots, X(N_g \times N + 1), X(N_g \times N + 2), \dots, X(NN)]^T \quad (4.24)$$

which is needed in the residuals of the principal model equations

$$\vec{F} = [F(1), F(2), \dots, F(N), F(N+1), \dots, F(2N), \dots, F(N_g \times N + 1), F(N_g \times N + 2), \dots, F(NN)]^T \quad (4.25)$$

where $NN = (N_g + 1) \times N$; N is the number of grid points; $X(i)$ and $F(i)$ are the solution value and residual of model equation at grid i .

$X(1) \rightarrow X(N_g \times N)$ represents the concentration of all N_g gaseous components ($C_{Aj}, j = 1, N_g$) at all grid points

$X(N_g \times N + 1) \rightarrow X(NN)$ represents the temperature T at all grids.

Define

$$\vec{X}^{k+1} = \vec{X}^k + \vec{\delta}^k \quad (4.26)$$

where \vec{X}^{k+1} and \vec{X}^k are the current and previous solution vectors and $\vec{\delta}^k$ is the correction (increment) vector for the following set of simultaneous linear equations

$$\underline{J}(\vec{X}^k)\vec{\delta}^k = -\vec{F}^k \tag{4.27}$$

The Jacobian matrix \underline{J} may be represented as

$$\underline{J} = \begin{bmatrix} \frac{\partial F(1)}{\partial X(1)} & \dots & \frac{\partial F(1)}{\partial X(i)} & \dots & \dots & \frac{\partial F(1)}{\partial X(NN)} \\ \vdots & & & & & \\ \frac{\partial F(i)}{\partial X(1)} & & & & & \frac{\partial F(i)}{\partial X(NN)} \\ \vdots & & & & & \\ \frac{\partial F(NN)}{\partial X(1)} & & & & & \frac{\partial F(NN)}{\partial X(NN)} \end{bmatrix} \tag{4.28}$$

The increment vector $\vec{\delta}^k$ is expressed as:

$$\vec{\delta}^k = [\delta(1), \delta(2), \dots, \delta(NN)]^T \tag{4.29}$$

The Jacobian is an $NN \times NN$ matrix. Using the theory of augmenting, the augmented matrix [$NN \times (NN+1)$] can be written as:

$$\underline{A} = \left| \underline{J}; -\vec{F}(\vec{X}^k) \right| \quad (4.30)$$

In seeking a solution to the sets of linear equations (4.27) with augmented matrix of coefficients, the Gauss - Jordan complete elimination method is employed with the maximum pivot strategy (Carnahan et al., 1969).

A number of subprograms are developed to execute the different aspects of the problem leading to a complete solution. A detailed flowchart of the numerical algorithm is given in Figure 4.1. A summarized description of the algorithm follows: The relevant data are read in. The grid structure is then set up and time is advanced by one step. The reaction rates are then calculated and the new reaction front radii in the solids are determined (if reacting) by solving the equations governing the movement of the reaction front [eq. (3.20)] with time, employing a Runge - Kutta method of order four. The overall conversion of the solid species is determined from the integral technique and the net pellet conversion is obtained from the pellet weight and overall conversions. The fluxes of the individual gaseous components described by eq. (4.21) are evaluated following Gauss - Seidel iterative technique. The fluxes are first initialized using linear approximation and subsequently updated through the iterative procedure. The right hand side vector, residuals, of the principal model equations [eqs. (4.19) and (4.20)] are evaluated. If the residuals are greater than a tolerance value, concentrations of all components and temperature are solved for via Newton - Raphson technique after setting up the Jacobians (as described earlier). If the conversion is not complete, or the time is less than the maximum reaction time, all the structural, thermophysical and transport parameters (ε , d_p , r_{gb} , μ , k^e , C_p^e , ΔH_i) are updated based on the new reaction front radii and the whole process is repeated for the new time.

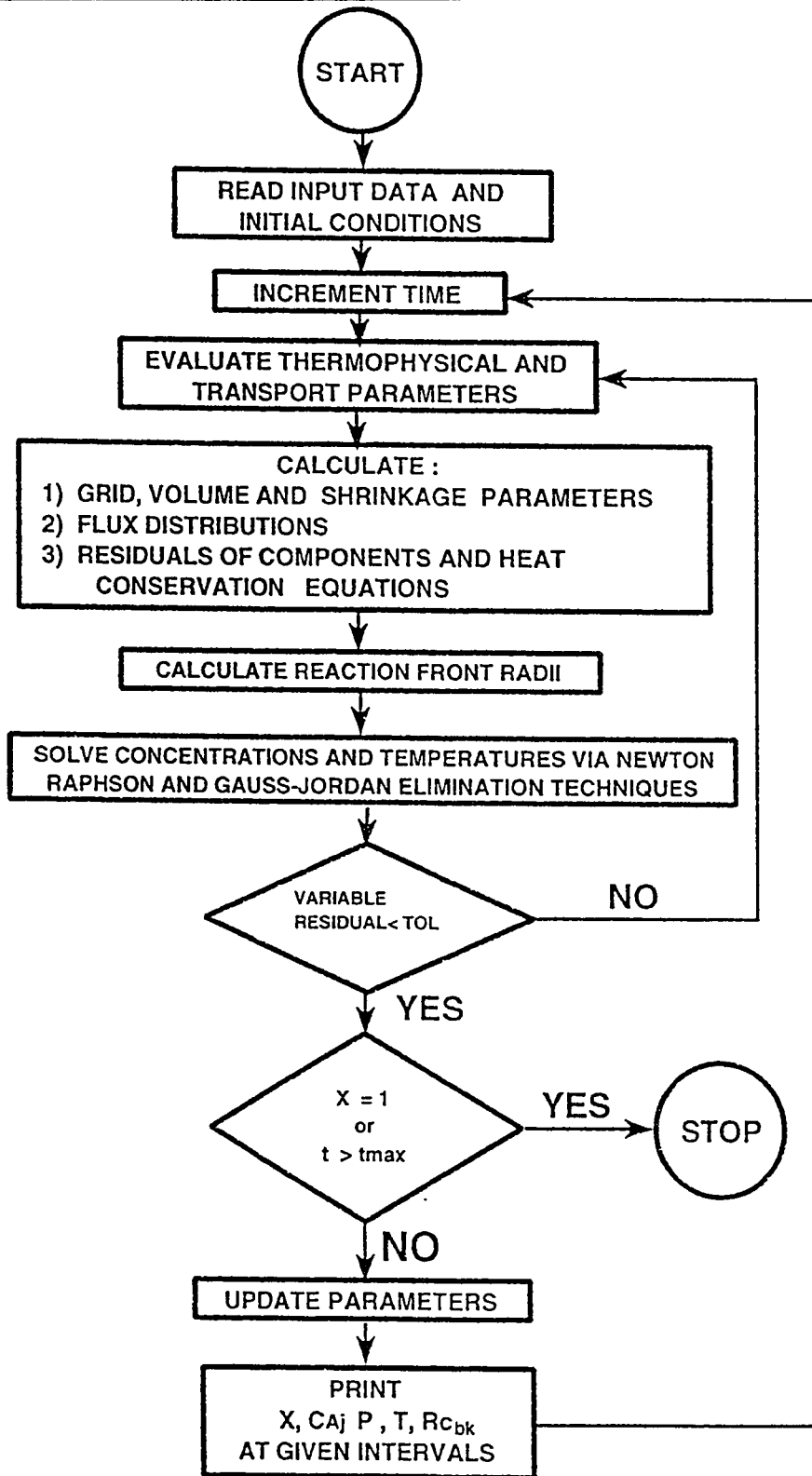


Figure 4.1. Numerical Solution Algorithm

CHAPTER 5

BINARY SIMULATION : MODEL VALIDATION

5.1 Introduction

As it was noted from the overview of past modeling efforts presented in Chapter 2, any successful mathematical formulation has either to favorably compare with experimentally obtained data (if available) or with existing models or both. However, there is no experimental data reported as yet in the literature that resulted from a reaction of multiple solid species (in pellet form) in an atmosphere of multicomponent diffusing gases. Therefore, in seeking out validation of the present formulation, two asymptotic cases for which experimental data exist are considered.

- i) Carbon gasification reaction and
- ii) Nickel oxide / Hematite reduction.

Both of these scenarios involve only two gaseous components each, and thus, the tag "binary" simulation. It should be reiterated here that the multicomponent model developed is also reducible (applicable) to limiting cases of simple reactions and binary simulations.

In this chapter, the application of the multicomponent model in predicting conversion trends of the asymptotic cases considered is demonstrated. Section 5.2 explores the match between experiment and model at various bulk gas temperatures and important observation and conclusion relevant to understanding the simulation results of Chapter 6 is presented in Section 5.3.

5.2 Case Studies

5.2.1 Carbon Gasification Reaction

Carbon gasification reaction has been studied experimentally at various times for a wide range of temperatures, primarily because of its importance in a number of industrial processes. It is basically a single reaction scheme with two gaseous components and can be represented as:



The reaction follows Langmuir - Hinshelwood kinetics and the rate expression is:

$$Rate = \frac{k_1 P_{CO_2}}{1 + k_2 P_{CO} + k_3 P_{CO_2}} \quad (5.2)$$

where k_2 and k_3 have the following values (Wu, 1949):

$$k_2 = 3.26 \times 10^{-11} \exp\left\{\frac{253,000}{R_g T}\right\} \quad kPa^{-1} \quad (5.3)$$

$$k_3 = 1.74 \times 10^{-3} \exp\left\{\frac{27,700}{R_g T}\right\} \quad kPa^{-1} \quad (5.4)$$

The kinetic rate constant k_1 , considered as an Arrhenius type function of temperature, is not known a priori. In a modelling exercise reported by Hastaoglu and Hassam (1988), the pre-exponential factor and the activation energy in the expression for k_1 were backed out by matching model

predictions with experimental data. The complete expression for k_1 reported is:

$$k_1 = 10.8 \exp\left\{\frac{-219,000}{R_g T}\right\} \frac{\text{mol}}{\text{kPa m}^2 \text{s}} \quad (5.5)$$

The experiments were conducted on disk shaped pellets formed from spherical carbon powder (grains) at atmospheric pressure over a temperature range of 800 - 1100°C. The complete experimental data is summarized in Table 5.1. Table 5.2 presents the additional data used in the modelling exercise in matching the experimentally obtained results (Hassam and Hastaoglu, 1988). The set - up used in conducting the experiment is shown in Figure 5.1. This figure is included to give a physical insight into the nature of the experimental setting used in the study of gas - solid reactions generally.

The results of the modeling exercise are illustrated in Figure 5.2. It can be clearly seen that, within a small error bound, the match between experiment and model predictions is very satisfactory. Although the experiments were performed for temperature range of 800 - 1100°C, only data values for 900 - 1100°C were reported. This resulted from the consideration that, the concentration of gaseous components and temperature can be assumed to equal their respective bulk values with negligible error (Hastaoglu and Hassam, 1988). The match of the model with experiment is relatively weak at the lower temperature of 900°C (approximately 15 % error) for the conversion range covered, as is clearly presented in Table 5.3. At this temperature, the conversion attained is only about 5 % after 3 hours of reaction. This offers significant clue to the strong temperature dependence of carbon gasification reaction and the strong chemical reaction resistance. This

Table 5.1 Experimental data for carbon gasification reaction

Material	NS Carbon black of Cabot Corporation
Grain diameter (spherical), μm	0.0375
Surface area, m^2 / g	25
Pelletizing pressure, kPa	71,000
Half pellet thickness (R_p), mm	1.283 - 1.448
Initial porosity of pellet (ϵ_o)	0.665
Bulk gas stream flow rate, m^3 / s	8.33×10^{-5}
Bulk gas pressure, kPa	101.3
Bulk gas temperature, K	1073 - 1373

Table 5.2. Data used in the modelling work for carbon gasification reaction

Solid property	Value
Thermal conductivity (k_s), $W/m.K$	1.89
Specific heat (Cp_s), $kJ/kg K$	1.49
Emissivity (θ)	0.8
Product porosity (ε_p)	0.35
density (ρ_s), kg/m^3	1800
Molecular weight (M_s), $kg/kmol$	12

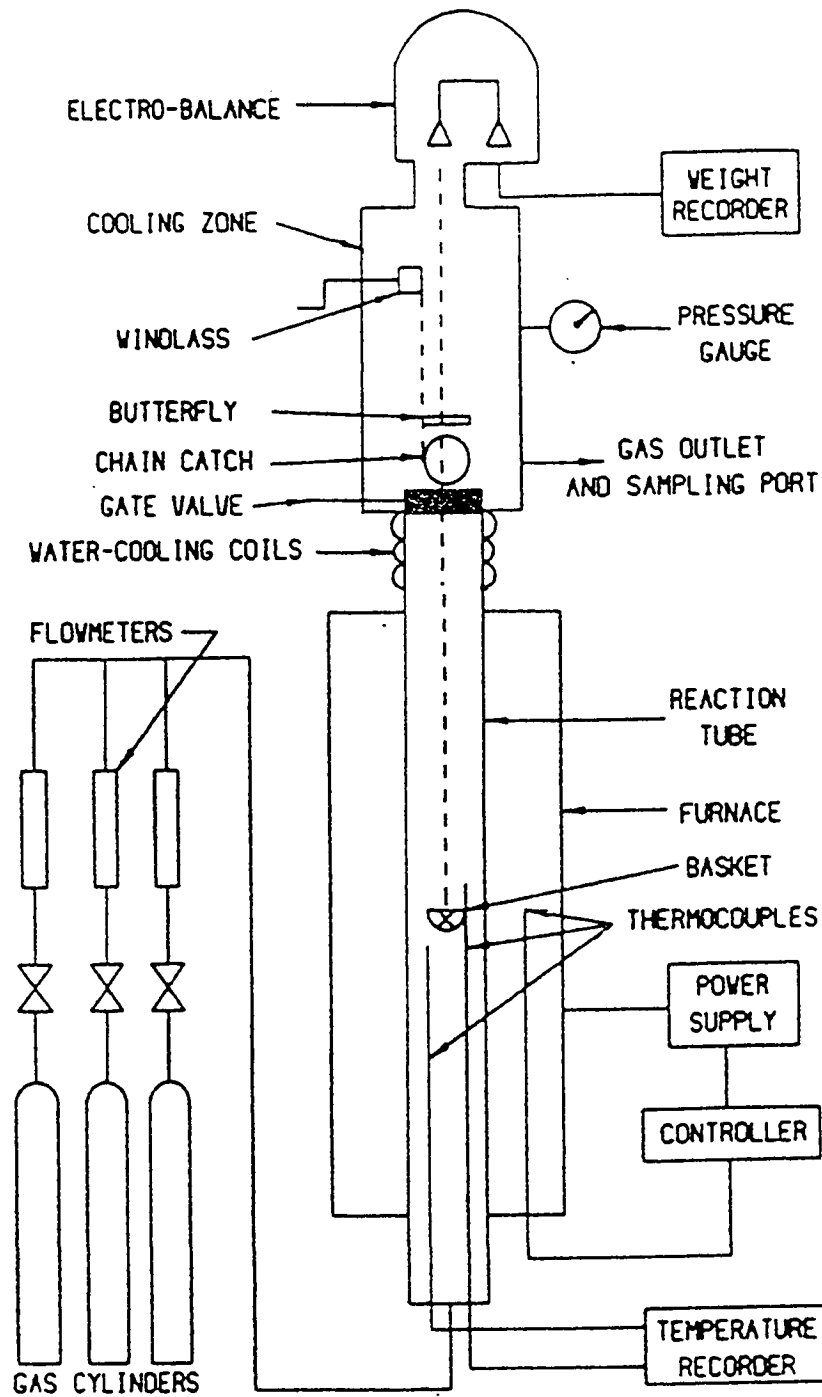


Figure 5.1. Schematic diagram of the TGA experimental set - up
(Hassam, M. S., 1988)

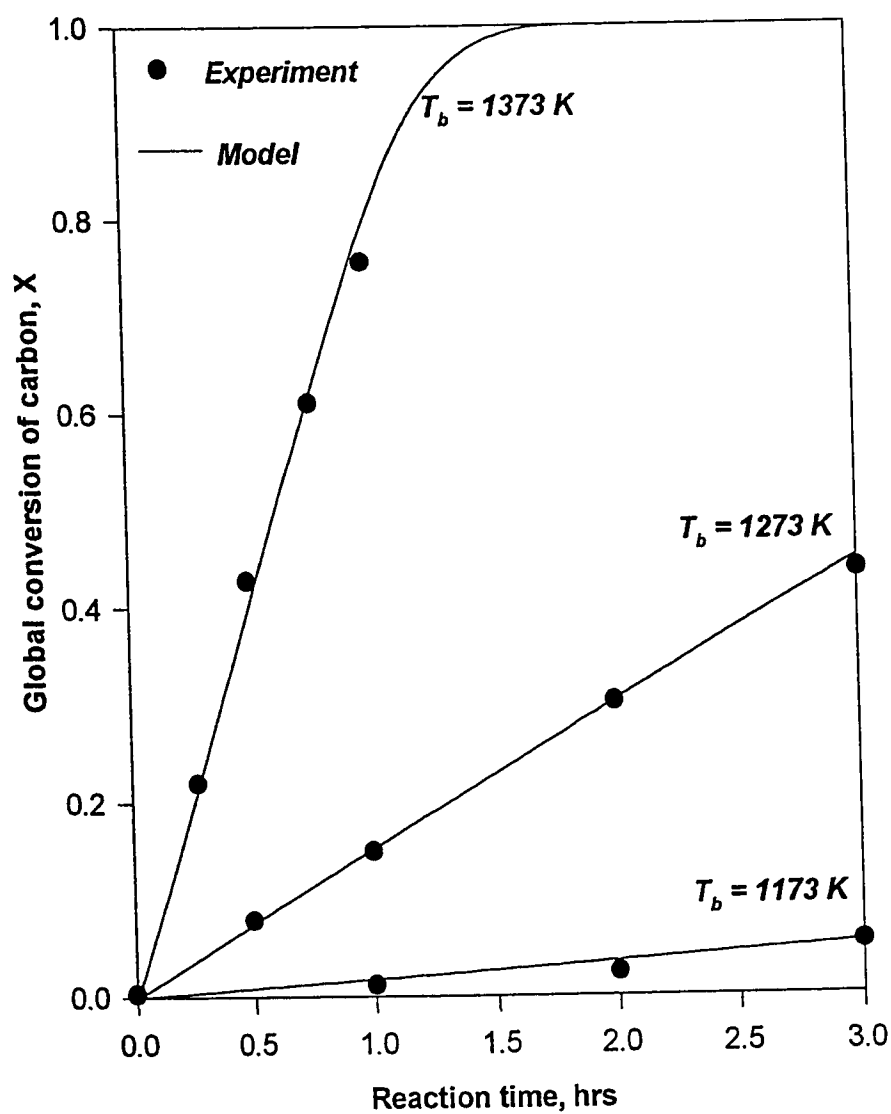


Figure 5.2. Comparison of transient model prediction with experimental data for carbon gasification reaction at various bulk gas temperatures

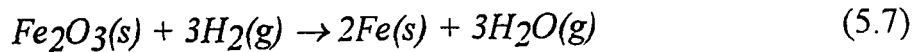
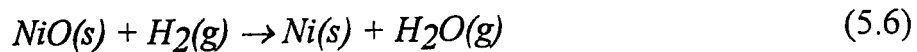
Table 5.3. Comparison between model and experimental values for carbon conversion at various bulk gas temperatures.

Solid Conversion			
Time (hr)	Experiment	Model	% Error
@ 900 °C			
0	0	0	0
1.0	0.00834	0.0101	- 21
2.0	0.02083	0.024	- 15.3
3.0	0.050	0.057	- 14
@ 1000 °C			
0	0	0	0
0.5	0.075	0.0749	0.13
1.0	0.1458	0.148	- 1.51
2.0	0.30	0.309	- 3.1
3.0	0.4333	0.4389	- 3.6
@ 1100 °C			
0	0	0	0
0.2727	0.2167	0.2169	- 0.09
0.50	0.425	0.409	3.7
0.7727	0.6083	0.6161	- 1.5
1.0	0.7542	0.78	3.4

also explains why heat and mass transfer limitations are considered negligible under the operating condition (900°C). At higher temperatures (1000 - 1100°C), the agreement between model and experiment is excellent (within 3 % error). This result clearly demonstrates the capability of the model in predicting conversion trends of single gas - solid reactions within acceptable error bound as is revealed from a further examination of Table 5.3.

5.2.2 Reduction of Nickel Oxide / Hematite Mixture

The reduction of nickel oxide / hematite mixture with hydrogen is of practical industrial importance, typically in the selective recovery of a more valuable metallic component from mixed ores (e.g., the recovery of nickel from lateritic ores) and the preparation of certain metal oxide catalysts among others. The experimental results and description of materials used that follow shortly are from Szekely and Hastaoglu (1976). The overall stoichiometry of the multiple reaction is represented as:



This is a system with "four solids" ($N_s = 4$) and "two gaseous" ($N_g = 2$) components described by "two reactions" ($N_r = 2$). It is worthwhile to note that, the experimental results for the simultaneous reactions describing the NiO / hematite reduction is one of the closest sets of data available for the multireaction, multicomponent scenario envisioned in evolving the model.

The reactions are assumed to follow first order kinetics and are essentially considered irreversible. Thus, the rates are:

$$Rate_1 = k_1 C_{H_2} \quad (5.8)$$

$$Rate_2 = k_2 C_{H_2} \quad (5.9)$$

In a manner similar to the one described under carbon gasification, the investigators modeled the system using a simplified pseudo - steady state approach to back out the kinetic parameters k_1 and k_2 . The approximate values of the parameters are:

$$k_1 = 1.0737 \times 10^{-10} \exp\left\{-\frac{12,780}{R_g T}\right\}, \quad m/s \quad (5.10)$$

$$k_2 = 1.956 \times 10^{-12} \exp\left\{-\frac{13,837}{R_g T}\right\}, \quad m/s \quad (5.11)$$

The experiments were carried out using a set - up similar to the one shown in Figure 5.1. A brief description of the experimental approach follows: Helium gas, used as the inert carrier, is first introduced into the system, such that only *He* gas was initially present in the pellet. The flow of *He* is stopped and *H₂*, the reactant gas, is introduced into the reaction zone maintained at the reaction temperature (581 - 608 K). It should be pointed out that all the experiments were carried out under atmospheric pressure. The complete data utilized in the experiments are presented in Table 5.4. The supplementary data used in the simulation work is given in Appendix A (Table A1).

Table 5.4 Experimental data for NiO / Fe₂O₃ reduction

Grains:		
	NiO	Fe ₂ O ₃
• Grain diameter, μm	0.18	0.2
• Grain shape, F_g	spherical, 3	spherical, 3
• Surface area, m^2 / g	5.32	5.65
Pellet:		
• Pelletizing pressure, kPa	272 - 1360	
• Half pellet thickness (R_p), mm	0.317 - 0.4448	
• Initial porosity of pellet (ϵ_o)	0.51	
Bulk gas stream properties:		
• Flow rate, m^3 / s	8.33×10^{-5}	
• pressure, kPa	101.3	
• Temperature, K	581 - 608	

The results of the present model studies are presented in Figures 5.3 and 5.4, corresponding to bulk temperatures of 581 and 608 K respectively. The match between model and experimental overall conversion is in general fairly good. However, as can be observed in Figure 5.4, at the early stages of the reaction (below two minutes of reaction time), there seems to be a sigmoidal behavior exhibited in the experimental results, which is not well represented by the model. The early mis-match may have possibly resulted from the catalytic effect of nickel on the reduction of hematite, although, the reduction of hematite is observed to be extremely slow under the operating conditions considered. A stronger explanation to the observed deviation could be in the reasonable insinuation that, there is still an "induction effect", whereby the reaction becomes fully developed only after an exposure time elapses. That period (in this case upto 2 minutes) can be considered as the induction period. Examination of Table 5.5 clearly indicates that, at the later stages of the reaction when most of the nickel oxide grains have reacted, the model prediction of the conversion trend improved tremendously (within approximately 2 % error). In addition to the overall conversion, Figure 5.4 also displays two solid lines, labeled, NiO and Fe₂O₃ respectively. These lines represent the individual solid conversion trends predicted by the present model. It is essential to note that, this model is capable of accounting for the conversion trends of individual grain types inside the overall solid matrix - the pellet. The conversion trends predicted for both NiO and Fe₂O₃ are consistent with the results of measurements reported from chemical analysis of the partially reacted solid specimen, represented by the square and triangular dots on Figure 5.4 for NiO and Fe₂O₃ respectively. For a complete picture of the partially reacted solid matrix, the reader is referred to

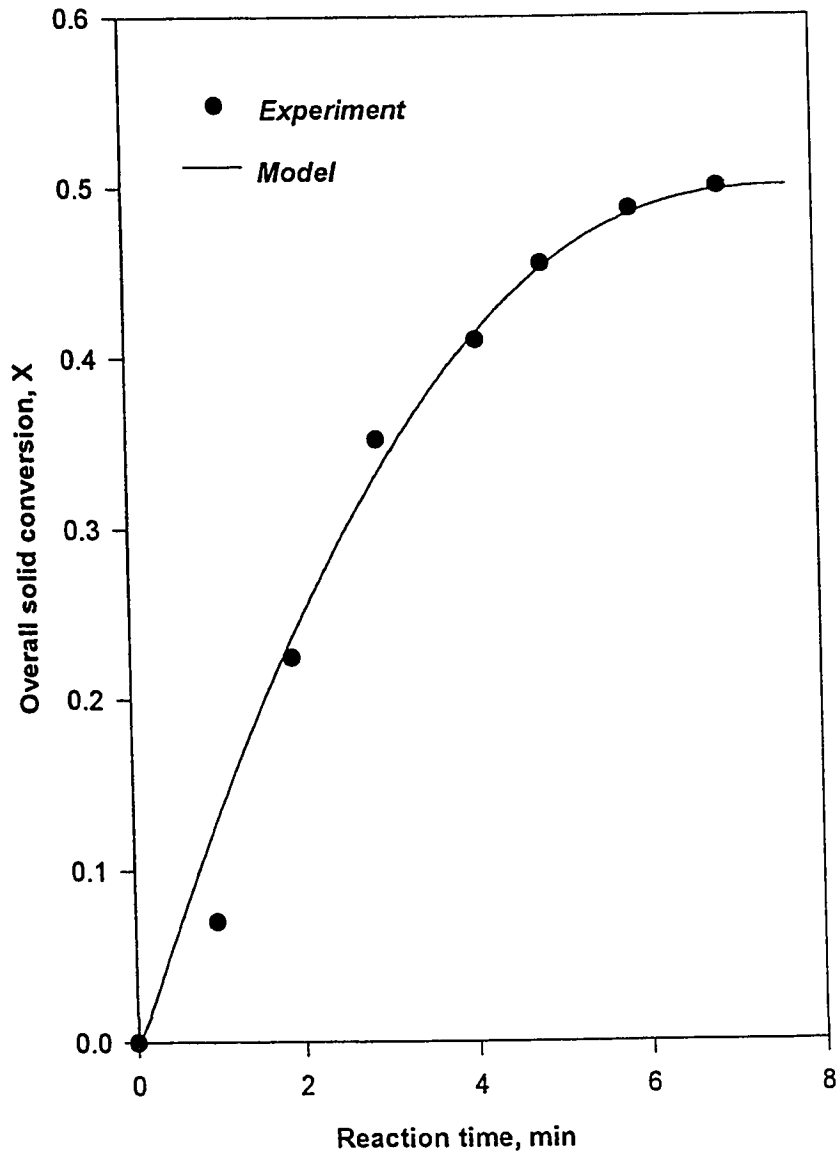


Figure 5.3 Comparison of transient model prediction with experimental data for Nickel Oxide / Hematite reduction at $T_b = 581$ K and $d_p = 8.9 \times 10^{-4}$ m for 50% NiO and 50 % Fe_2O_3 .

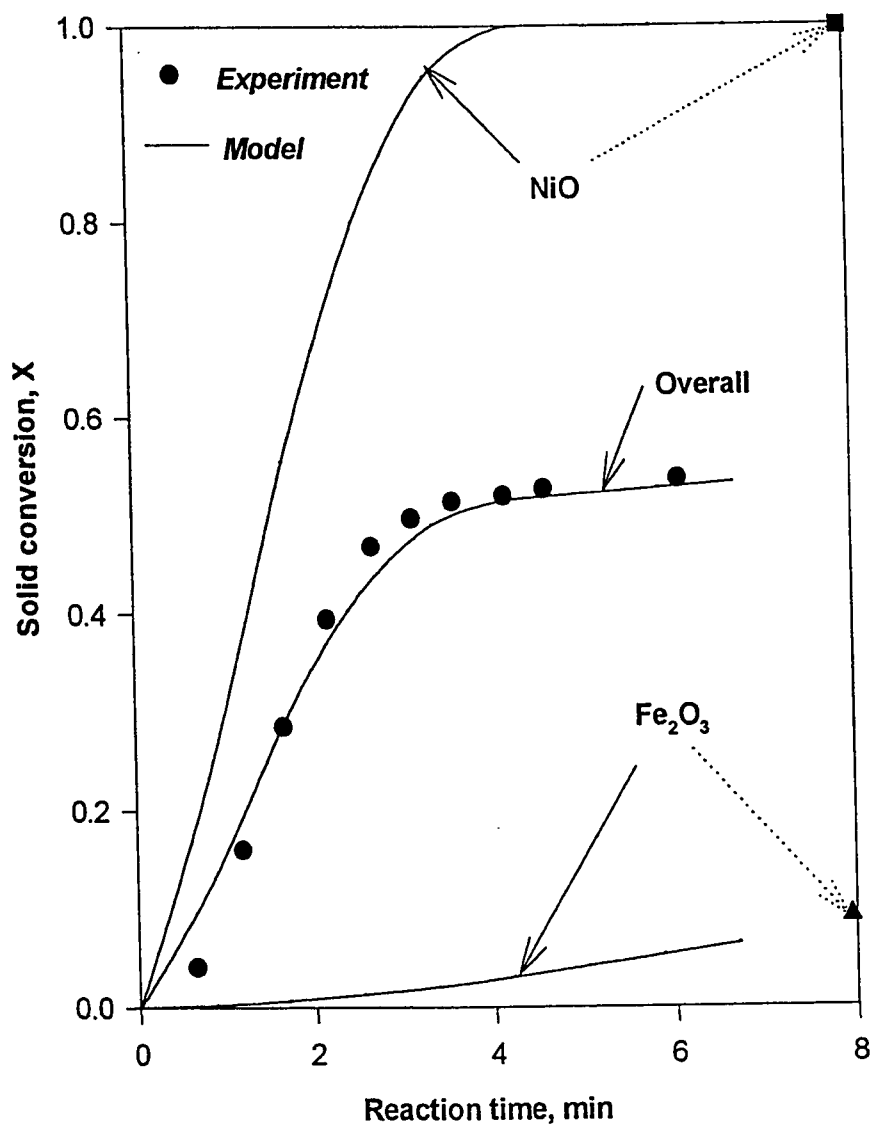


Figure 5.4 Comparison of transient model prediction with experimental data for Nickel Oxide / Hematite reduction at $T_b = 608$ K and $d_p = 8.9 \times 10^{-4}$ m for 50% NiO and 50% Fe_2O_3 .

Table 5.5. Comparison between model and experimental values for NiO / Fe₂O₃ mixture conversion at bulk gas temperatures of 581 and 608 K.

Overall Solid Conversion			
Time (min.)	Experiment	Model	% Error
@ 581 K			
0	0	0	0
1.923	0.2244	0.2361	5.2
2.9487	0.3525	0.3319	5.84
4.1025	0.41026	0.415	1.15
4.8718	0.45512	0.4538	0.29
5.8974	0.4872	0.4843	0.59
6.923	0.50	0.4985	0.4
@ 608 K			
0	0	0	0
1.0	0.16	0.17	6.25
1.4857	0.2857	0.264	7.6
2.0	0.3943	0.3528	10.5
2.971	0.4971	0.44	10.2
3.4286	0.51429	0.47	7.8
4.0	0.52	0.51	1.92
4.457	0.5271	0.525	0.4

Szekely and Hastaoglu (1976), in which a clearly sectioned, partially reacted specimen that initially consisted of nickel oxide / hematite mixture is presented.

5.3 Observation and Conclusion

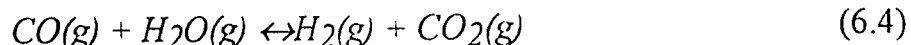
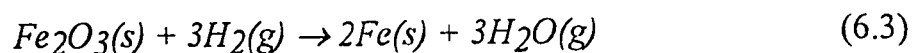
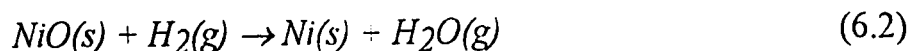
It has been clearly demonstrated in this chapter that, the present model is capable of predicting conversion - time trends in a number of gas - solid reactions, and particularly in the gasification of carbon and the reduction of nickel oxide / hematite mixture within allowable error bounds. It is however evident that, none of the results presented thus far incorporated the multicomponent consideration that constitute one of the cornerstones of this study. It should be re-emphasized that, there is not as yet any data in the literature that explicitly considers multicomponent diffusing environment, in which a number of solid species are reacting simultaneously via complex reaction pattern. It is therefore pertinent that, some results consistent with this conception is presented in this study and thus, Chapter 6 is fully devoted to exploring the effects of various parameters on the system behavior using one such scenario hypothesized.

CHAPTER 6

MULTICOMPONENT SIMULATION

6.1 Introduction

It was noted in the introduction to the thesis (Chapter 1), that most industrially important reactions not only follow complex reaction schemes, but are also accompanied by multicomponent diffusion mechanisms as a result of the active gaseous reactants and inerts. And such reactions are sometimes carried out with the solid matrix comprising different types of solid grains, some of which could be inert and some could play catalytic roles and some are reactants / products in the overall reaction. Using the case studies presented in Chapter 5 as a background and basis, a hypothetical scenario is envisioned in which four sequential reactions are considered to be taking place simultaneously. It should be noted that the general model will be applied to this specific scenario. These reactions are respectively, carbon gasification, reduction of nickel oxide / hematite mixture and a homogeneous reaction between CO and H₂O (water - gas - shift reaction). The reactions can be written as:



Except for the water - gas - shift reaction (hereafter referred to as "WGS reaction") represented by equation (6.4), equations (6.1) - (6.3) are actually reproduced from Chapter 5, where the detailed kinetics of both carbon gasification and NiO / Fe₂O₃ reduction are presented. The WGS reaction is mildly exothermic to the right and maximum conversion at equilibrium is attained at the lowest temperatures (Satterfield, 1991). The heat of reaction is approximately 40 kJ/mol at standard temperature (25 °C).

In modeling this system, three simplifying assumptions were made with respect to the WGS reaction: (i) The shift in the reaction is largely to the right over the temperature range considered and thus, the reverse reaction is considered negligible. (ii) The kinetics is described by a simple second order rate in CO and H₂O concentrations. (iii) The effect of solid - solid interactions on the WGS reaction is considered negligible. It is worthwhile to indicate that, introduction of this particular reaction in the overall scheme is partly because of the possibility of such reaction taking place inside the pellet considering the gaseous reactants and products of the heterogeneous reactions and in part by the desire to incorporate and study the effect of a homogeneous reaction in the grand structure.

In the following sections, various aspects of the scheme above are examined and discussed. Concentrations and temperature profiles in the pellet both temporally and spatially are critically discussed in Section 6.2. The effects of various bulk properties, inert solid and pellet porosity on the conversion of the solid matrix are presented in Section 6.3.

6.2 Concentration and Thermal Gradients Inside the Pellet

6.2.1 Diffusion and Reaction Effects

One of the strong features of this model is that, it accounts for the multicomponent diffusion mechanism prevalent in most practical reaction scenarios. The reaction scheme considered in this chapter [eqs. (6.1) - (6.3)] have two gaseous reactants (CO_2 and H_2) and two products (CO and H_2O). Initially, the pellet is completely purged with inert gas (N_2), thus, prior to the commencement of the reaction, no active gaseous reactant was present inside the pellet matrix. Therefore, in all, there are five gaseous components diffusing into and out of the pellet.

Figures 6.1 - 6.6 illustrate the radial concentration profiles in both dimension and dimensionless forms at the base case (bulk temperature, $T_b = 1173$ K; bulk pressure, $P_b = 101.3$ kPa and pellet half thickness, $R_p = 3.28 \times 10^{-4}$ m), corresponding to 1, 60, and 480 seconds of reaction times respectively. These figures are presented for the purpose of giving a qualitative picture of the profiles within the pellet at different times of the reaction. Figures 6.1 and 6.2 show the concentration profiles after one second of reaction. However, the time step, dt , initially 5×10^{-3} s, was being continuously increased with the progress of the reaction. Therefore, although the profiles in these figures (developed as they appear) correspond to only one second of reaction time, they actually resulted after about 50 iterations.

The concentration profiles through the pellet for all the three cases presented ($t = 1, 60, \text{ and } 480$ s) indicate that the reactions are influenced by both diffusion and kinetic resistances. Two extreme possibilities exist when both diffusion and chemical reaction take place simultaneously; (i) diffusion controlled; (ii) kinetic controlled. It needs to be mentioned here

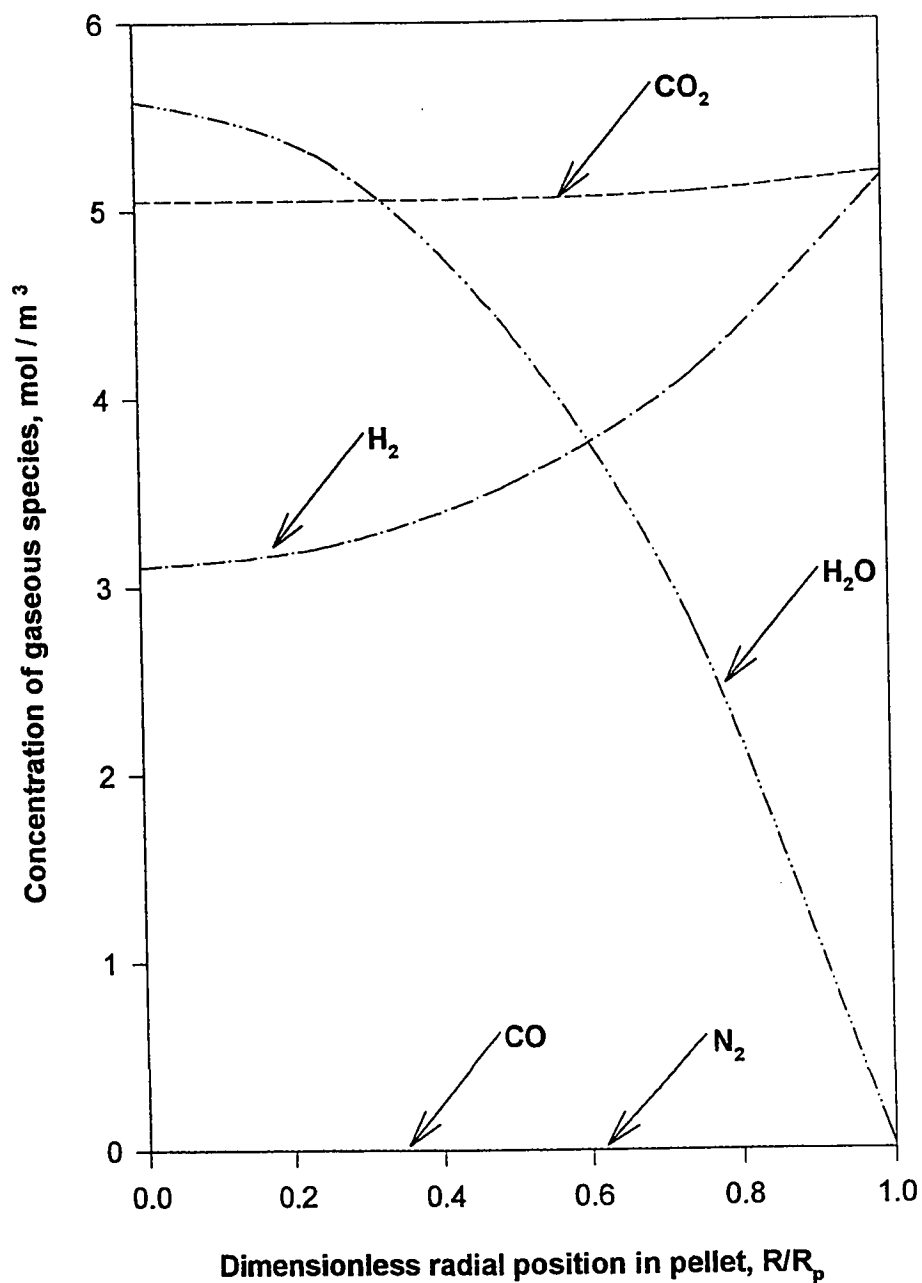


Figure 6.1. The radial concentration profile at: $t = 1$ s, $GXT = 1.95 \times 10^{-5}$,
 $T_b = 1173$ K, $P_b = 101.3$ kPa and $R_p = 3.28 \times 10^{-4}$ m.

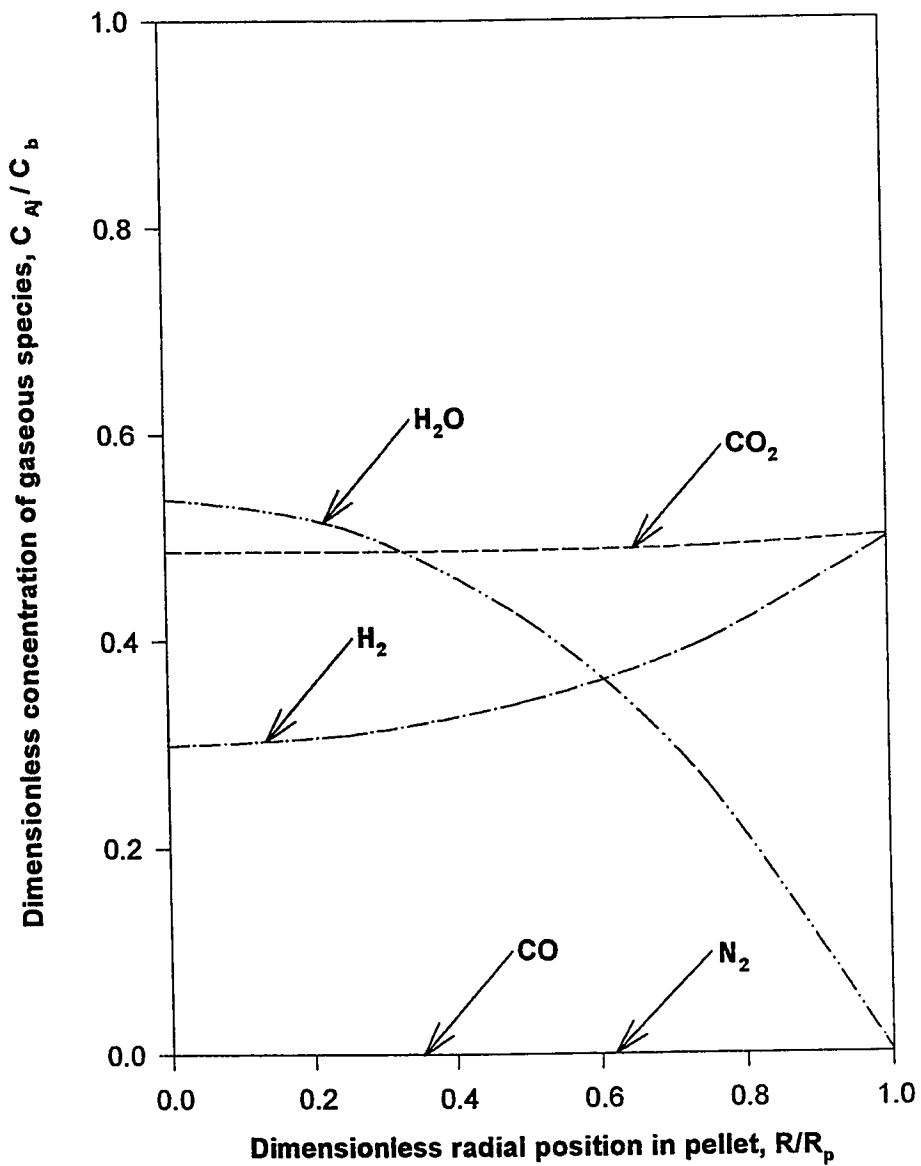


Figure 6.2. The radial concentration profile at: $t = 1$ s, $GXT = 1.95 \times 10^{-5}$, $T_b = 1173$ K, $P_b = 101.3$ kPa, $C_b = 1.04$ mol/m³ and $R_p = 3.28 \times 10^{-4}$ m.

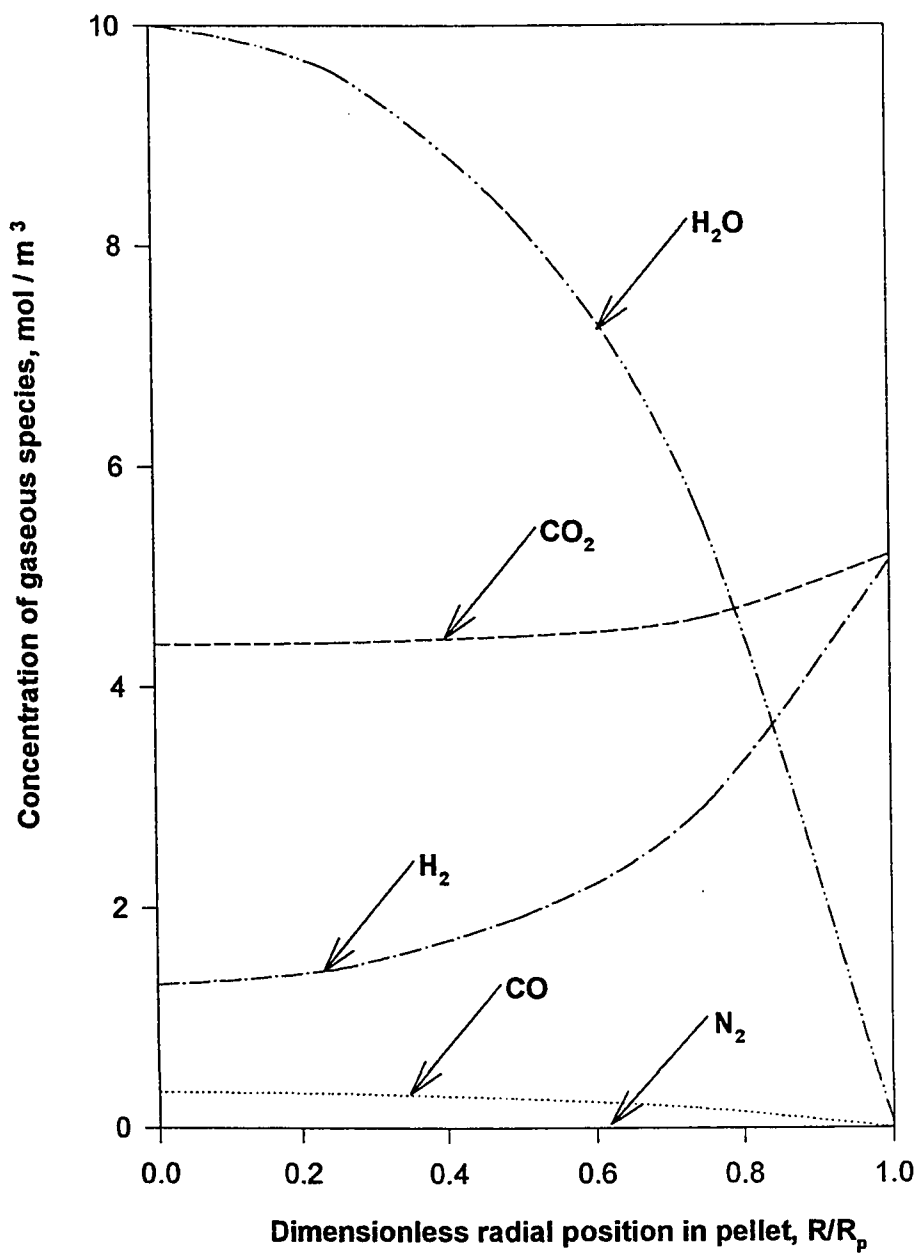


Figure 6.3. The radial concentration profile at: $t = 60$ s, $GXT = 0.012$, $T_b = 1173$ K, $P_b = 101.3$ kPa and $R_p = 3.28 \times 10^{-4}$ m.

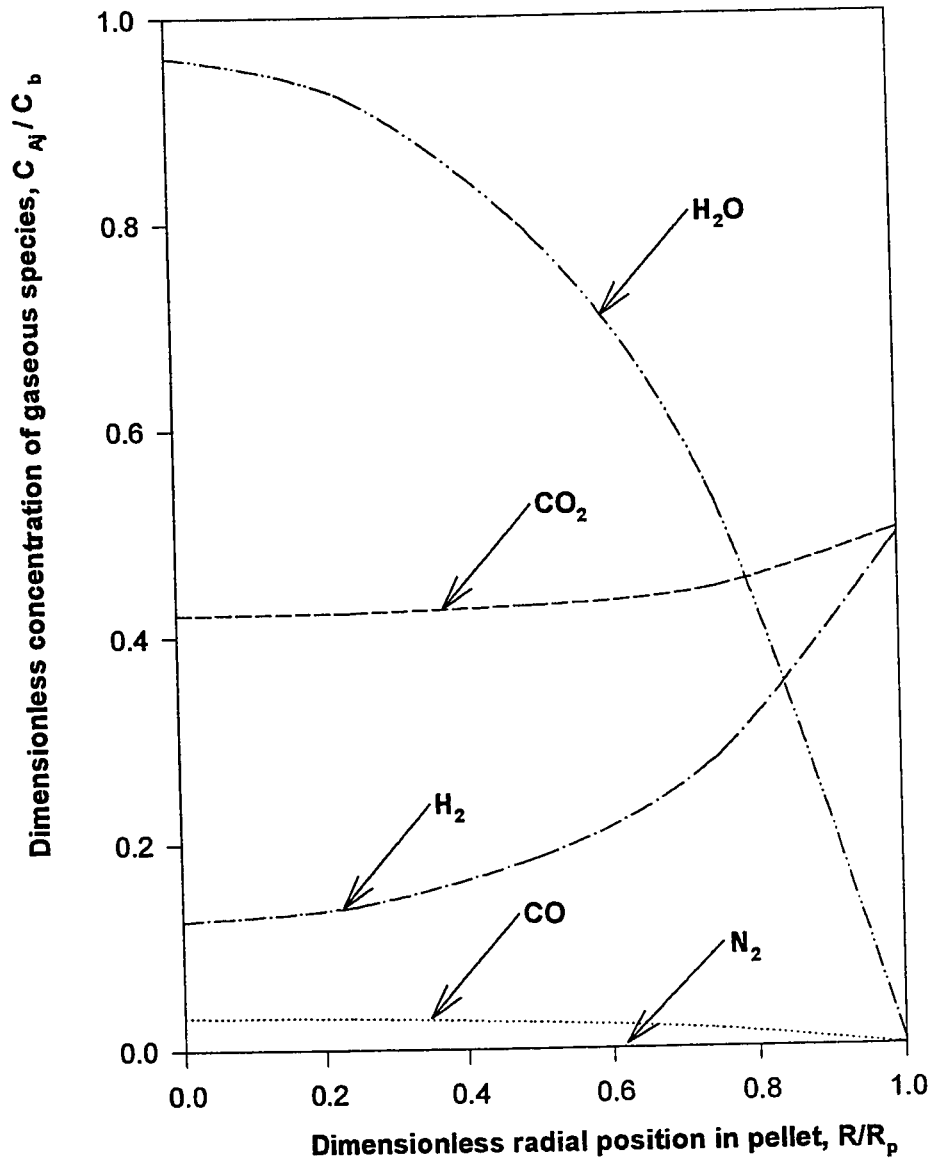


Figure 6.4. The radial concentration profile at: $t = 60$ s, $GXT = 0.0123$, $T_b = 1173$ K, $P_b = 101.3$ kPa, $C_b = 1.04$ mol/m³ and $R_p = 3.28 \times 10^{-4}$ m.

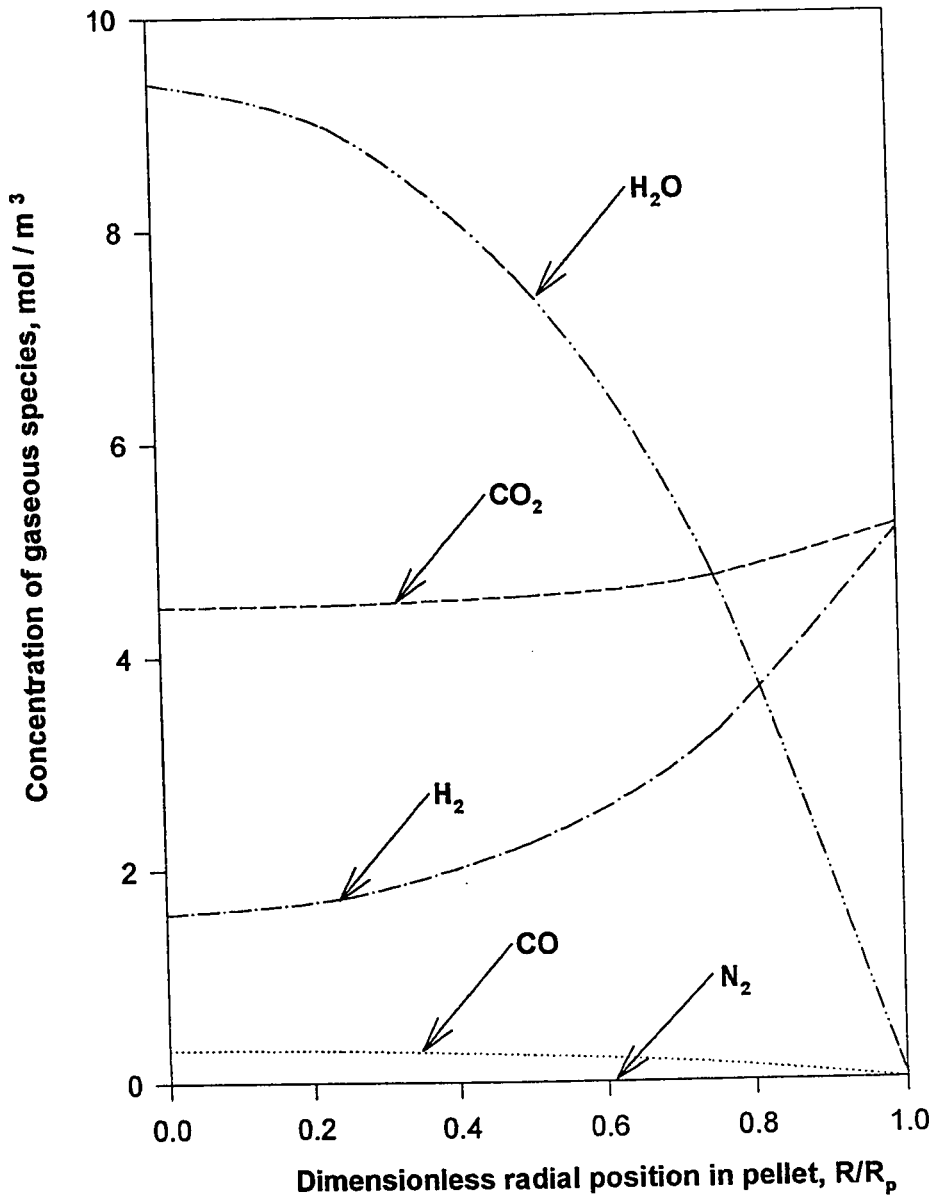


Figure 6.5. The radial concentration profile at: $t = 480$ s, $GXT = 0.093$, $T_b = 1173$ K, $P_b = 101.3$ kPa, and $R_p = 3.28 \times 10^{-4}$ m.

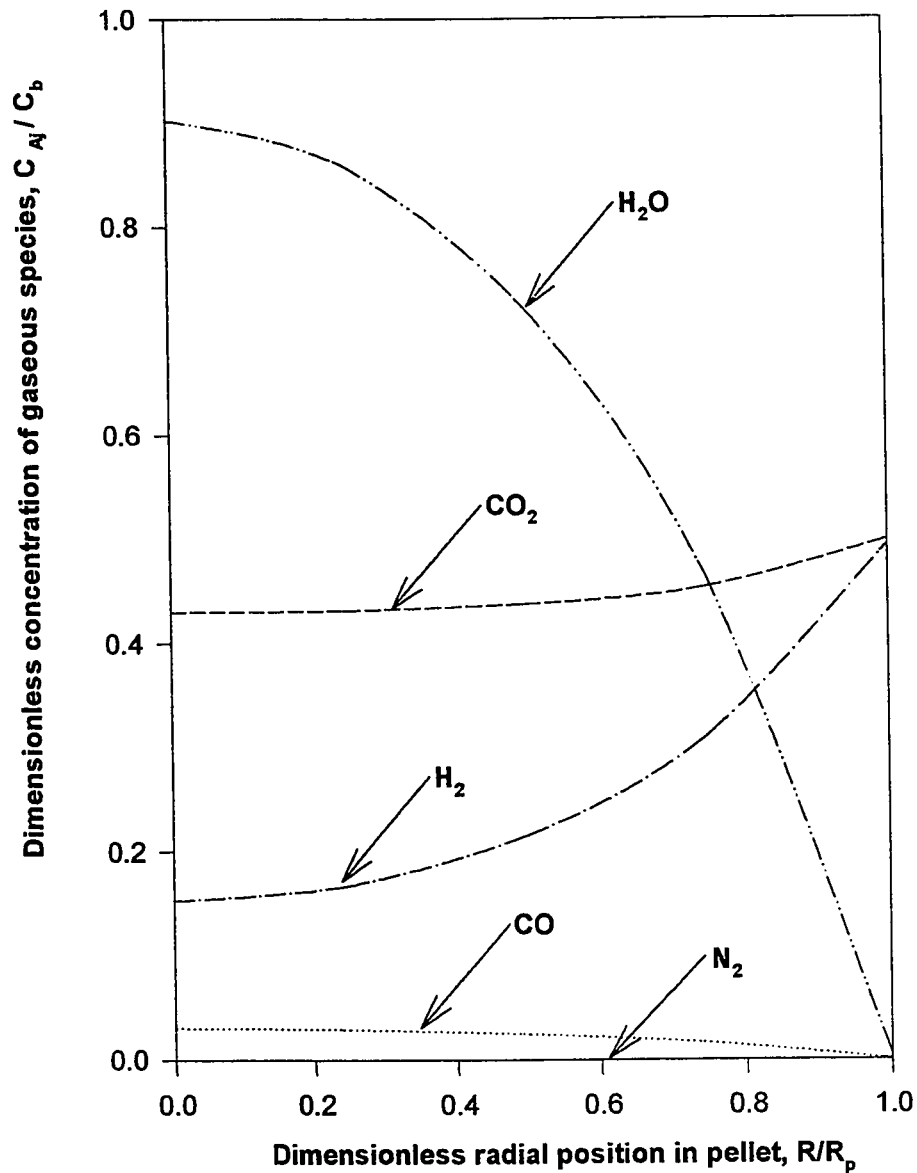


Figure 6.6. The radial concentration profile at: $t = 480$ s, $GXT = 0.093$, $T_b = 1173$ K, $P_b = 101.3$ kPa, $C_b = 1.04$ mol/m³ and $R_p = 3.28 \times 10^{-4}$ m.

that since both CO_2 and H_2 are produced from the WGS reaction, it becomes especially difficult to isolate the concentration profiles and restrict the explanation to the more straightforward situation (without the WGS reaction). Thus, the approach adopted is focused on the overall behavior observed.

If the reactions were diffusion controlled, the intrinsic rate of reaction would be faster than the rate of diffusion into the pellet. This implies that, any reactant gas diffusing into the pellet would be consumed at or near the pellet surface and, therefore, a very steep concentration profile of the reactant gases results with high concentrations (closely approaching their respective bulk values) at the pellet surface ($R/R_p=1.0$), which drops to near zero a short distance into the pellet. If the reactions are kinetically controlled however, the rate of diffusion into the pellet would have been greater than the intrinsic reaction rate. Thus, the concentration profile of the reactant gases would be nearly equal across the pellet. Reaction would occur throughout the pellet at the same time and the radii of the grains would decrease at approximately the same rate.

Close examination of Figures 6.1 - 6.4 clearly shows that the concentration profiles are in general between the two extremes outlined above. Thus, the reaction can safely be considered to be both kinetic and diffusion controlled. This situation may be called intermediate or diffuse regime. However, while the observation made is true for H_2O and H_2 , same cannot be concluded on CO and CO_2 as evidenced by the near flat profiles observed. The flatness in the concentration profile of CO_2 seen in all the figures does indicate a severe kinetic resistance and fast diffusion into the pellet. This is, however, very consistent with the slow rate of conversion observed experimentally under the same operating conditions in the carbon gasification reaction. In fact, carbon conversion of only about 5 % was

attained after 3 hours of reaction (see Figure 5.2)

The concentration of the reactant gases (CO_2 and H_2) are expected to deplete inwardly and a negative gradient in concentration is expected for the product gases (H_2O and CO). However, the product gases in the WGS reaction (H_2 and CO_2) being the reactants in the simultaneous reactions of carbon gasification and nickel oxide / hematite reduction, more than offset the amount of the same consumed at the early stages of the reaction. This effect is visibly seen in the transient concentration profile shown in Figure 6.7. The results of a bigger pellet size ($R_p = 3.28 \times 10^{-2}$ m) shown in Figure 6.8, even more clearly represent the behavior observed. The initial increase and subsequent decrease and leveling off of the concentration profile of H_2 seen in Figure 6.8 is consistent with the observation made above. Another interesting feature of this figure is that, the amount of H_2O produced by the $\text{NiO}/\text{Fe}_2\text{O}_3$ reduction cause the concentration of H_2O to reach a maximum of about 8 mol/m^3 . It started to decrease after about 120 seconds of reaction. This behavior is actually expected, since significant amount of the H_2O produced comes from the reduction of NiO and the reaction is almost complete after 120 seconds. This probably explains the increasing part of the curve. The decreasing region can be attributed to the amount consumed in the WGS reaction, which is more dominant than the Fe_2O_3 reduction and, thus, the resultant H_2O tends towards depletion.

Comparison of Figures 6.7 and 6.8 clearly shows the effect of pellet size on the overall concentration profiles and by extension on the solid conversion. The inert gas, N_2 , almost instantaneously depleted to zero after start of the reaction and immediately leveled off for the smaller pellet ($R_p = 3.28 \times 10^{-4}$ m). For the bigger pellet ($R_p = 3.28 \times 10^{-2}$ m) however, complete depletion was not attained until after 240 seconds of reaction. This result is

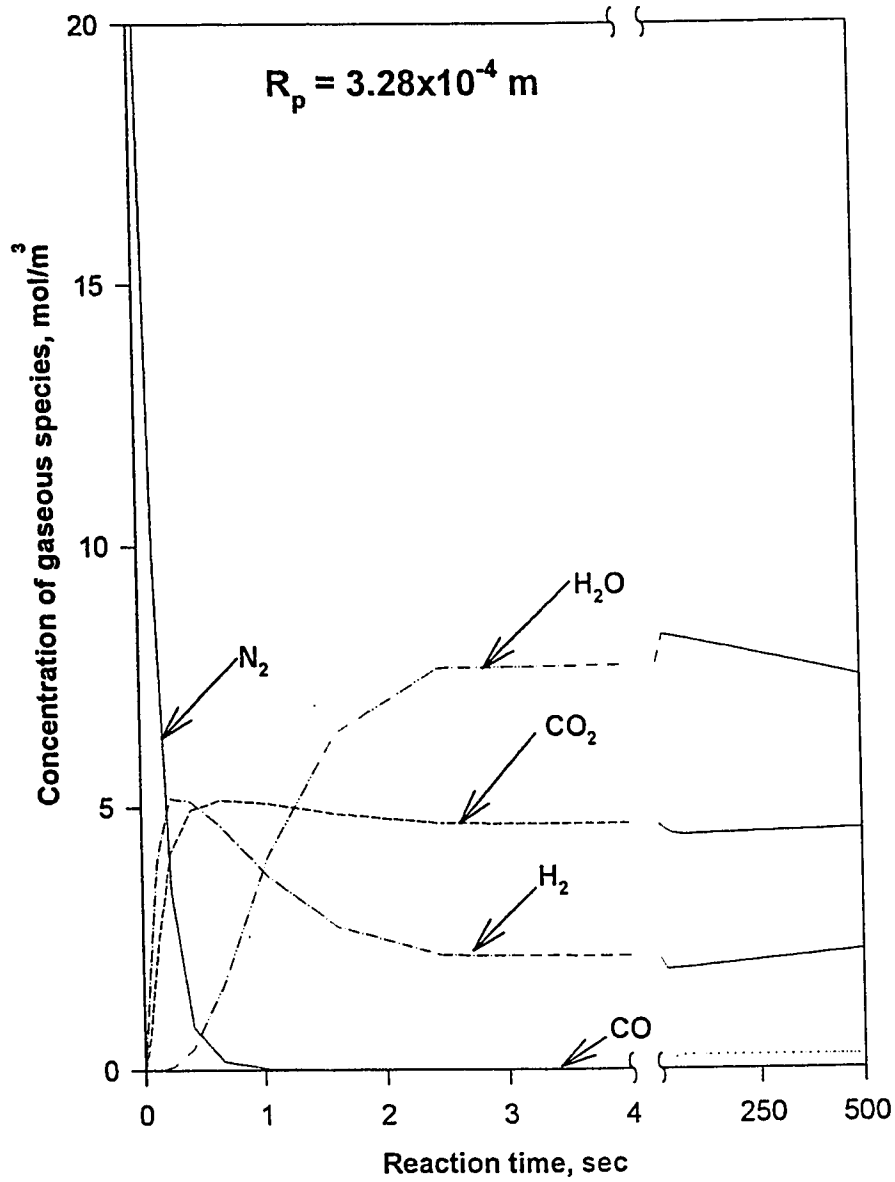


Figure 6.7. The transient concentration profile at: $R/R_p = 0.5$, $T_b = 1173 \text{ K}$, $P_b = 101.3 \text{ kPa}$, and $R_p = 3.28 \times 10^{-4} \text{ m}$.

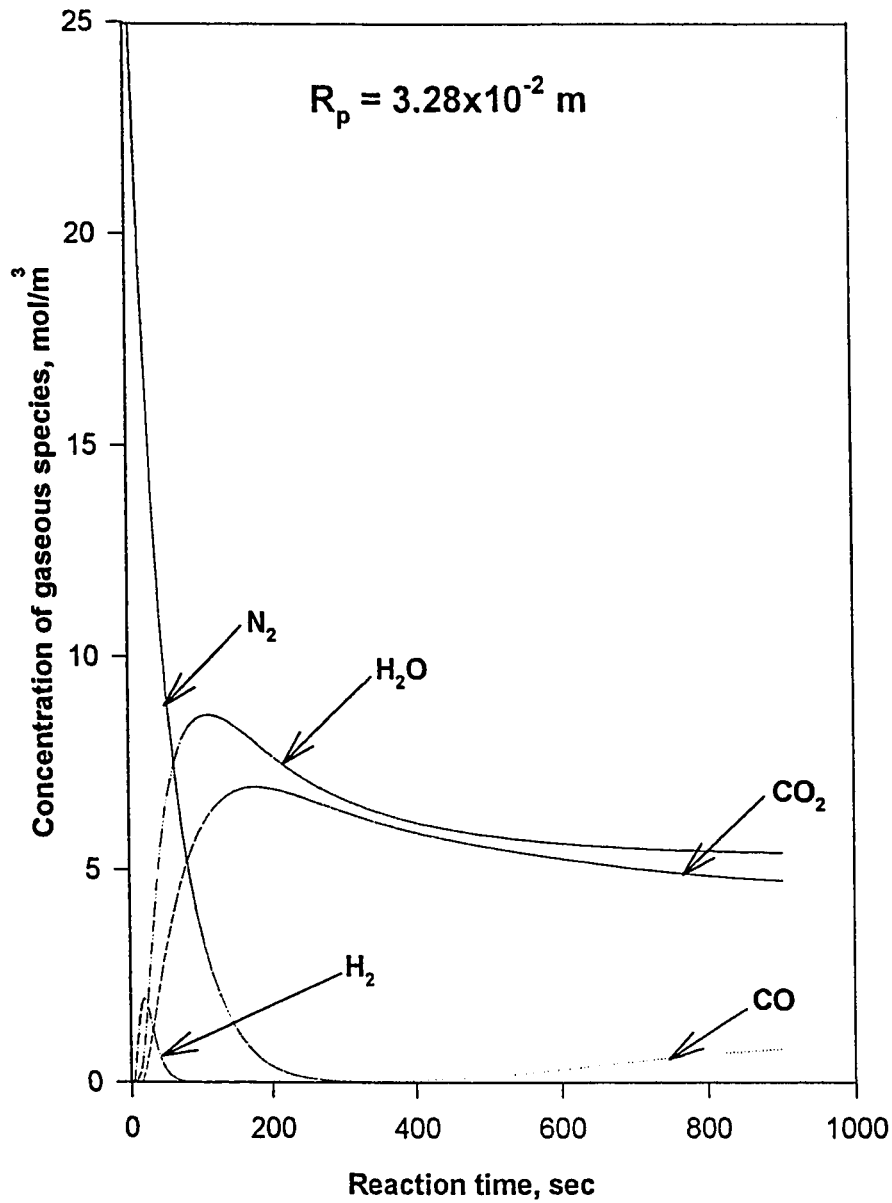


Figure 6.8. The transient concentration profile at: $R/R_p = 0.5$, $T_b = 1173 \text{ K}$, $P_b = 101.3 \text{ kPa}$, and $R_p = 3.28 \times 10^{-2} \text{ m}$.

consistent with the theoretical expectations. Since the operating conditions are kept same (including bulk concentrations) in both cases, it is obvious that increase in pellet size increases the diffusion path followed by the reactant gases and as such the entire diffusion process is slowed. On the other hand, increase in pellet weight is tantamount to increase in the overall active ingredients (solid reactants) and under the same operating conditions, a slower rate of reaction is envisaged. Moreover, as has been explained earlier, both internal diffusion and reaction resistances are visibly seen to be present in the system and thus, it can be concluded that, the behavior in these figures is consistent with theoretical expectations.

Figure 6.9 shows the local conversion profiles of individual solid reactants along the radius of the pellet after 480 seconds of reaction for a half pellet thickness (R_p) of 3.28×10^{-4} m. The corresponding overall pellet conversion (GXT) at that instant is 9.2 %. The steepness of the profiles becomes most pronounced towards the outer layer of the pellet. Thus, the solid grains are almost completely converted to products in that region and almost unreacted in the inner core. NiO grains are converted to Ni much faster than either carbon or Fe_2O_3 . This is consistent with the experimental results shown in Figures 5.2 through 5.4. As was noted in Chapter 5, in carbon gasification reaction at temperatures of 900 °C and below, there is practically no conversion even after 480 seconds of reaction. Further, the conversion of Fe_2O_3 is relatively much slower compared to that of NiO as shown in Figure 5.4. In fact, only conversion of about 2 % is attained in Fe_2O_3 grains after 8 minutes of reaction, when NiO grains have long leveled off after reaching complete conversion ($GX_{BK} = 1.0$). Taking into account the different scales used for the local conversion of carbon, Fe_2O_3 and NiO (Figure 6.9), it can clearly be seen that, the conversion profile is almost flat for carbon indicating

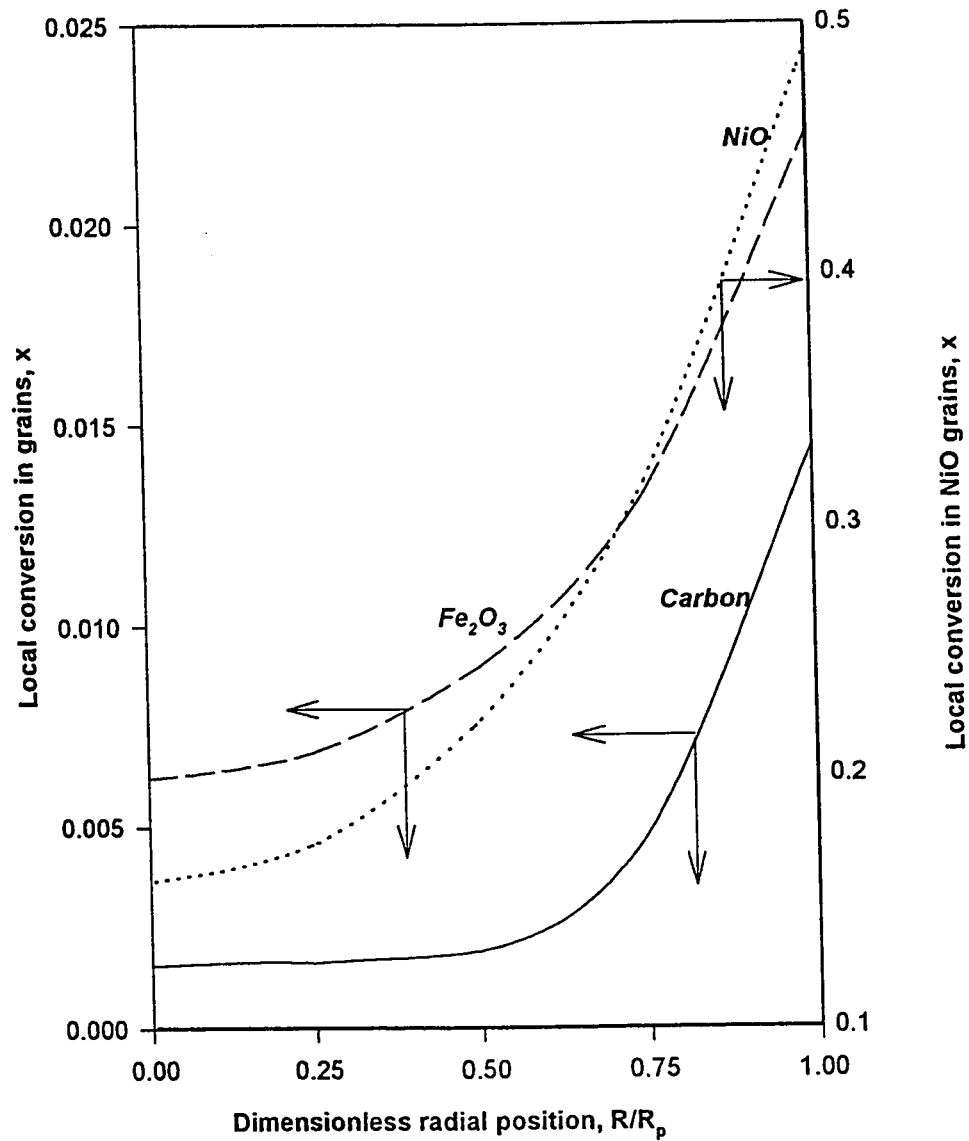


Figure 6.9. Local conversion along radius of pellet at: $t = 480$ s, $GXT = 0.093$, $T_b = 1173$ K, $P_b = 101.3$ kPa, $C_b = 1.04$ mol/m³ and $R_p = 3.28 \times 10^{-4}$ m.

decrease in grain radii at approximately the same rate. This is a further evidence to the kinetically controlled regime discussed above. On the other hand, the NiO profile provides evidence of diffusion control in the nickel oxide reaction. This is clear from the grain radius profile with radius approaching initial value a short distance into the pellet. On the overall however, Figure 6.9 clearly demonstrates the magnitude of each grain - type conversions which are consistent with and within the framework of the conceptualization of the grain model.

To further examine the possibility of external mass transfer limitations, series of runs were made with varying bulk gas flow rates in the range 8.33×10^{-7} - 8.33×10^{-1} m³/s (base case is 8.33×10^{-5} m³/s). Although the results of the runs are not presented here, it was observed that, there is practically no effect of the gas flow rate on the overall conversion. Thus, the conclusion is drawn that there is no external transport limitations for such thin pellets. Moreover, at the low Reynolds number usually encountered in laboratory reactors, the mass and heat transfer coefficients are quite insensitive to changes in flow rates, so that for noticeable effect to be observed, the flow rates have to be varied over very wide range. For thicker or larger pellets, however, the external transport limitations do become important.

6.2.2 Thermal Gradient

Thus far, only concentration gradients inside the pellet were discussed. The simultaneous solution to the continuity and energy equations yield temperature profiles both temporally and spatially. Figures 6.10 and 6.11 show the temperature profiles inside the pellet after just one second of reaction for a pellet of $R_p = 3.28 \times 10^{-4}$ m. It can be seen that, while there is

visibly internal gradient (specifically 8 K) from the surface to the center of the pellet, the temperature shot to over 960 K from an initial value of 400 K after only one second of reaction. This indicates a rather small resistance of heat transfer for such reaction schemes. However, this heat up may be very important in reactions which last a short time, perhaps less than one second. Typical examples are flash pyrolysis and combustion.

A transient temperature history is shown in Figure 6.12. The overlap between the temperature profiles at the surface ($R/R_p = 1.0$), center ($R/R_p = 0$) and midway between the center and the surface ($R/R_p = 0.5$) is also a clear indication that, for the size of the pellet considered, the internal heat transfer resistance is almost negligible. The overall pellet temperature almost suddenly attained the bulk value of 1173 K (specifically after 5 seconds of reaction). As the pellet size increases however, the effect of the internal resistance becomes pronounced. Figure 6.13 presents the temperature history for a pellet size of $R_p = 3.28 \times 10^{-2}$ m. The surface temperature in this case reached about 1000 K, which is almost 400 K higher than the center value after 200 seconds of reaction time. The simplest explanation to this observation is as follows: since the reaction is occurring over a large volume for the bigger pellet, the heat generated is correspondingly higher. However, a higher heat transfer coefficient in the external gas film resulting from the smaller pellet size (heat transfer coefficient being approximately proportional to the inverse square root of the pellet diameter) enables the heat generated in the pellet to be transferred to the flowing gas faster resulting in lower temperature rises in the pellet at a given time. As the pellet size increases, the depth of penetration of the reactant gas along the pellet center increases and the reaction at earlier times would only occur in a finite zone nearer to the surface.

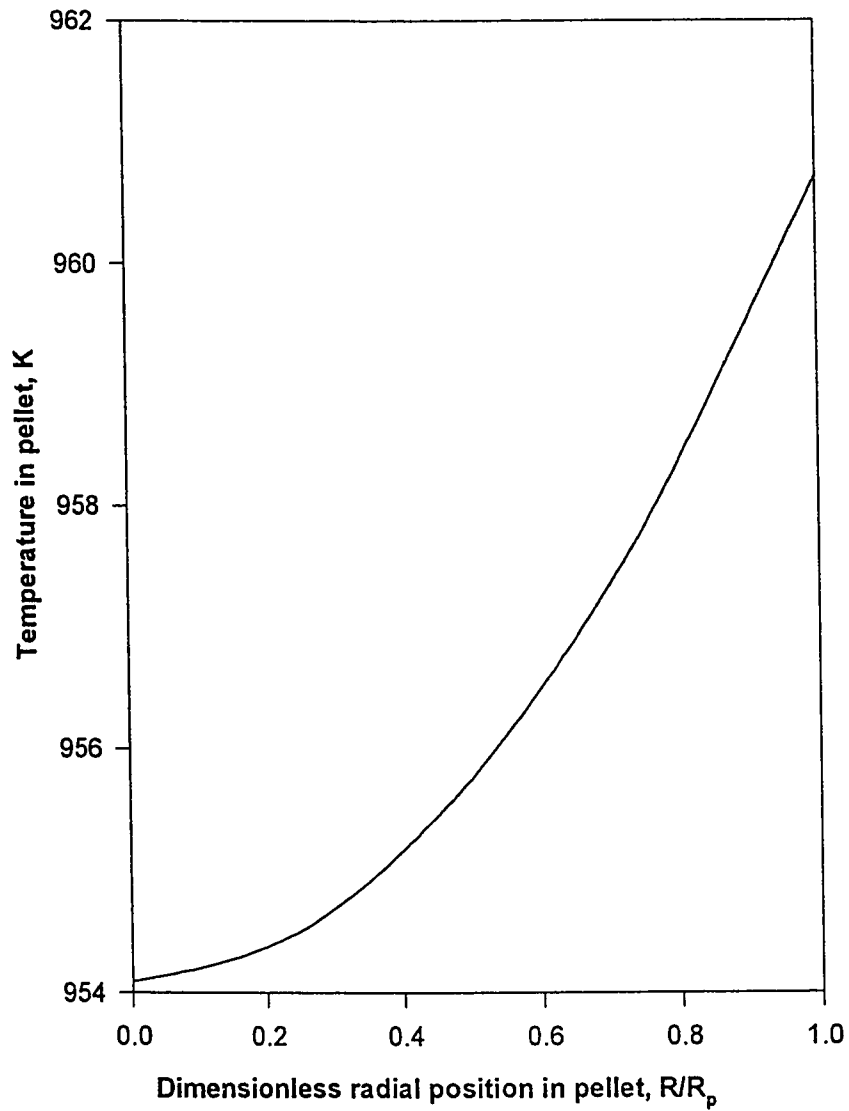


Figure 6.10. The radial temperature distribution: $t = 1$ s, $GXT = 1.95 \times 10^{-5}$,
 $T_b = 1173$ K, $P_b = 101.3$ kPa, and $R_p = 3.28 \times 10^{-4}$ m.

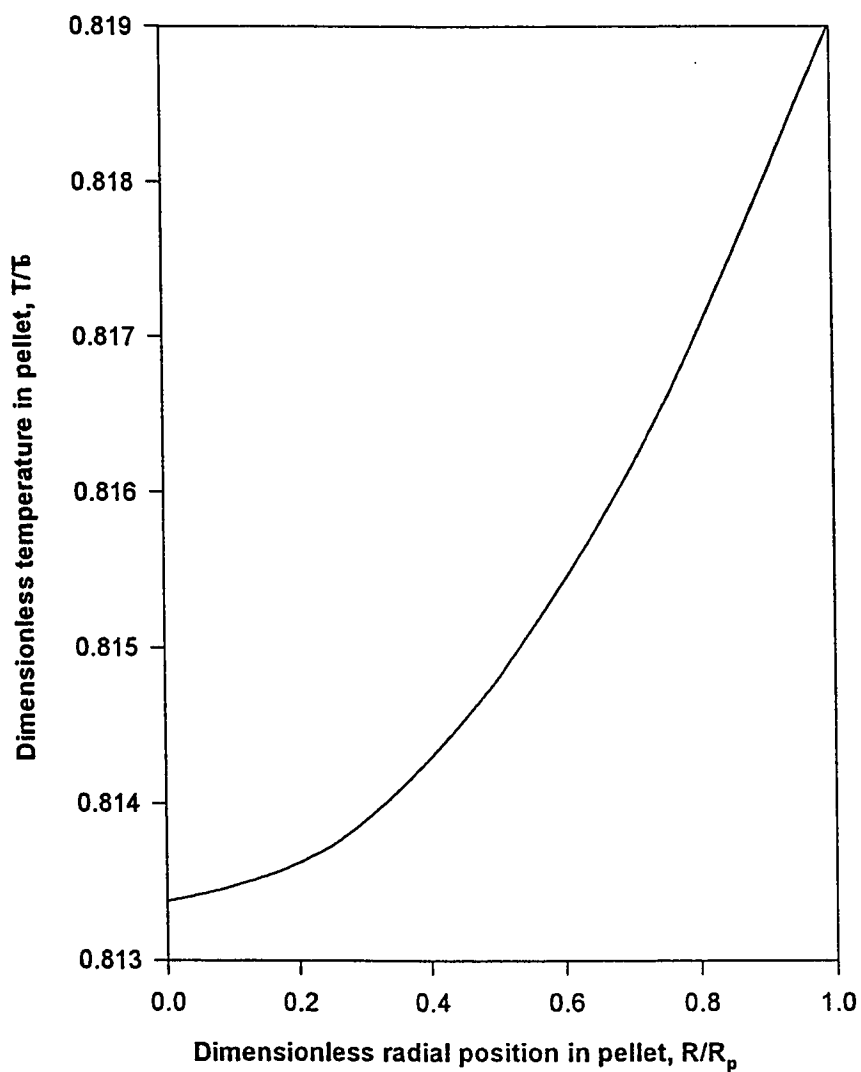


Figure 6.11. The dimensionless radial temperature profile at: $t = 1$ s, $GXT = 1.95 \times 10^{-5}$, $T_b = 1173$ K, $P_b = 101.3$ kPa, and $R_p = 3.28 \times 10^{-4}$ m.

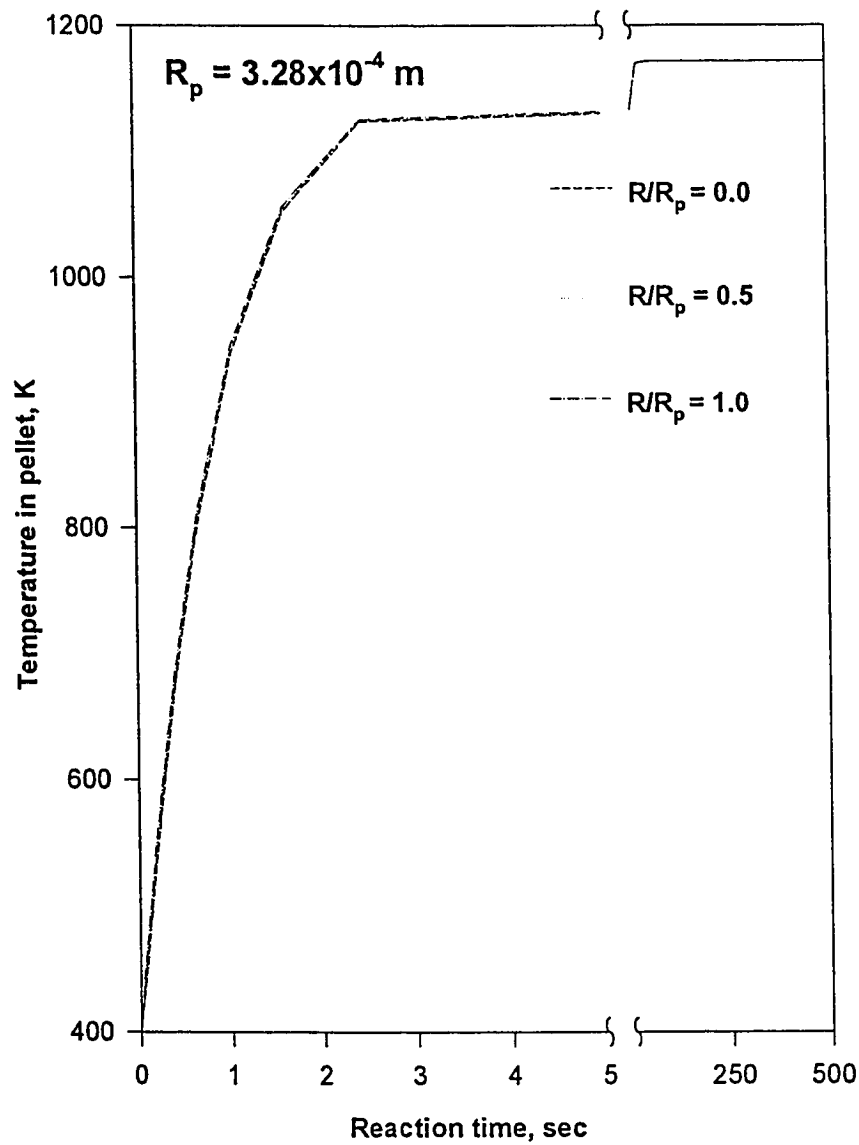


Figure 6.12. The temperature history in pellet at: $T_b = 1173 \text{ K}$,
 $P_b = 101.3 \text{ kPa}$ and $R_p = 3.28 \times 10^{-4} \text{ m}$.

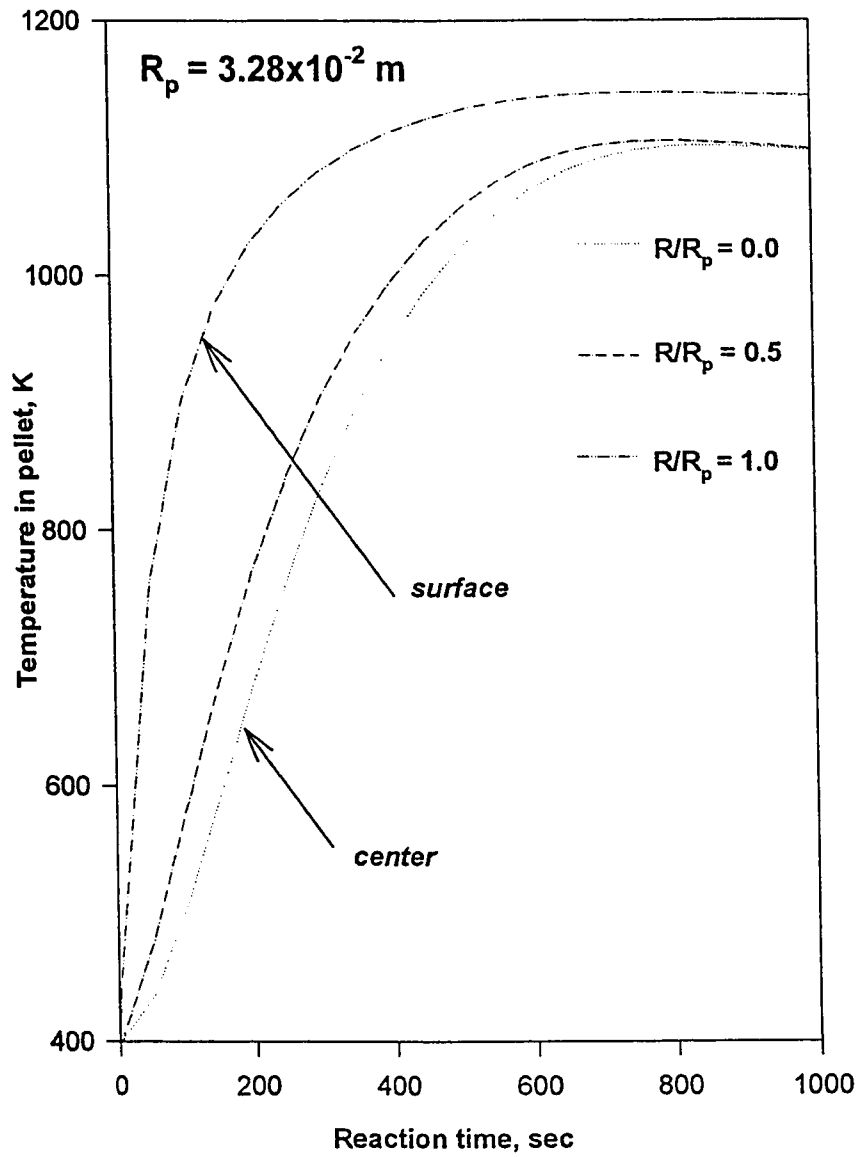


Figure 6.13. The temperature history in pellet at: $T_b = 1173 \text{ K}$, $P_b = 101.3 \text{ kPa}$ and $R_p = 3.28 \times 10^{-2} \text{ m}$.

6.2.3 System Stability

Multiplicity of steady states could conceivably occur as a consequence of some strong non - linearity in the heat generation term in the right hand side of equation (3.22). However, according to Luss (1968), the range of Thiele modulus over which it occurs is quite narrow and for rather drastic parameter values, the Thiele modulus was found to be only between 0.47 and 0.49. Thus he concluded that, the internal temperature gradients are unlikely to cause particle instability for the pellet sizes investigated.

Although the scope of this work does not cover the investigation of steady state multiplicity, it should be noted that, interfacial concentrations and temperature gradients inside the pellet widen the range of operating conditions which may lead to the occurrence of multiple steady states. Moreover, when the resistance to diffusion leads to significant concentration gradients, multiplicity of steady states could arise leading to a hysteresis in the reaction rate upon increase and subsequent decrease of the reaction temperature. This behavior is particularly unfavorable for smooth industrial operations. However, the interfacial concentration and temperature gradients have been shown to be negligible. This, coupled with the speedy attainment of bulk temperature throughout the pellet after commencement of reaction (especially for the pellet sizes considered) leads to the conclusion that, there is no multiplicity under the prevailing conditions.

Nonetheless, the magnitude of the effect of instability in the system is not undermined and since this model is intended to be extended to simulate larger pellets, it should take into account the possibility of the existence of steady states multiplicity. This aspect may form the basis for further study.

6.2.4 Conclusion

In conclusion, the effects of both external and internal mass and heat transfer have been assessed qualitatively. The reactions studied are both diffusion and kinetic controlled, i.e., intermediate regime, where magnitude of each varies with the individual reactions. The external mass and heat transfer limitations have been shown to be negligible, except for extremely rapid reactions where there is the possibility of external mass transfer resistance and temperature gradients of some significance. Only for unrealistic situations is it likely that particle instabilities might occur for the pellet sizes examined; and even then only for a very narrow range of temperature.

6.3 Parametric Study

6.3.1 Effect of Bulk Temperature

Figures 6.14 - 6.18 show the effect of the temperature of the bulk gas stream in the range 873 - 1373 K on the conversion of solid reactants. It can be seen that, increase in the bulk temperature favors the overall conversion up to 1173 K. Above this temperature, the effect is negative leading to reduced conversions. Typically, at 1373 K, a very dramatic behavior in the conversion trend is observed. Some degree of leveling - off of the conversion is seen and overall conversion of about 9 % is attained after 100 seconds of reaction (see Figure 6.18), which is much smaller than the conversion attained at a lower

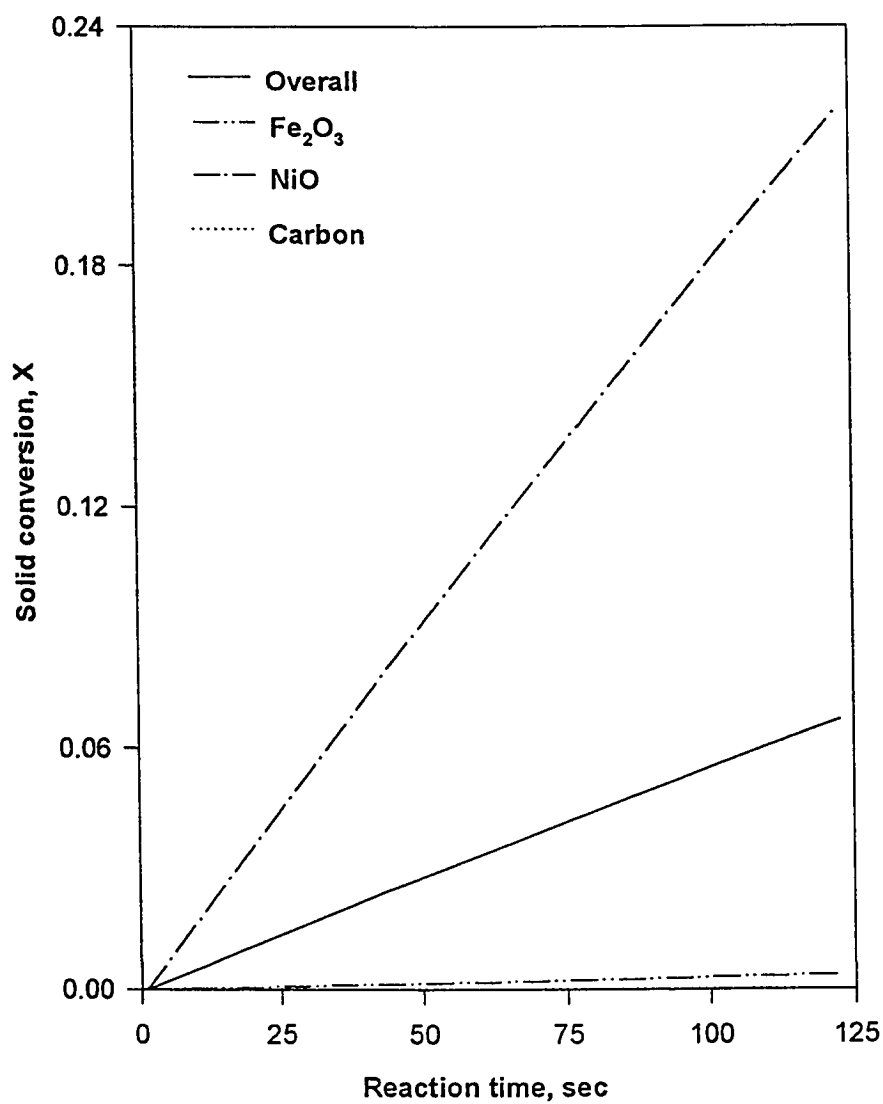


Figure 6.14. Effect of bulk temperature on conversion at: $T_b = 873$ K, and $P_b = 101.3$ kPa.

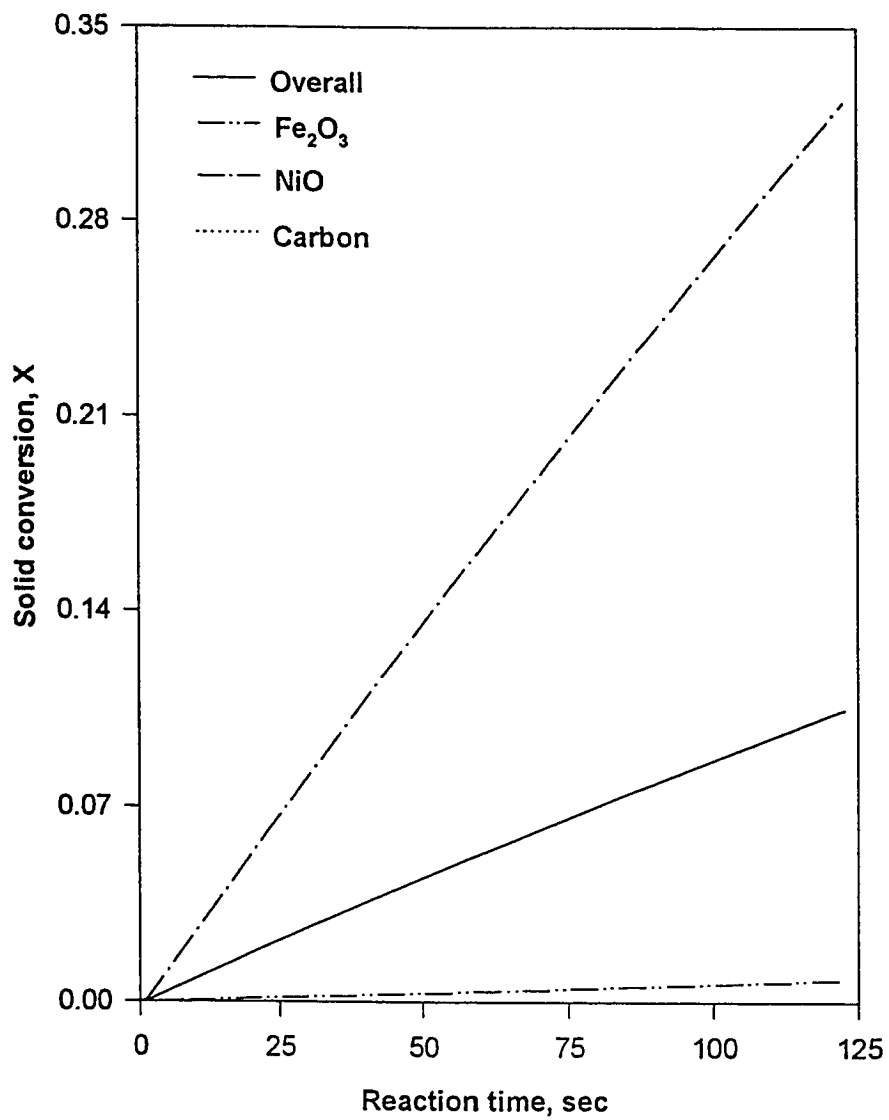


Figure 6.15. Effect of bulk temperature on conversion at: $T_b = 973$ K, and $P_b = 101.3$ kPa.

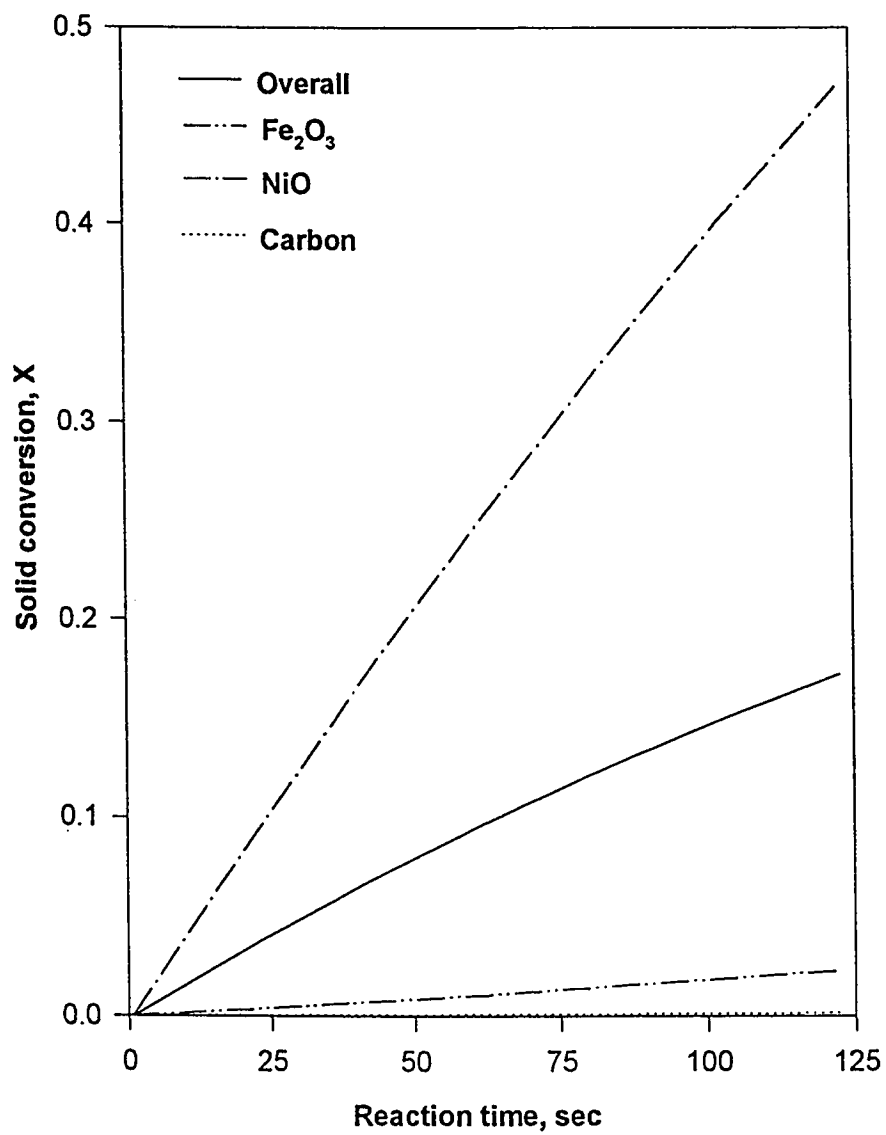


Figure 6.16. Effect of bulk temperature on conversion at: $T_b = 1173$ K, and $P_b = 101.3$ kPa.

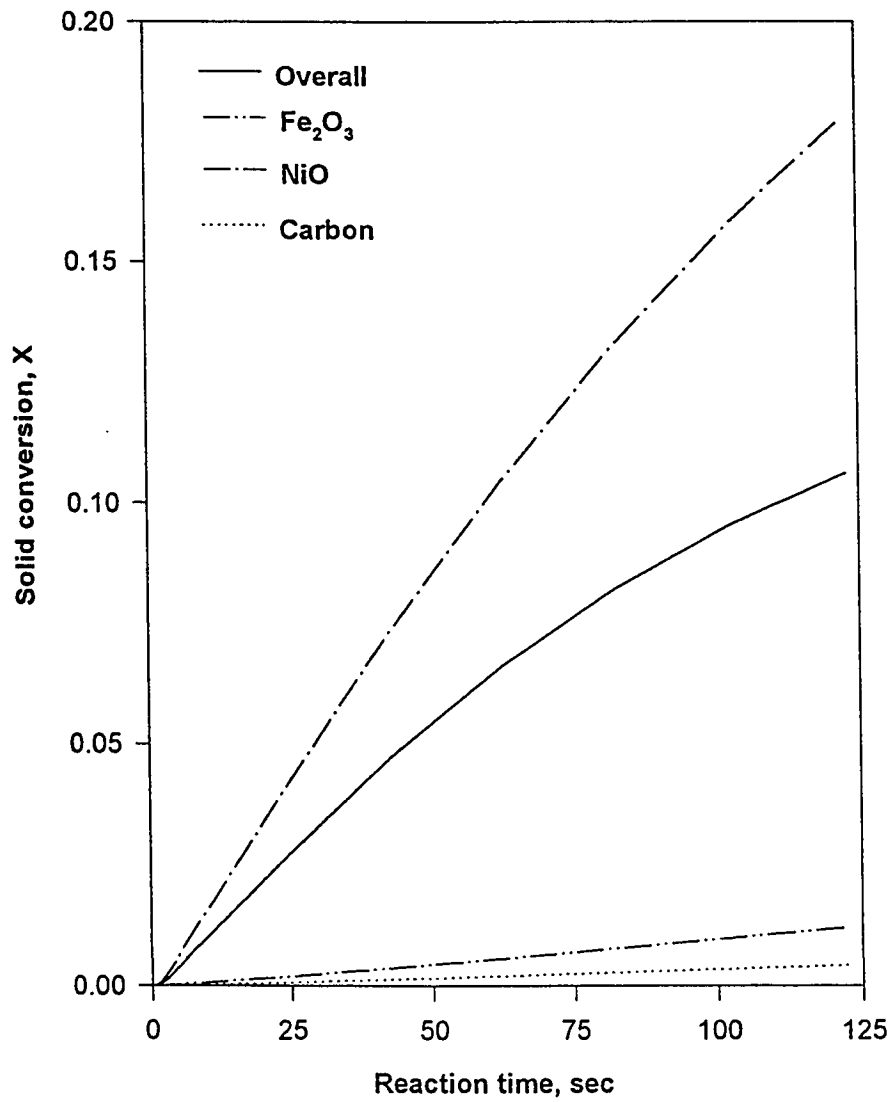


Figure 6.17. Effect of bulk temperature on conversion at: $T_b = 1273$ K, and $P_b = 101.3$ kPa.

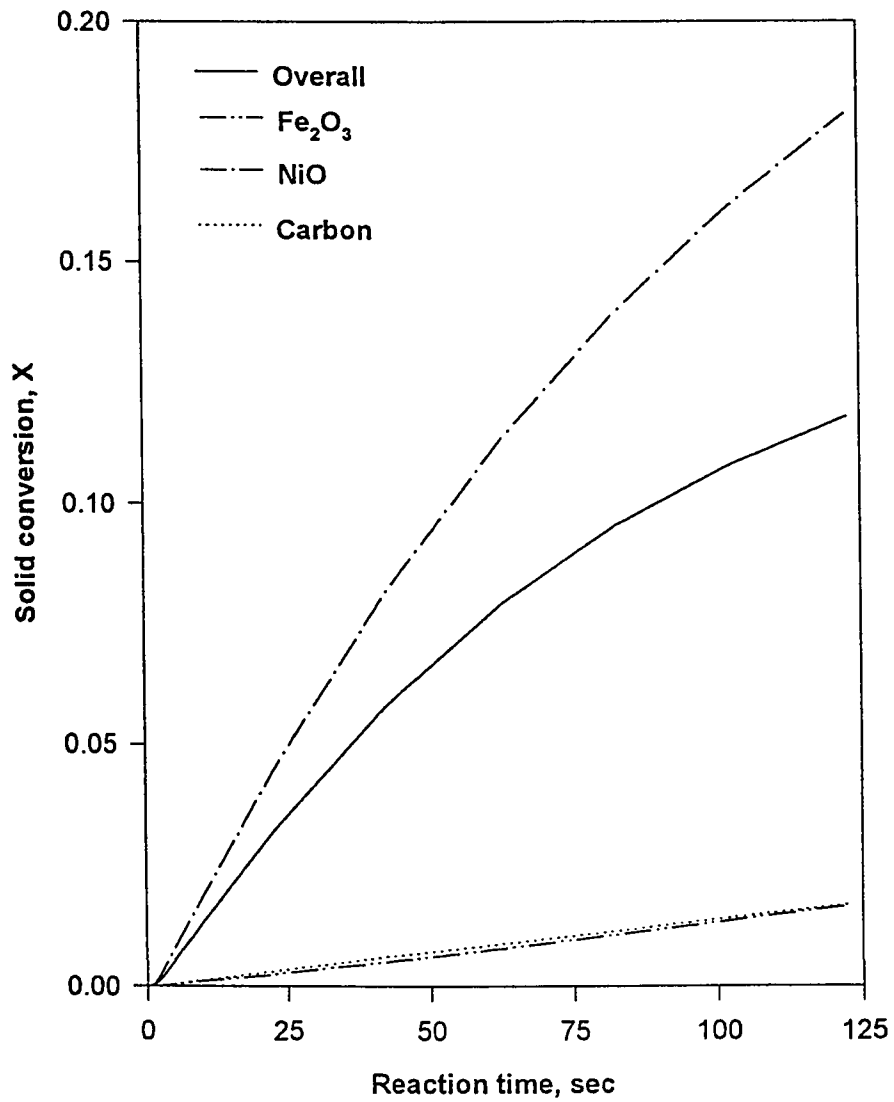


Figure 6.18. Effect of bulk temperature on conversion at: $T_b = 1373$ K, and $P_b = 101.3$ kPa.

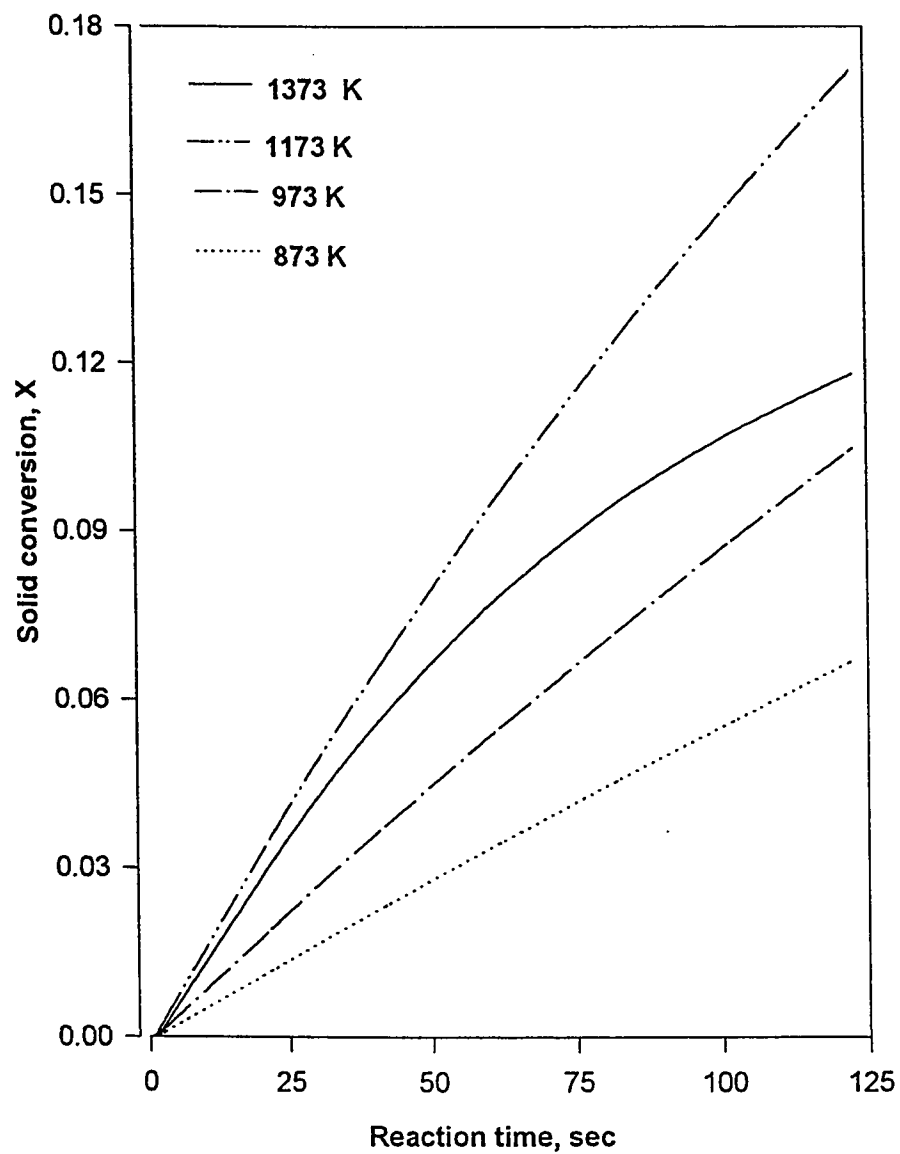


Figure 6.19. Effect of bulk temperature on the overall solid conversion at $P_b = 101.3$ kPa.

temperature of 1173 K (15%) for the same reaction time as illustrated in Figure 6.19. This behavior can be explained from the following consideration: at very high temperatures, both NiO and Fe₂O₃ grains lose their shapes and collapse. This effect has been observed experimentally in the reduction of NiO / Fe₂O₃ mixture even at temperatures slightly above 900 °C. Thus, at 1000 °C, the effect of sintering (which is not accounted for in the present simulation runs) could even be more pronounced in these grains. The competing nature of the reactions in the system also explains. However, carbon grains are very stable at these temperatures and in fact, as can be observed from Figures 6.14 - 6.18, the carbon conversion actually increased throughout with increasing temperature. In effect, the study of the effect of bulk gas temperature helps identify the optimum temperature value above which negative effect results (drop in solid conversion trend), while still keeping the temperature high enough not to suppress the more temperature dependent reactions.

6.3.2 Effect of Bulk Pressure

Figures 6.20 through 6.24 show the effect of bulk pressure on conversion over the pressure range 101.3 - 1013 kPa. The experiments for both carbon gasification and NiO / Fe₂O₃ reduction were carried out at atmospheric pressure. It can be seen from Figure 6.20 that, the maximum NiO conversion reached after 8 minutes of reaction is only about 27 % for the base case ($T_b = 1173$ K and $P_b = 101.3$ kPa). It is interesting to note that, in the reduction of NiO / Fe₂O₃ mixture alone, the conversion of NiO is seen to have reached an asymptotic value of about 99 % in only 4 minutes of reaction corresponding to bulk temperature of 608 K (see Figure 5.4). Therefore, the

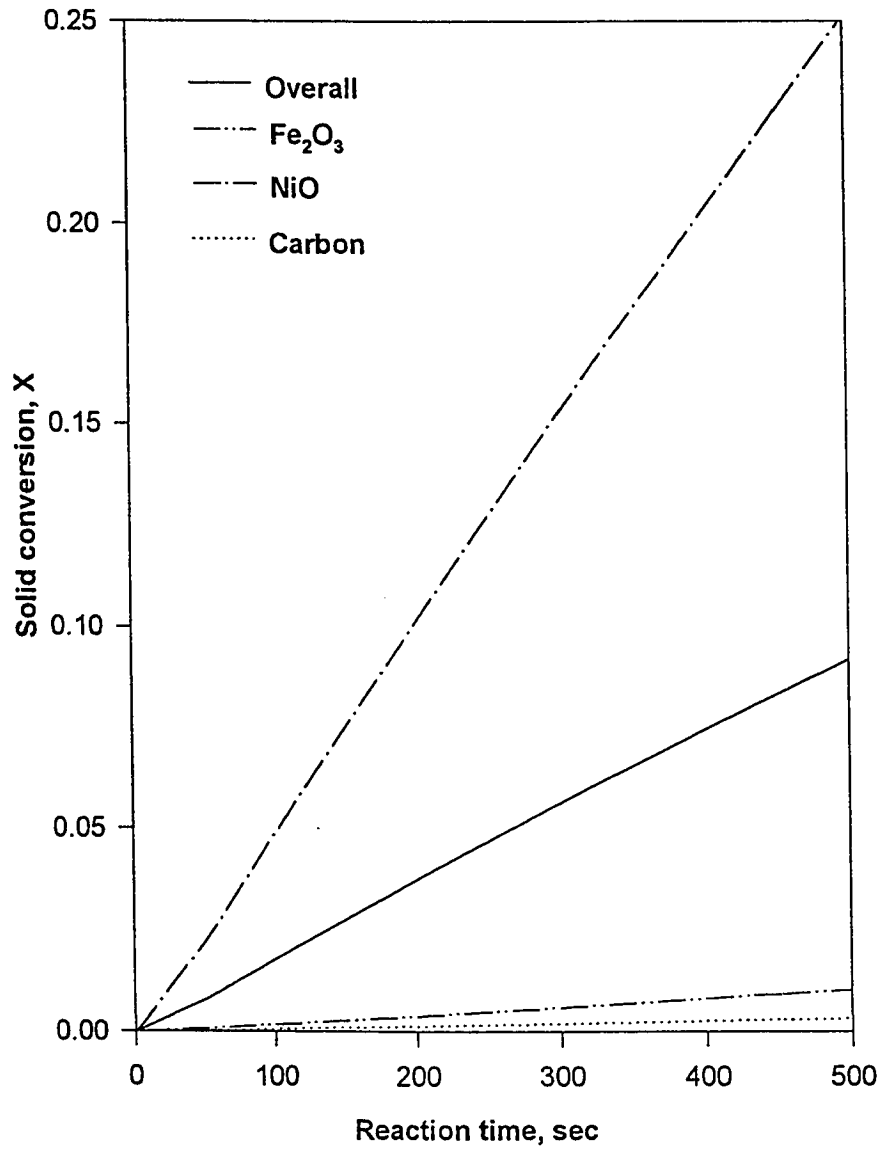


Figure 6.20. Effect of bulk Pressure on conversion at $T_b = 1173$ K and $P_b = 101.3$ kPa.

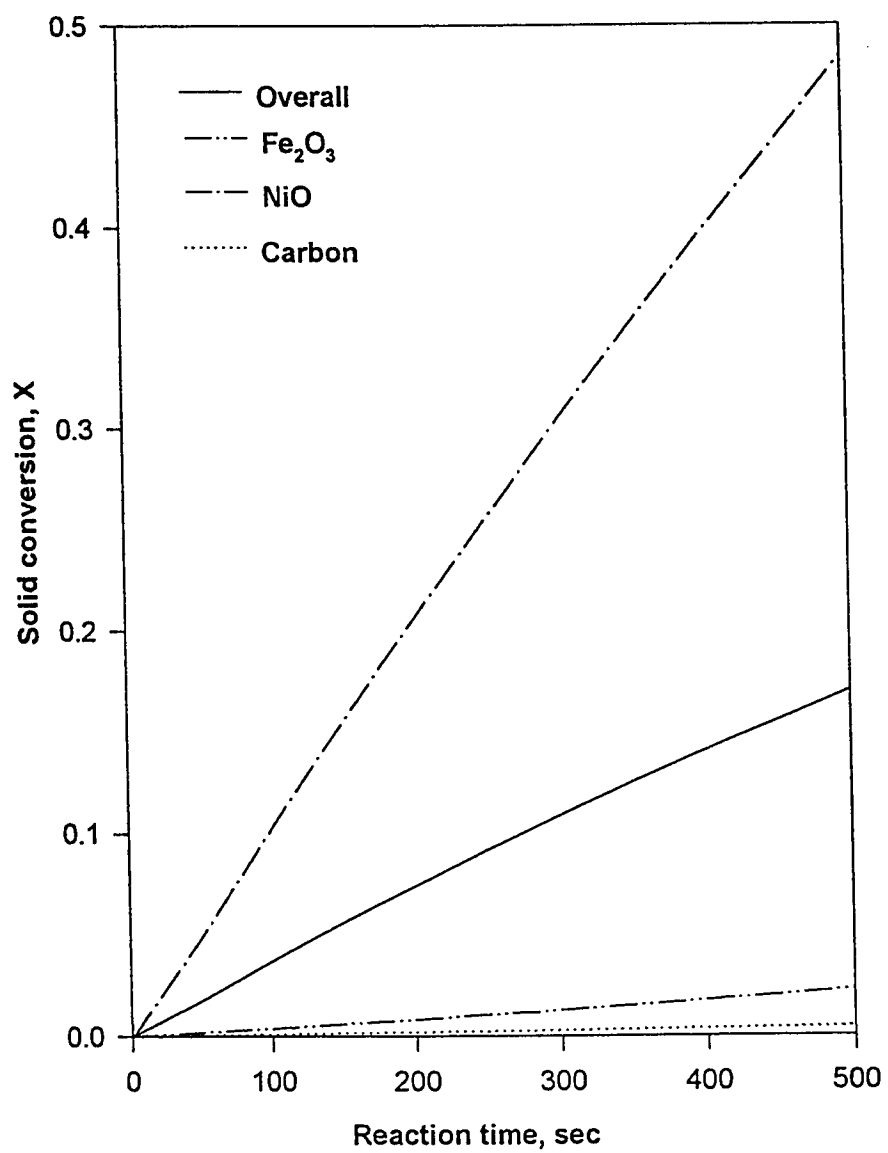


Figure 6.21. Effect of bulk Pressure on conversion at $T_b = 1173$ K and $P_b = 202.6$ kPa.

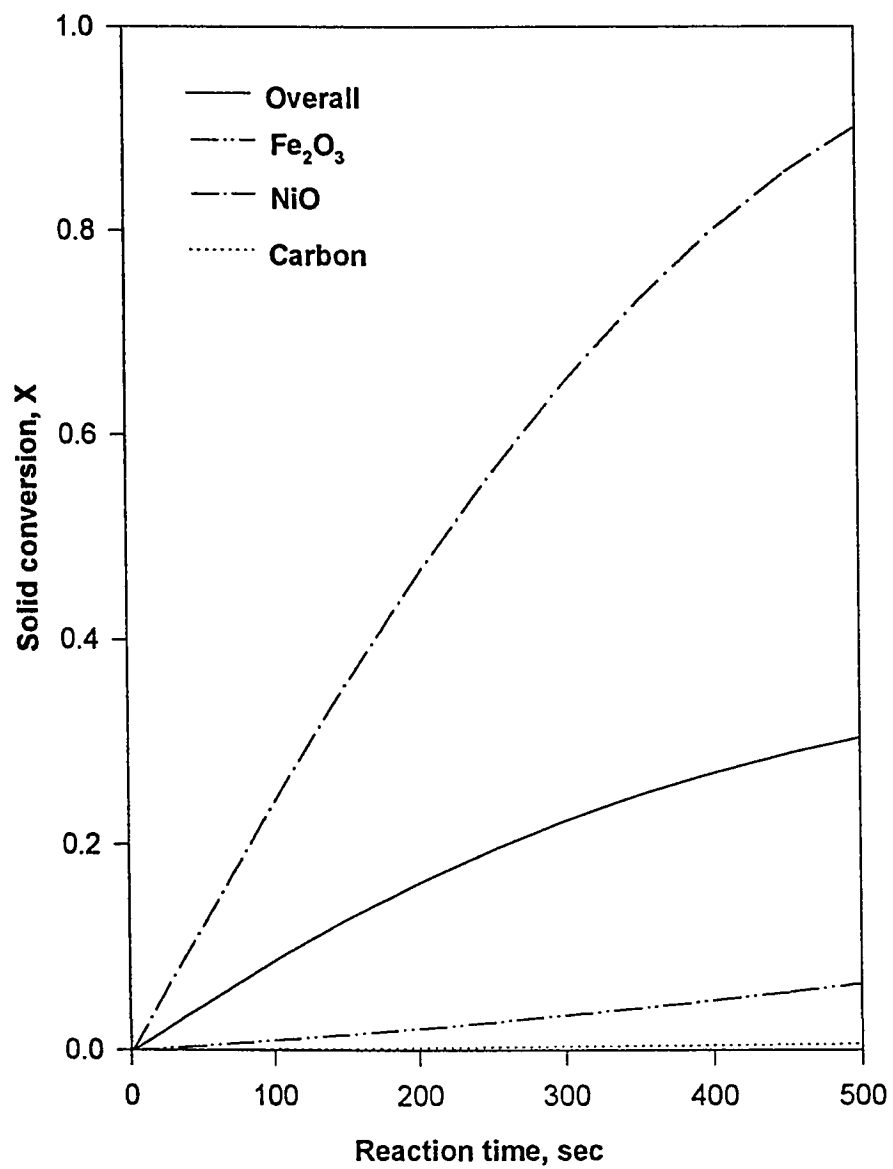


Figure 6.22. Effect of bulk Pressure on conversion at $T_b = 1173$ K and $P_b = 506.5$ kPa.

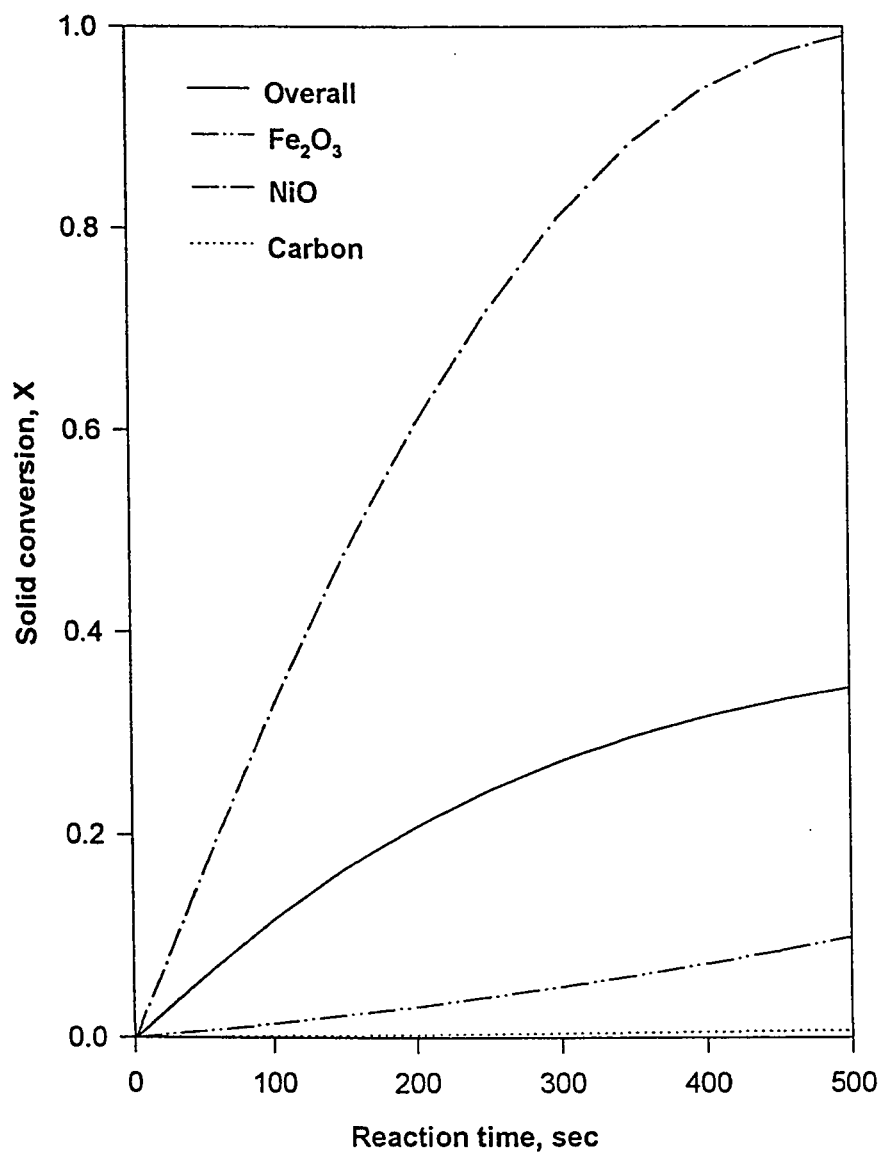


Figure 6.23. Effect of bulk Pressure on conversion at $T_b = 1173$ K and $P_b = 701.9$ kPa.

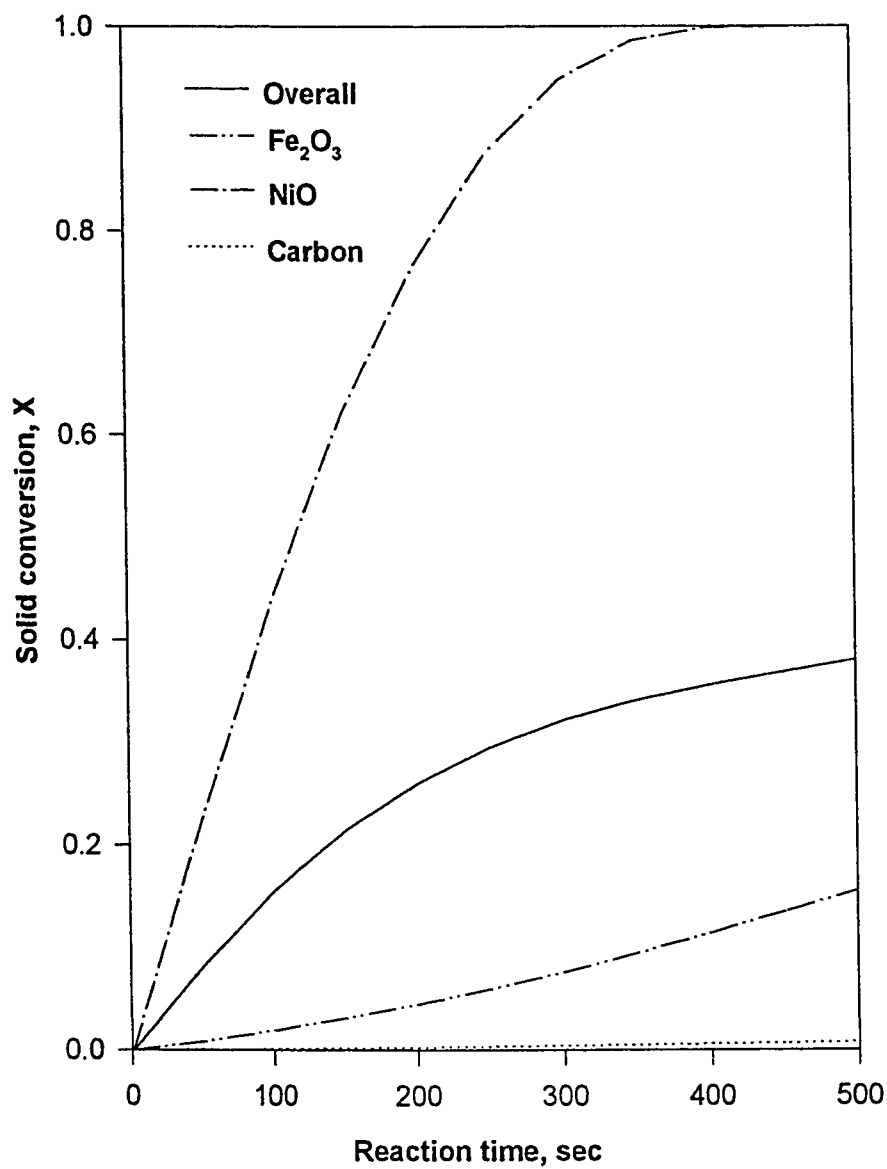


Figure 6.24. Effect of bulk Pressure on conversion at $T_b = 1173$ K and $P_b = 1013$ kPa.

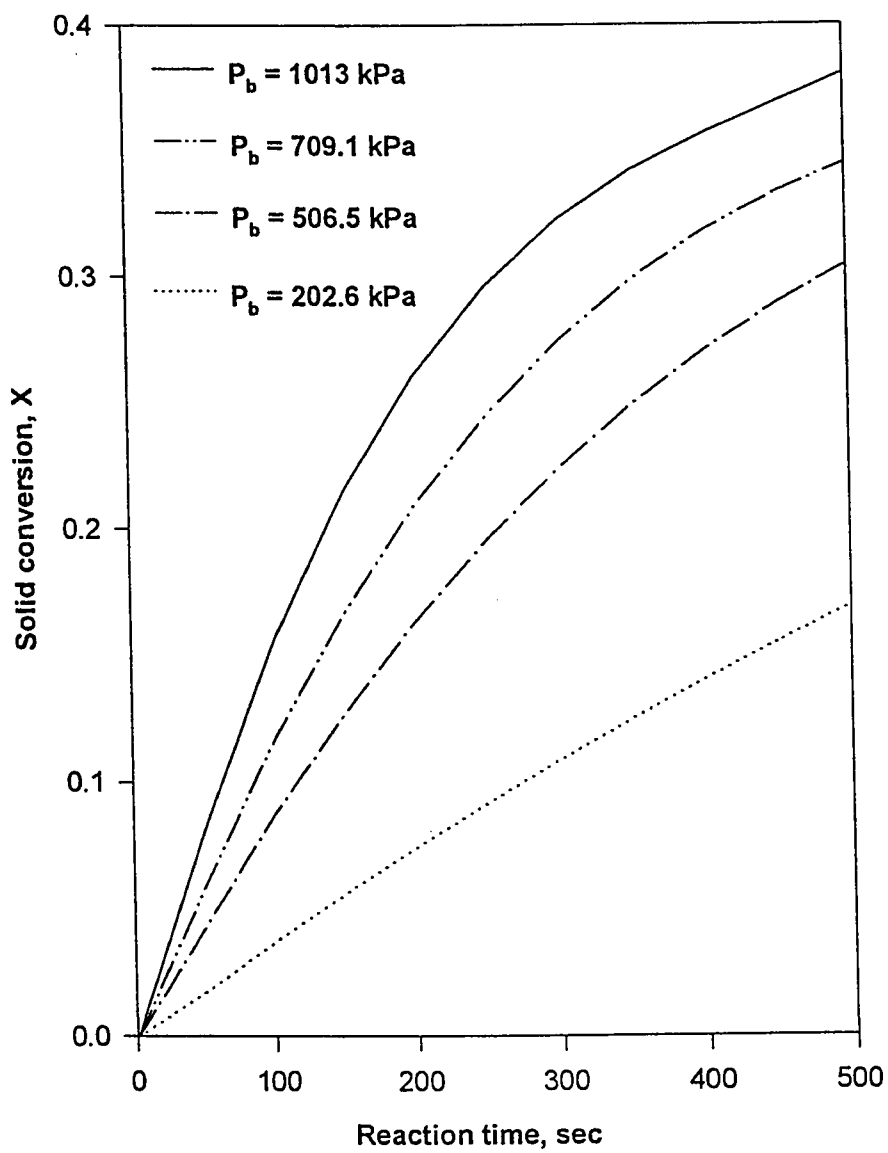


Figure 6.25. Effect of bulk Pressure on overall solid conversion at $T_b = 1173$ K.

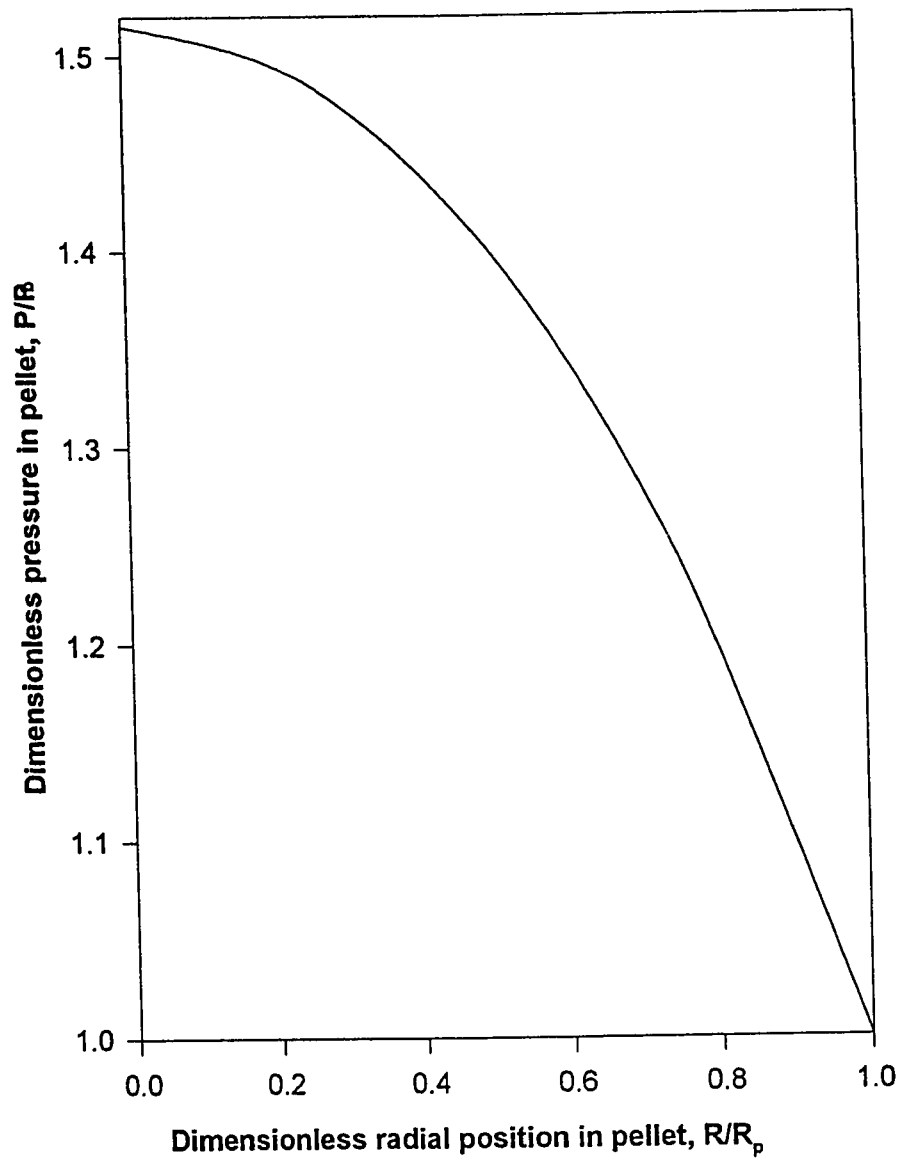


Figure 6.26. The radial pressure distribution at : $t = 480$ s, $GXT = 0.093$,
 $T_b = 1173$ K, $P_b = 101.3$ kPa. and $R_p = 3.28 \times 10^{-4}$ m.

lower conversion attained in this case could be attributed in part to the high bulk gas temperature effect explained in Section 6.3.1 and, of course, in part to the presence of two additional reactions in the system. However, Figures 6.21 - 6.24 clearly illustrate the drastic effect of increasing the bulk pressure on both the grain and overall conversions. Summary of the effect of bulk pressure on the overall conversion over the pressure range considered for reaction time of up to 500 seconds is presented in Figure 6.25. The explanation to this trend lies in the excessive pressure build up inside the pellet resulting in a steep pressure gradient and that provides severe resistance to the inward diffusional process and facilitates diffusion of product gases out of the pellet. Figure 6.26 shows the dimensionless radial pressure distribution for a pellet with a half thickness $R_p = 3.28 \times 10^{-4}$ m after 480 seconds of reaction. Pressure build up of about 50 % is seen at the inner core of the pellet. In conclusion, these figures have closely established the sensitivity of the overall solid conversion to bulk pressure changes and the behavior is very consistent with expectations.

6.3.3 Effect of Inert Gas in the Bulk Stream

The influence of inert gas in the bulk stream on the time - conversion relationship has been computed for $T_b = 1173$ K and $P_b = 101.3$ kPa. The inert gas considered in this case is nitrogen. Mole fraction of N_2 in the bulk stream, X_{bi} , is varied from 0 to 0.5 and the results are presented in Figures 6.27 - 6.29. These figures show the conversion of each of the solid grain - types: carbon, NiO and Fe_2O_3 respectively up to 7 minutes of reaction. With increasing inert gas, the overall conversion drops. This is because the amount of gaseous reactants (H_2 and CO_2) that diffuse into the pellet from the bulk

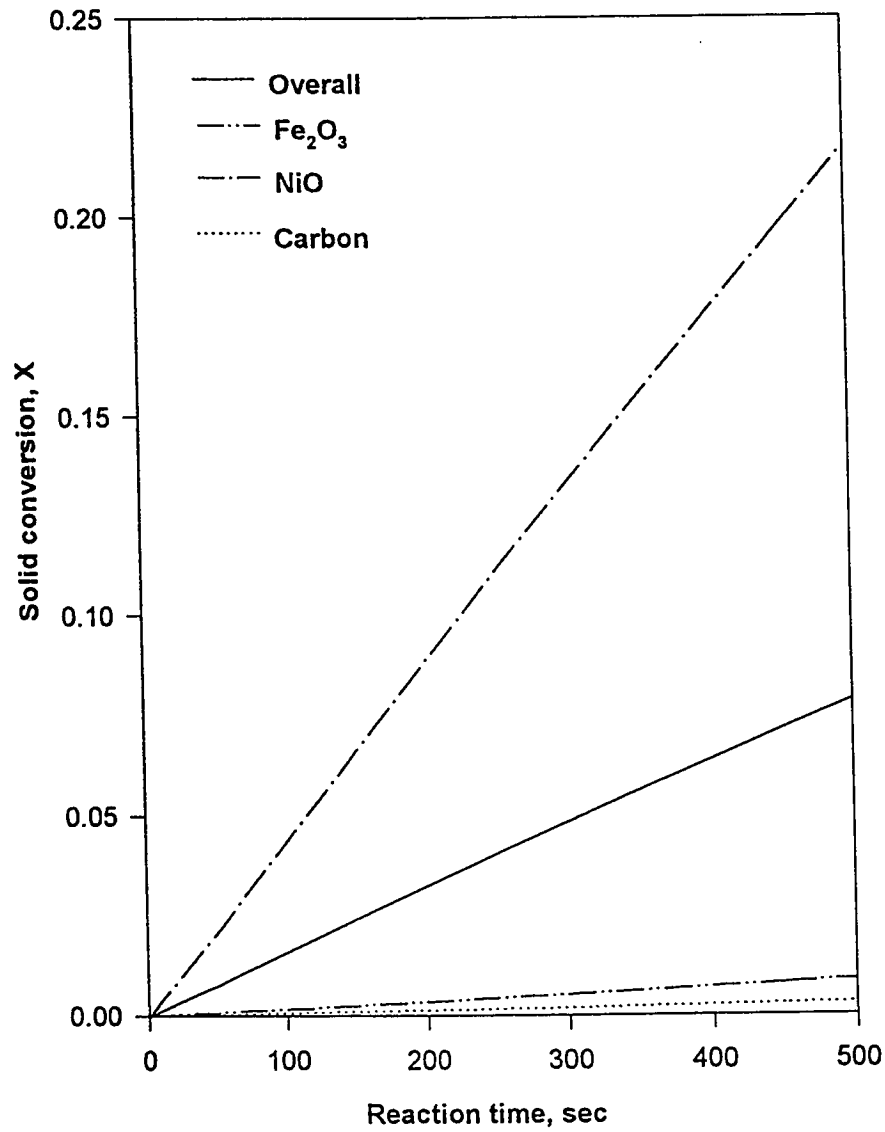


Figure 6.27. Effect of inert gas (N₂) in the bulk stream on conversion at:
 $T_b = 1173$ K $P_b = 101.3$ kPa. and $X_{bi} = 20\%$.

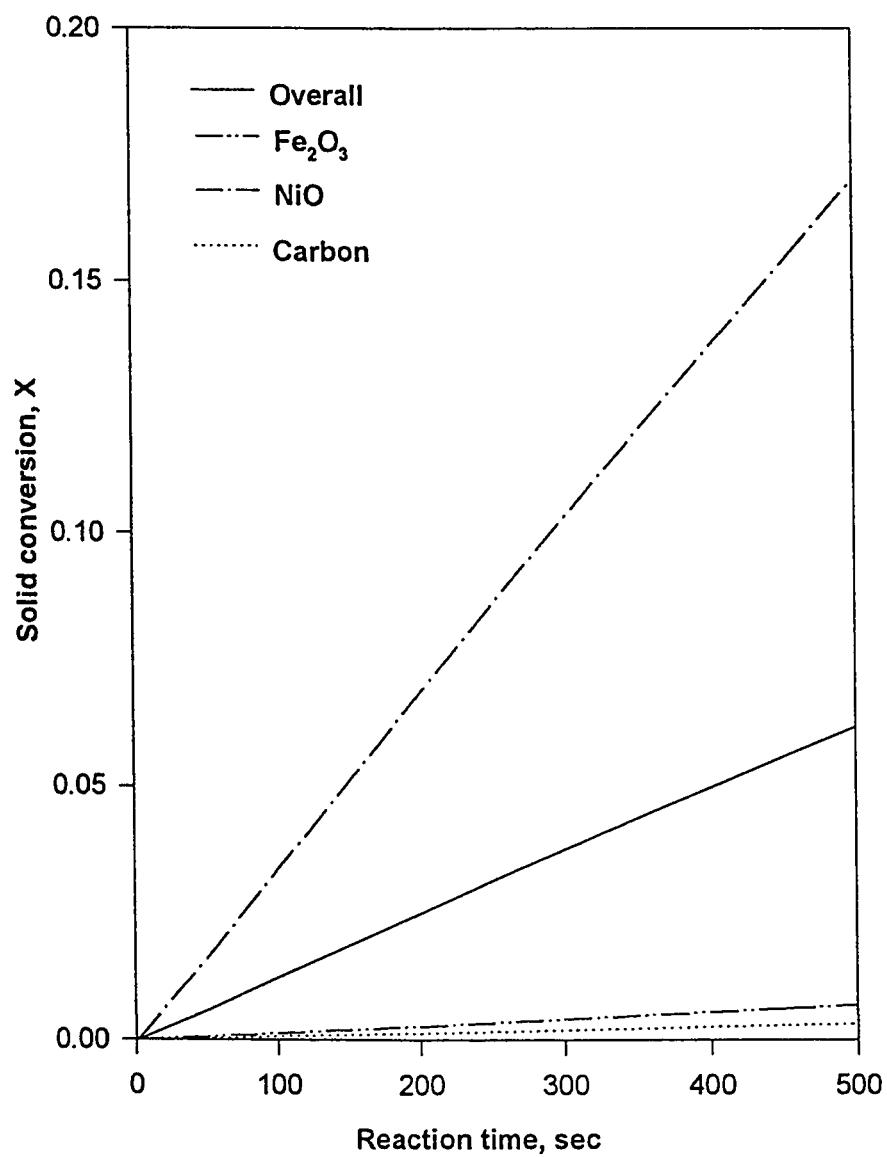


Figure 6.28. Effect of inert gas (N₂) in the bulk stream on conversion at:
 $T_b = 1173$ K $P_b = 101.3$ kPa. and $X_{bi} = 30\%$.

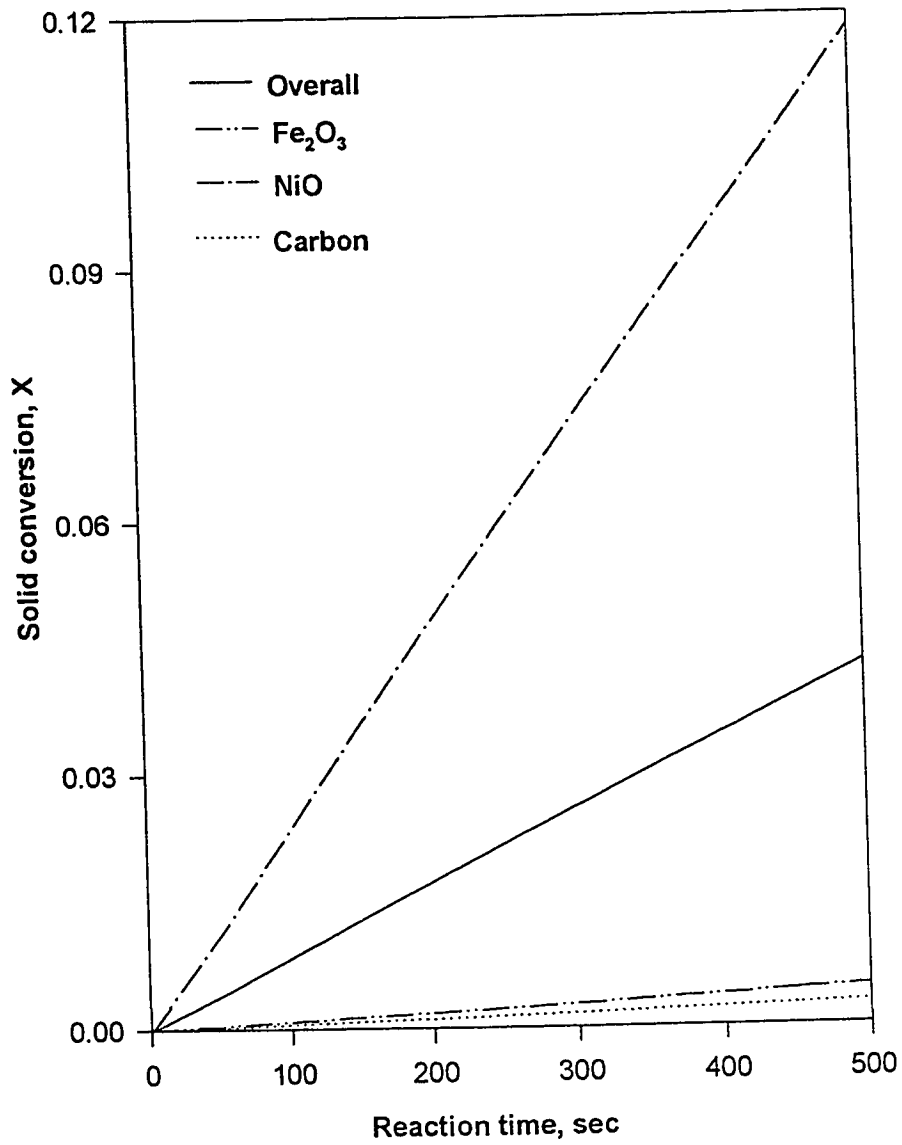


Figure 6.29. Effect of inert gas (N₂) in the bulk stream on conversion at:
 $T_b = 1173 \text{ K}$ $P_b = 101.3 \text{ kPa}$. and $X_{bi} = 50\%$.

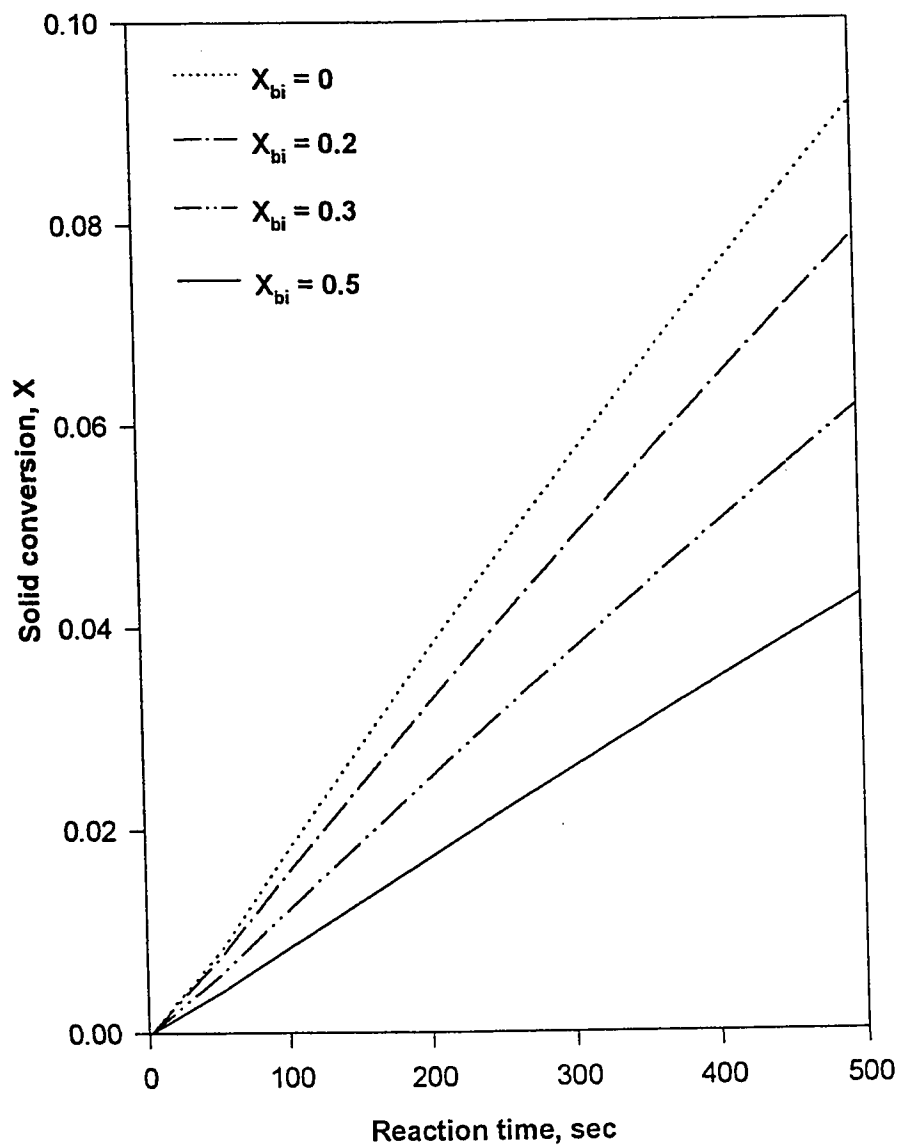


Figure 6.30. Effect of inert gas (N_2) in the bulk stream on overall solid conversion at: $T_b = 1173$ K, $P_b = 101.3$ kPa.

gas stream is proportionately decreased with increasing inert concentration. This is, however, offset by the products of the WGS reaction (H_2 and CO_2). Thus, the effect of the inert gas in the bulk stream on the conversion is not as pronounced as would otherwise appear. Figure 6.30 presents this effect in summary over the range considered.

6.3.4 Effect of Pellet Porosity

The pellet porosity is especially a very important parameter that helps interpret several aspects of the processes taking place inside the pellet. Figures 6.31 - 6.34 present the effect of pellet porosity, ε , on conversion at $T_b = 1173 \text{ K}$ and $P_b = 101.3 \text{ kPa}$. The pellet porosity is varied from 0.1 to 0.8 (the base case is 0.556). The increase in the overall conversion from about 2 % with $\varepsilon = 0.1$, to about 20 % with $\varepsilon = 0.8$ is clearly seen from these figures.

At a porosity of 0.1, the pore diameter is correspondingly small and thus higher internal surface area per pore for the reaction. However, the number of pores becomes correspondingly small and this also creates steep diffusional resistance to the reactant gas, which is at atmospheric pressure. And at the early stages of the reaction process, diffusional steps can be envisaged to be faster than the reaction owing largely to the smaller pressure gradients along the radius of the pellet and to the induction period explained previously. Thus, chemical reaction can be considered to be limiting at the early stages of the reaction and consequently, hindering the diffusional processes (because of small pore diameter) for the time range of 3 minutes and hence retards the overall conversion. This observation is consistent with

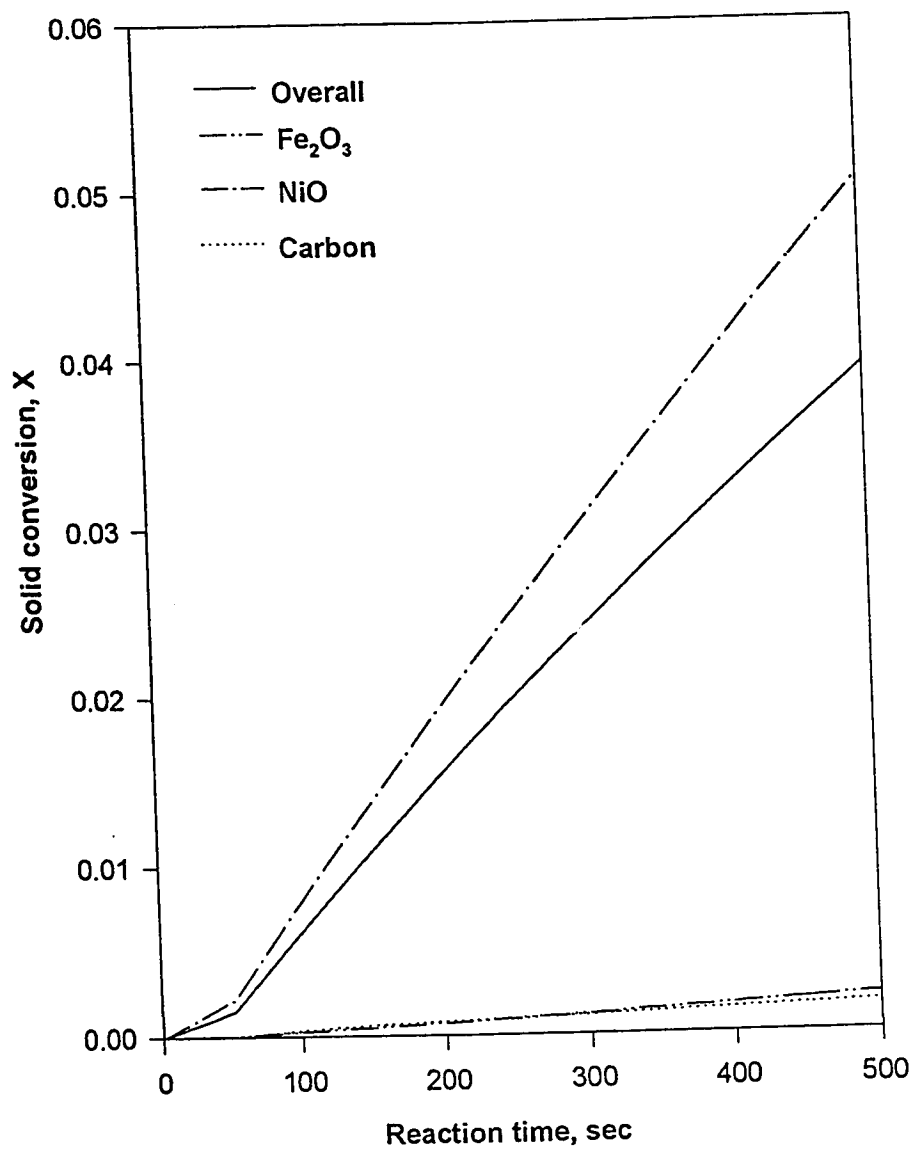


Figure 6.31. Effect of pellet porosity on conversion at: $T_b = 1173$ K,
 $P_b = 101.3$ kPa. and $\varepsilon = 0.1$

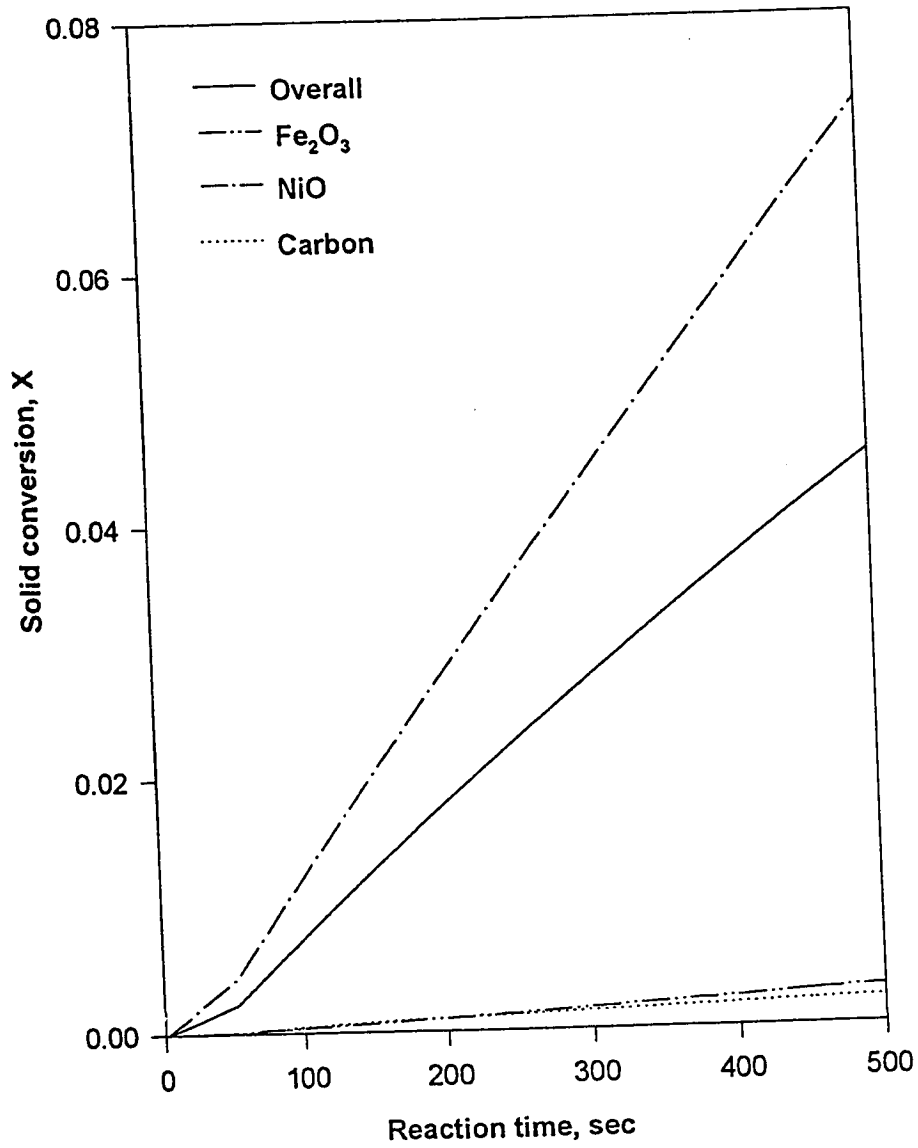


Figure 6.32. Effect of pellet porosity on conversion at: $T_b = 1173$ K,
 $P_b = 101.3$ kPa. and $\varepsilon = 0.2$

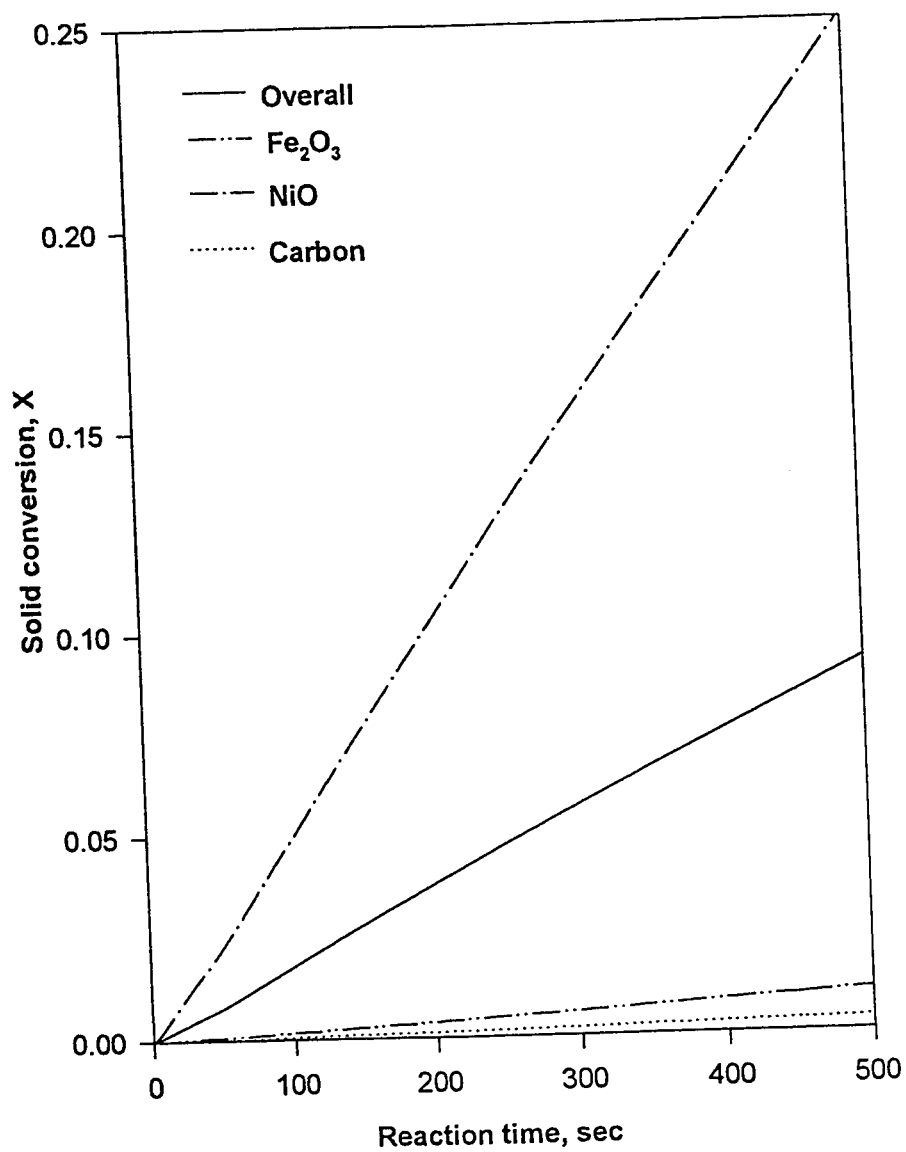


Figure 6.33. Effect of pellet porosity on conversion at: $T_b = 1173$ K,
 $P_b = 101.3$ kPa. and $\varepsilon = 0.556$

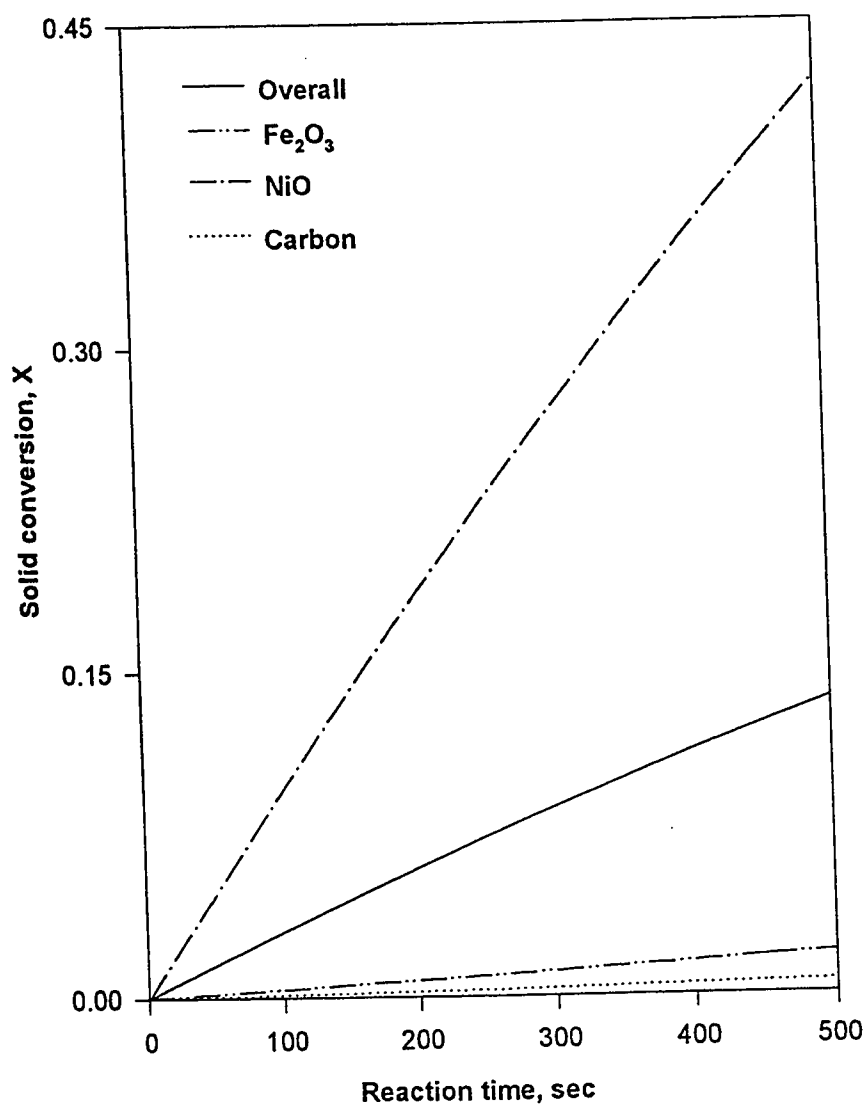


Figure 6.34. Effect of pellet porosity on conversion at: $T_b = 1173$ K,
 $P_b = 101.3$ kPa. and $\varepsilon = 0.8$

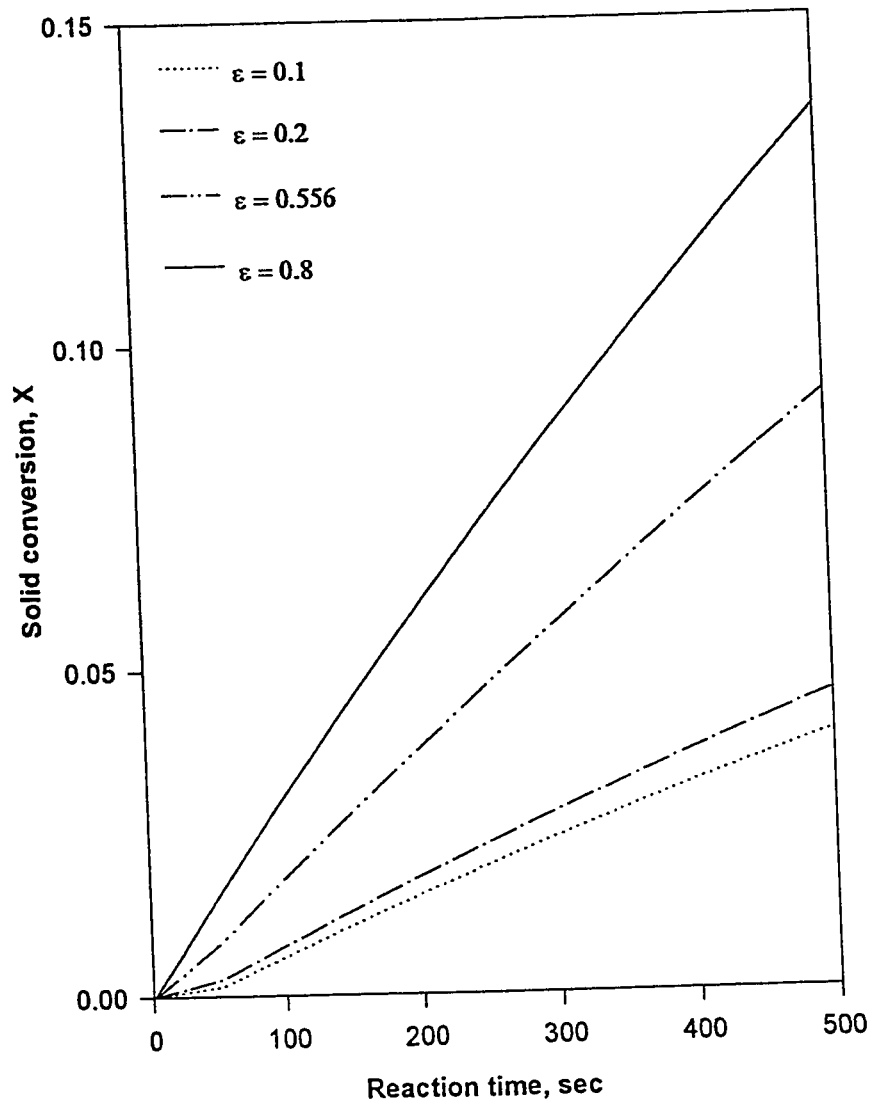


Figure 6.35. Effect of pellet porosity on overall solid conversion at:
 $T_b = 1173$ K, $P_b = 101.3$ kPa.

theory and the experimental results. The relative magnitude of the influence of pellet porosity over the range considered is presented in Figure 6.35.

6.3.5 Effect of Inert Solid Inside Pellet

The effect of inert solid inside the pellet matrix on conversion at $T_b = 1173$ K and $P_b = 101.3$ kPa for inert weight fraction, W_{fi} , over the range 5 - 50 % is shown in Figures 6.36 - 6.39. The inert solid considered in this investigation is silicon, Si. As can be seen from the figures, the influence of inert solid on the conversion of solid is in line with the trend expected. Increase in fractional composition of inert solid, W_{fi} , decreases the conversion. It should be noted that the total weight of the pellet is kept constant while varying the amount of inert solid inside. And therefore, increase in inert solid content invariably amounts to proportional decrease of the active reactants. Thus, the explanation to the trend observed comes principally from the increase in diffusion path of the reactant gases, which is imminent with increases in inert on one hand and overall decrease in active (reacting) components in the solid matrix on the other. To buttress this point further, comparison of the effects of 5% and 50% inert weight fraction shows that, the overall conversion attained with 5 % inert is approximately twice that attained with 50 % inert at the same reaction time as is clearly shown in Figure 6.40.

It may be worthwhile to note that, if the overall pellet weight is varied commensurate with the increase in inert solid, the conversion trend could be seen to be reverse of what is illustrated in Figure 6.40. The explanation comes from the fact that, the particles near the surface expand resulting in pore closure for the case without inert, whereas, the presence of inerts prevents

complete pore closure and the amount of inerts present would therefore significantly affect the total solid conversion in the reverse direction to what is observed in Figure 6.40.

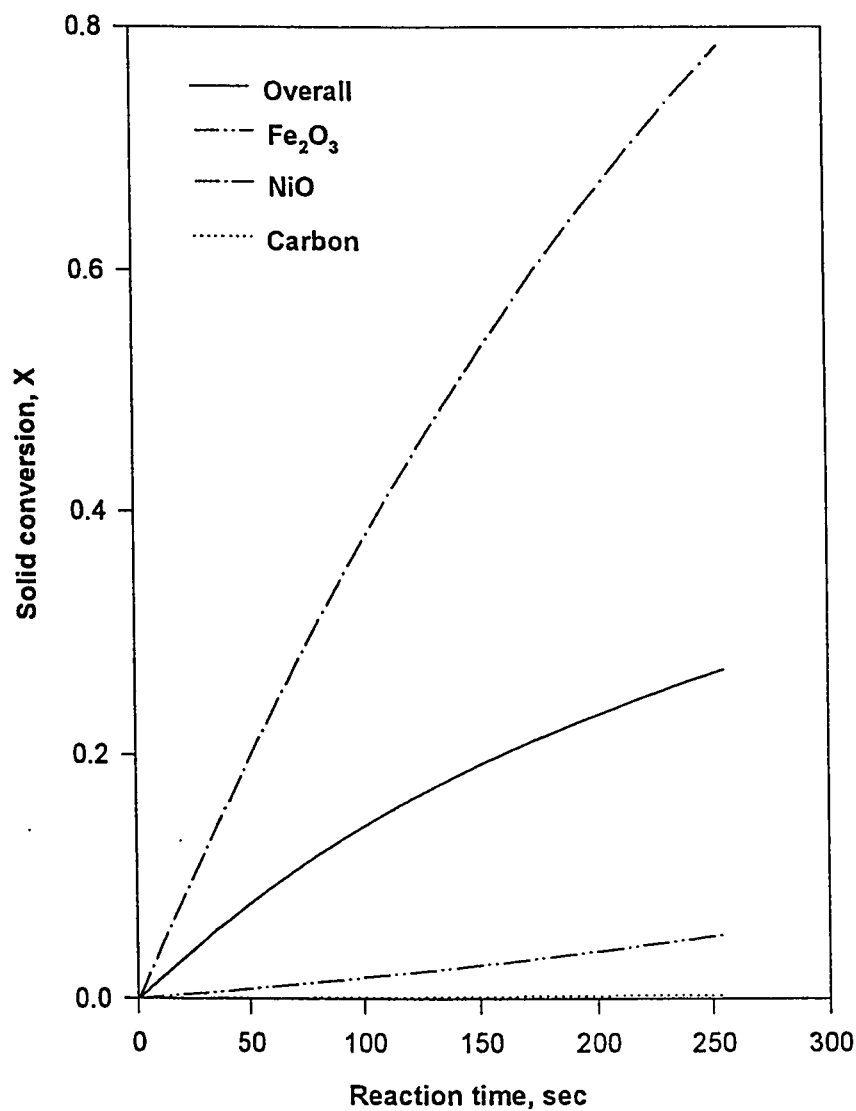


Figure 6.36. Effect of inert solid (Si) inside solid matrix on conversion at:
 $T_b = 1173$ K, $P_b = 101.3$ kPa. and $W_{fi} = 5\%$.

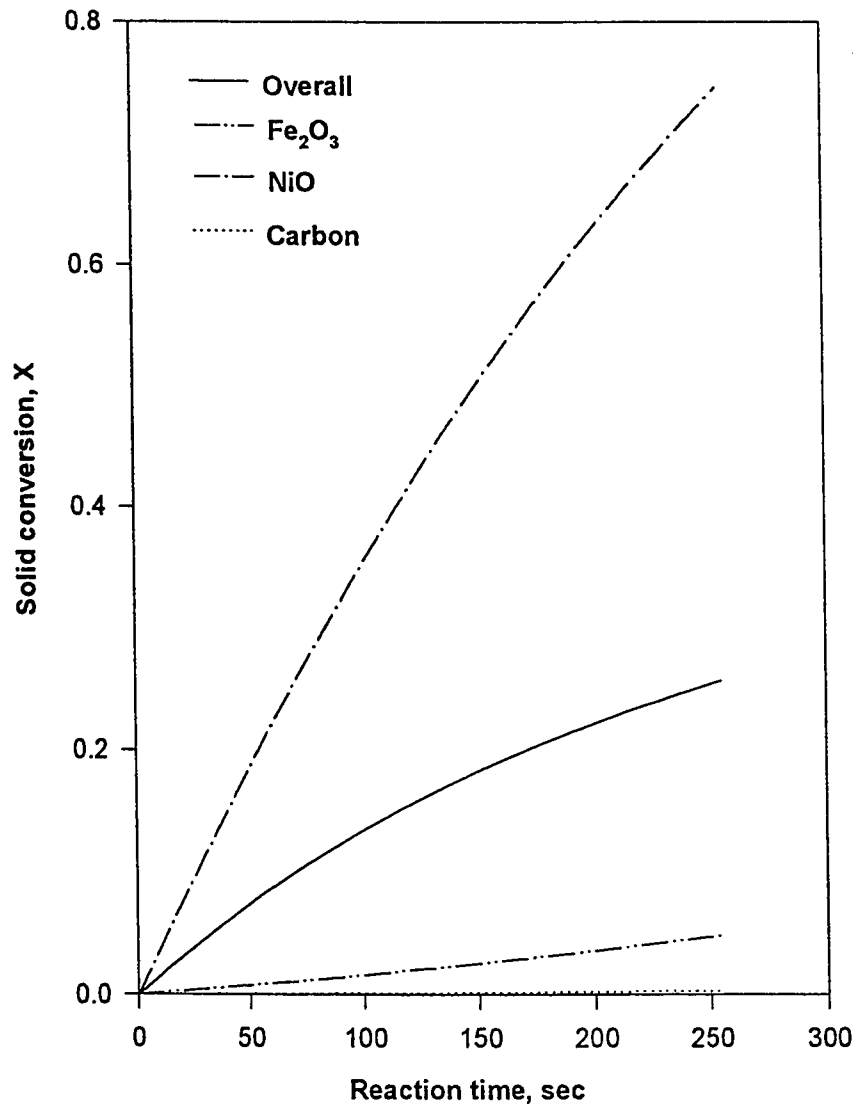


Figure 6.37. Effect of inert solid (Si) inside solid matrix on conversion at:

$T_b = 1173$ K, $P_b = 101.3$ kPa. and $W_{fi} = 10\%$.

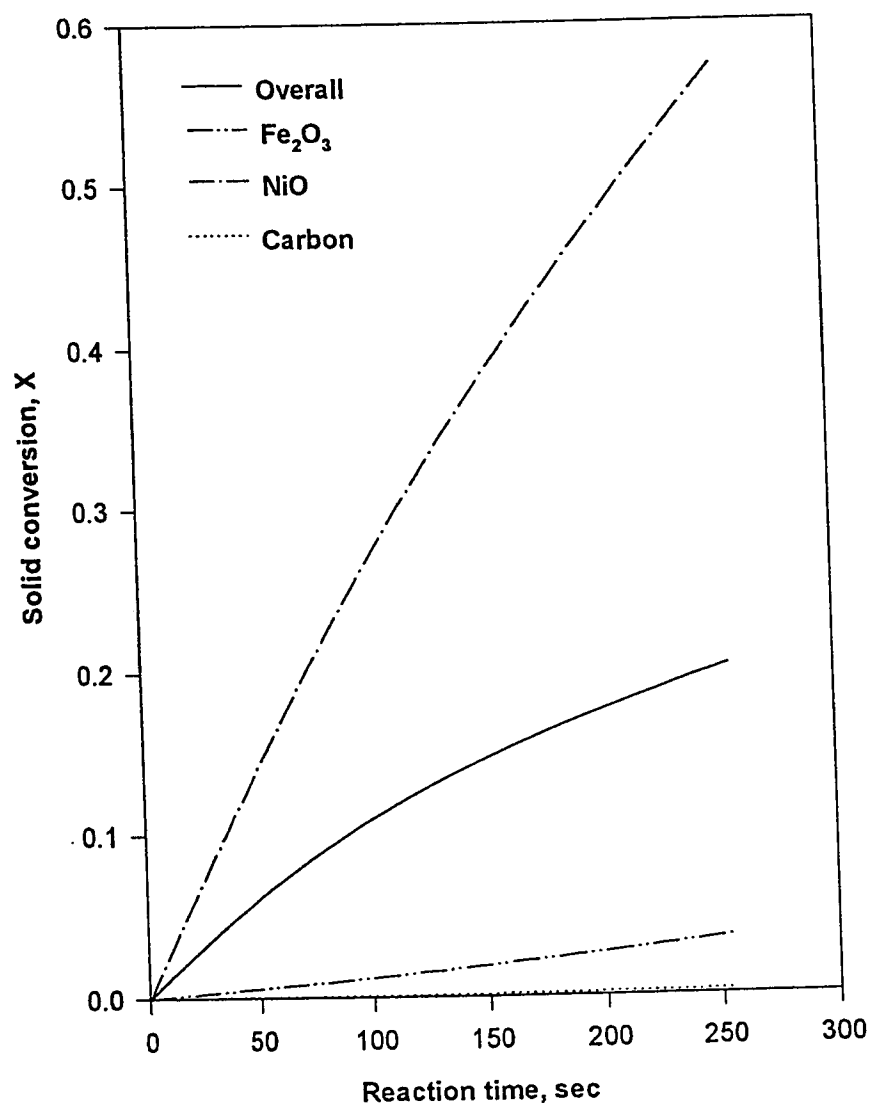


Figure 6.38. Effect of inert solid (Si) inside solid matrix on conversion at:

$T_b = 1173$ K, $P_b = 101.3$ kPa. and $W_{fi} = 30\%$.

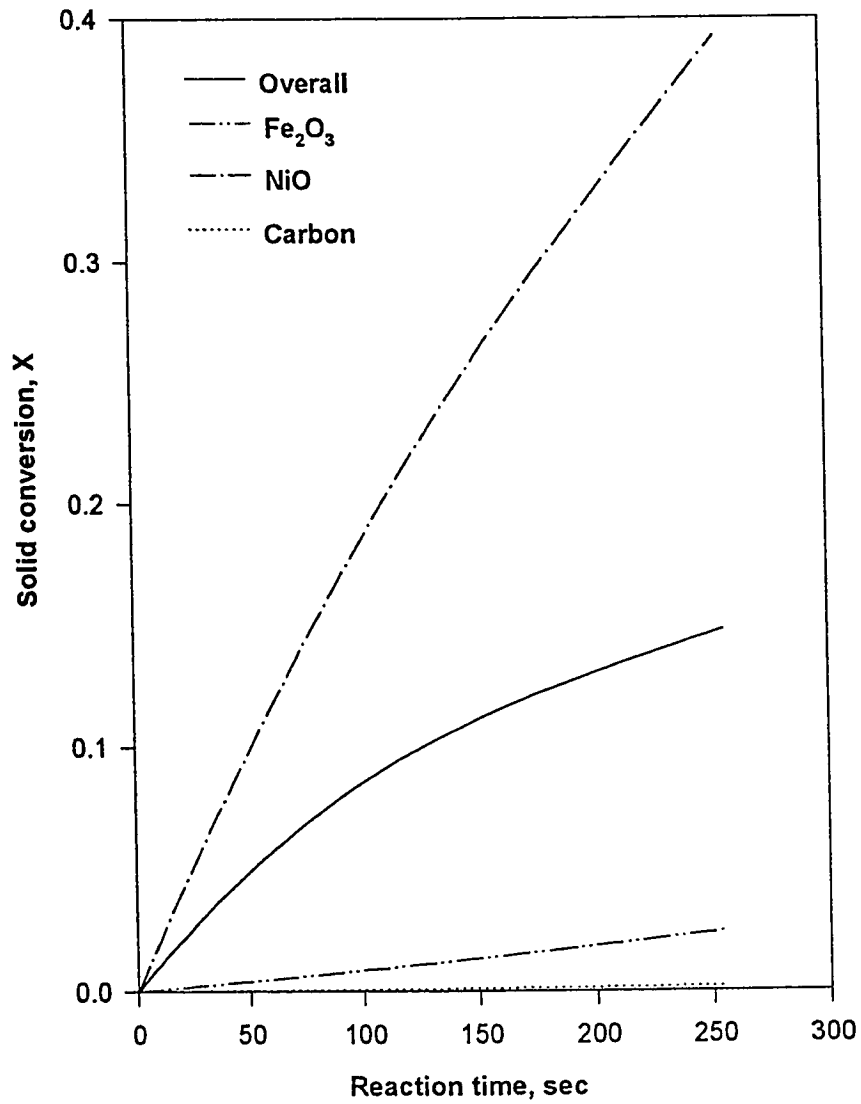


Figure 6.39. Effect of inert solid (Si) inside solid matrix on conversion at:
 $T_b = 1173$ K, $P_b = 101.3$ kPa. and $W_{fi} = 50\%$.

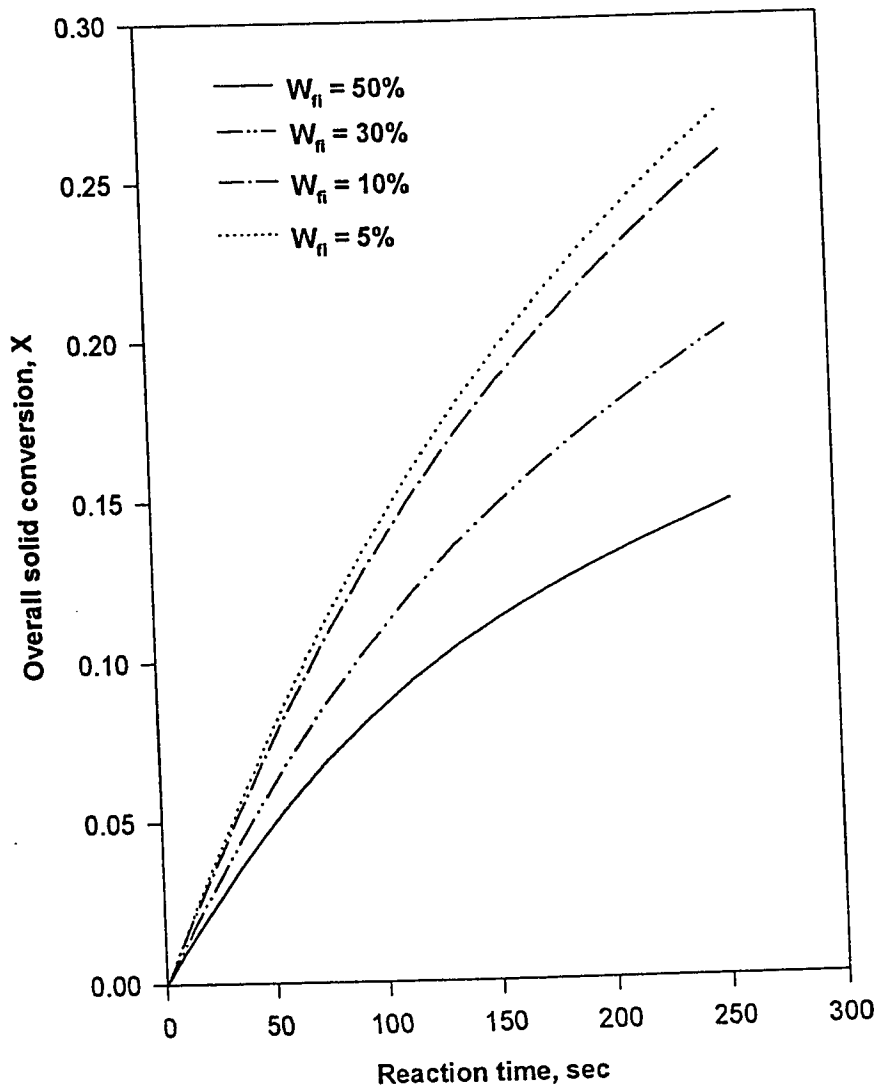


Figure 6.40. Effect of inert solid (Si) inside solid matrix on overall conversion at: $T_b = 1173$ K, $P_b = 101.3$ kPa.

CHAPTER 7

CONCLUSIONS AND RECOMMENDATIONS

7.1 Conclusions

- i) A unified approach has been used to develop a rigorous multi gas - solid reaction model successfully for the first time. The model was verified by comparing the simulation results with experimental data for two asymptotic cases; carbon gasification at 800 - 1100°C and NiO / Fe₂O₃ mixture reduction with hydrogen at 581 - 608 K. The match between model and experiment was found to be satisfactory in general.

- ii) Multicomponent simulation results that resulted from a consideration of four sequential reactions (carbon gasification, reduction of nickel oxide / hematite mixture and water gas shift reaction) are presented. From the analysis of the effects of external and internal mass and heat transfer, it was found that, the reactions studied are both diffusion and kinetic controlled, i.e., intermediate regime, in which the magnitude of each varies with the individual reactions. It is established that, the external mass and heat transfer effects are negligible for the pellet sizes studied, except for extremely rapid reactions where there is the possibility of external mass transfer resistance and temperature gradients of some significance.

- iii) A detailed parametric study shows that, increasing bulk pressure enhances both the grain and the overall solid conversion and this is shown to be resultant from the excessive pressure build up inside the pellet leading to severe resistance to the inward diffusional process. The overall solid conversion has been shown to increase with increasing bulk temperature up to 1173 K, above which decrease resulted. This was attributed primarily to the competitiveness of the reactions leading to fast consumption of reactants at elevated temperatures.
- iv) As for the results of the influences of pellet porosity and inert solid on conversion, it was shown that, increasing these parameters enhances the solid conversion. Increase in pellet porosity results in smaller pressure gradients and hence reduced resistance in the path of the diffusing gases while increase in fractional composition of inert solid results in increase in the diffusion path of the reactant gases.

7.2 Recommendations

- i) It is recommended that, experiments with large number of reactions and reactants, consistent with this formulation be carried out and the results compared with model prediction.
- ii) The principal significance of the single pellet model is in its integration in the design and simulation of a number of commercially important systems such as Fluidized and Fixed Bed Reactors. Examples include pyrolysis of wood in circulating fluidized bed and hydrodesulfurization

- in fixed bed among others. Therefore it is recommended that the generalized model developed be integrated over such systems.
- iii) The model can be extended to simulate a number of interesting environmental problems. Typical areas include decay (decomposition) and evaporation of volatile organic compounds in the subsurface. In such studies, the soil particles are envisaged as agglomerating to form the pellet.
 - iv) Sintering becomes very significant at elevated temperatures. Since most gas - solid reactions take place at high temperatures and considering the general nature of the model developed, the effect of sintering should be incorporated in the model formulations.
 - v) The viscous flow parameters become especially important at elevated pressures. This effect has already been established in the literature. Therefore, the pressure expression should be modified to account for non - ideality, thus, making it possible to simulate very high pressure scenarios.
 - vi) The effect of instability in gas - solid reaction leading to multiplicity of steady states is an important consideration, especially, in view of the general nature of the scheme developed. Investigation of this aspect is highly recommended in future work.

NOMENCLATURE

a, b, c	stoichiometric coefficients
a_{ij}, b_{ik}	coefficients of gaseous component A_j and Solid B_k respectively, in reaction i
A, C	gaseous components
A_j	gaseous component j as reactant or product
$(Ar)_i$	specific reaction surface or area per unit volume of gross reaction space, m^{-1}
B, D	solid components
B_k	solid component k as reactant or product
B_0	permeability of the medium, m^2
C_{A_j}	concentration of gaseous component A_j , mol/m^3
$C_{A_{j0}}, C_{A_{jN}}, C_{A_{jb}}$	initial, surface and bulk concentrations of gaseous component A_j , mol/m^3
C_p^e	effective heat capacity of pellet, $kJ/kg.K$
C_{pA}	heat capacity of component A_j , $kJ/kmol.K$
C_{pG}	heat capacity of gas, $kJ/kmol.K$
C_{pS}	heat capacity of solid, $kJ/kg.K$
$C_{A_j,inf}$	interface concentration of gaseous component A_j , mol/m^3
d_p	characteristic mean pore diameter, m
dr	grid size, m
dt	time step, s
$D_{A_j}^p$	effective diffusivity of component A_j through the product
D_{ij}	binary diffusivity, m^2/s

D_{ij}^e	effective binary diffusivity, m^2/s
$D_{i,k}^e$	effective Knudsen diffusivity, m^2/s
$f_i(\vec{\mathbf{A}})$	the intrinsic reaction rate term per unit surface area for reaction i based on a pivot component
$\vec{\mathbf{F}}$	vector of residuals, Newton's method
F_g	grain shape factor
$F(i)$	residual of model equation at grid i
F_p	pellet shape factor
GX_{Bk}	global conversion of grain types B_k
GXT	Overall pellet conversion
h_c	external heat transfer coefficient, $W/m^2.K$
ΔH_i	heat of reaction i , $kJ/gmol$
$\underline{\underline{J}}$	Jacobian matrix
k_1, k_2	rate constants
k^e	effective thermal conductivity of pellet, $W/m.K$
k_c	mass transfer coefficient, m/s
k_m	thermal conductivity of gas mixture, $W/m.K$
k_s	thermal conductivity of solid, $W/m.K$
M_{Bk}	molecular weight of grain type B_k , $kg/kmol$
n	time level
n_{A_j}, n_{B_k}	number of moles of components A_j and B_k respectively
N	number of grid points
N_{A_j}	flux of component A_j , $mol/m^2.s$
N_g	number of gaseous components
$N_{A_j}^P$	flux through the product layer of component A_j , $mol/m^2.s$
N_r	number of reactions
N_s	number of solid components

Nu	Nusselt number
P_1, P_0	structural parameters
P	pressure inside the pellet, <i>kPa</i>
P_b	bulk pressure, <i>kPa</i>
P_c	critical pressure, <i>kPa</i>
P_r	Prandtl number
$r_{C_{Bk}}$	reaction front radius of grain type B_k , μm
$r_{g_{Bk}}$	radius of grain type B_k at any time t , μm
r	location of grid points, m
$r_{O_{Bk}}$	initial radius of grain type B_k , μm
R_p	radius of pellet, m
R	radius of pellet at any time t , m
R_g	universal gas constant, $8.314 J/gmol.K$
Re	Reynolds number
Sc	Schmidt number
Sh	Sherwood number
T_b	bulk temperature, K
T^r	reference temperature (298 K), K
T_c	critical temperature, K
T_N	pellet surface temperature, K
T_r	reduced temperature, K
T	temperature in pellet, K
t	time of reaction, s
T_c	critical temperature, K
$V_{0,j}, V_j$	initial and instantaneous pore volume of the j th cell, m^3
W_{fi}	weight fraction of inert solid (Si) inside pellet
x_{Bk}	local conversion of grain type B_k
x_i	mole fraction of specie i
X(i)	solution value at grid i

\vec{X}	solution vector, Newton's method
X_{bi}	mole fraction of inert gas (N_2) in the bulk stream
Z_V	ratio of molal volume of product to reactant

Greek symbols

β	pellet shrinkage or swelling parameter
$\vec{\delta}$	correction to the solution vector
ε	pellet porosity at any time t
ε_{Bk}	porosity of the product layer
ε_{oBk}	initial porosity of grain type B_k
μ	viscosity of bulk gas, cp
μ_i	viscosity of component i , $kg/m.s$
μ_m	viscosity of gas mixture, $kg/m.s$
ν_{A_j}	stoichiometric coefficient of component A_j
Φ_{ij}	constant in the Wassiljewa's equation
ρ_{Bk}	density of grain type B_k , kg/m^3
ρ_s	density of solid, kg/m^3
σ	Boltzmann constant, $5.735 \times 10^{-8} W/m^2.K^4$
σ_{ij}	constant in the Lennard - Jones 12 - 6 potential function
τ	tortuosity factor
θ	emissivity
ω_{ij}	collision integral function

Abbreviations

CCM	Crackling Core Model
DGM	Dusty Gas Model

NM	Network Model
ODE	Ordinary Differential Equation
PDE	Partial Differential Equation
PM	Pore Model
PPP	Particle - Pellet Model
RPM	Random Pore Model
SIM	Sharp Interface Model
TGA	Thervogravimetric Analysis
VRM	Volume Reaction Model
WGS	Water - gas - Shift

BIBLIOGRAPHY

- Abu-El-Shar, W. Y., Experimental Assessment of Multicomponent Gas Transport Flux Mechanisms in Subsurface Systems, Ph.D. Thesis, University of Michigan, (1993).
- Ausman, J. M. and C. C. Watson, Mass Transfer in a Catalyst Pellet during Regeneration, *Chem. Eng. Sci.* **17**, 323 (1962).
- Avrami, M., Kinetics of Phase Change II. Transformation - time Relations for Random Distribution of Nuclei, *J. Chem. Phys.* **8**, 212 (1940).
- Behie, A. L., D. Berk, A. Jones, B. H. Lesser, and G. M. Gaucher, The Production of the Antibiotic Patulin in a 3-Phase Fluidized bed Reactor II. Longevity of the Biocatalyst, *Can. J. Chem. Eng.* **62**, 120 (1984).
- Bhatia, S. K. and D. D. Perlmutter, A Random Pore Model for Fluid - Solid Reactions: II. Diffusion and Transport Effects, *AIChE J.* **27**, 247 (1981).
- Bhatia, S. K. and D. D. Perlmutter, A Random Pore Model for Fluid Solid Reactions: 1. Isothermal, Kinetic Control, *AIChE J.* **26**, 379 (1980).
- Bhatia, S. K., Analysis of Distributed Pore Closure in Gas - Solid Reactions, *AIChE. J.* **31**, 642 (1985).

- Bird, R. B., W. E. Stewart, and E. N. Lightfoot, Transport Phenomena, 3rd ed., McGraw-Hill, New York, (1977).
- Bowen, J. H. and C. K. Chen, A Diffuse Interface Model for Fluid - Solid Reactions, *Chem. Eng. Sci.* **24**, 1829 (1969).
- Cao, G., Varma, A. and Strieder, W., Approximate Solutions for Nonlinear Gas - Solid Noncatalytic Reactions, *AIChE J.* **39**(5), 913, (1993).
- Calvelo, A. and J. M. Smith, Intrapellet Transport in Gas - Solid Reactions, *Chemeca Proceeding*, No. 3, 1 (1970).
- Carnahan, B., H. A. Luther, and J. O. Wilkes, Applied Numericals Method, John Wiley and Sons Inc., New York, (1969).
- Chilton, T. H., and A. P. Colburn, *Ind. Eng. Chem.* **26**, 1183 (1934).
- Christman, P. G. and T. F. Edgar, Distributed Pore - Size Model for the Sulfation of Limestone, *AIChE J.* **29**, 388 (1983).
- Christman, P. G., and T. F. Edgar, Distributed Pore Size Model for the Sulfation of Limestone, *AIChE Meet., Chicago* (1980).
- Chrostowski, J. W. and C. Georgakis, Pore Plugging Model for Gas - Solid Reactions, *ACS Symp. Ser., 65 (Chem. React. Eng., Houston)*, 225-37 (1978).
- Deb Roy, T. and K. P. Abraham, An Analysis of the Pressure Build - up Inside a Reacting Pellet During Gas - Solid Reactions, *Met. Trans.* **5**, 349 (1974).

- Dogu, T., A. Keshi, and G. Dogu, Single Pellet Moment Method for Analysis of Gas - Solid Reactions, *AIChE J.* **32**(5), 743 (1986).
- Doraiswamy, L. K. and B. D. Kulkarni, Chemical Reactor Design, eds.; Carberry, J. J. and A. Varma, pg. 239, Marcel Dekker Inc., New York (1987).
- Doraiswamy, L. K. and M. M. Sharma, Heterogeneous Reactions: Analysis, Examples and Reactor Design, Gas - Solid and Solid - Solid Reactions, vol. 1, pg. 450, John Wiley and Sons, New York (1984).
- Dossari, C. G., J. W. Tierney and Y. T. Shah, A Gas - Solid Reaction with Non - uniform Distribution of Solid - Reactant, *AIChE J.* **34**(11), 1878 (1988).
- El-Rahaiby, S. K., and Y. K. Rao, The Kinetics of Reaction of Iron oxide at Moderate Temperatures, *Met. Trans.* **10B**, 257 (1979).
- Evans, J. W., Gas- Solid Reactions : The Viscous Flow Term, *Can. J. Chem. Eng.* **50**, 811 (1972).
- Fahim, M. A. and J. D. Ford, Gas - Solid Reactions - II: Reduction of Cobalt sulfide in the presence of Calcium oxide, *Can. J. Chem. Eng.* **56**, 730 (1978).
- Fahim, M. A., N. Wakao and J. D. Ford, Gas - Solid Reactions I: A Grain Cell Model for Complex Reactions, *Can. J. Chem. Eng.* **56**, 725 (1978).
- Froment, G. F. and K. B. Bischoff, Chemical Reactor Analysis and Design, 2nd ed., pg. 215, John Wiley and Sons Inc., Singapore (1990).

- Gavalas, G. R., A Random Capillary Model with Application to Char Gasification at Chemically Controlled Rates, *AIChE J.* **26**, 577 (1980).
- Geankoplis, C. J., Mass Transport Phenomena, Holt : Reinehart and Winston, (1972).
- Georgakis, C., C. W. Chang and J. Szekely, A changing Grain Size Model for Gas - Solid Reactions, *Chem. Eng. Sci.* **34**, 1072 (1979).
- Gibson, J. B. and D. P. Harrison, The Reaction between Hydrogen sulfides and Spherical Pellets of Zinc oxide, *I & EC Proc. Des. Dev.* **19**, 231 (1980).
- Hashimoto, K. and P. L. Silveston, Gasification: Part I. Isothermal Kinetic Control Model for a Solid with a Pore size Distribution, *AIChE J.* **19**, 259 (1973).
- Hassam, M. S., Studies in Gas - Solid Reactions, Ms. Thesis, University of Calgary, (1987).
- Hastaoglu, M. A., Modelling of Packed Tower: Mass and Heat Transfer with Reaction, *Fuel*, in press (1995).
- Hastaoglu, M. A. and F., Berruti, A Gas-Solid Reaction Model for Flash Wood Pyrolysis, *Fuel* **68**, 1408 (1989).
- Hastaoglu, M. A. and M. G. Karnann, Modeling of Catalytic Carbon Gasification, *Chem. Eng. Sci.* **5**, 1121 (1987).

- Hastaoglu, M. A. and M. S. Hassam, A Gas-Solid Reaction Model - Variable Temperature, Pressure and Structural Parameters, *Can. J. Chem. Eng.* **66**, 419 (1988).
- Hastaoglu, M. A. and M. S. Hassam, Application of a General Gas - Solid Reaction Model to Flash Pyrolysis of Wood in a Circulating Fluidized Bed, *Fuel*. (in press) (1995).
- Haynes, H. W. Jr., Calculation of Gas Phase Diffusion and Reaction in Heterogeneous Catalysts: The Importance of Viscous Flow, *Can. J. Chem. Eng.* **56**, 582 (1978).
- Hite, R. H. and R. Jackson, Pressure Gradients in Porous Catalysts Pellets in the Intermediate Diffusion Regime, *Chem. Eng. Sci.*, **32**, 703 (1977).
- Ishida, M. and C. Y. Wen, Comparison of Kinetic and Diffusional Models for Gas - Solid Reactions, *AIChE J.* **14**, 311 (1968).
- Jackson, R., Transport in Porous Catalysts, Chem. Eng. Monograph, New York ; Elsevier, (1977).
- Jayaraman, V. K., V. Hlavacek, and J. Puszynski, An Expanding Core Model for a Heterogeneous Non - catalytic Gas - Solid Reactions, *Ind. Eng. Chem. Res.* **26**, 1048 (1987).
- Knudsen, M., Dei gesetze der molekularstromung und die inneren reibungsstromung der gase durch rohen, *Ann. Phys.* **28**, 75 (1909).

- Lindner, B. and D. Simonsson, Comparison of Structural Model for gas -Solid Reactions in Porous Solids, *Chem. Eng. Sci.* **36**, 1519 (1981).
- Luss, D. Sufficient Conditions for Uniqueness of the Steady State Solution in Distributed Parameter Systems, *Chem. Eng. Sci.* **23**, 1249 (1968).
- Luss, D. and A. Amundson, Maximum Temperature Rise in Gas - Solid Reactions, *AIChE J.* **15**, 194 (1969).
- Mantri, V. B., A. N. Gorkarn, and L. K. Doraiswamy, Analysis of Gas - Solid Reactions: Formulation of a General Model, *Chem. Eng. Sci.* **31**, 779 (1976).
- Mason, E. A. and A. P. Malinauskas, Gas Transport in Porous Media: The Dusty Gas Model, Chem. Eng. Monograph, New York; Elsevier, (1983).
- Park, J. and O. Levenspiel, The Crackling Model for the Multiparticle Reaction of Solid Particles, *Chem. Eng. Sci.* **32**, 233 (1975).
- Petersen, E., Reaction of Porous Solids, *AIChE J.* **3**, 443 (1957).
- Ramachandran, P. A. and J. M. Smith, A Single Pore Model for Gas - Solid Non - catalytic Reactions, *AIChE J.* **23**, 353 (1977a).
- Ramachandran, P. A. and J. M. Smith, Effect of Sintering and Porosity changes on the Rate of Gas - Solid Reactions, *Chem. Eng. J.* **14**, 137 (1977b).
- Ramachandran, P. A. and L. K. Doraiswamy, Analysis of Gas - Solid Reactions with Zero - Order Dependency on both Gas and Solid: Concept of Jumping Reaction Zones, *AIChE J.* **28**, 881 (1982).

- Ramachandran, P. A. and L. K. Doraiswamy, Modeling of Non - catalytic Gas-Solid Reactions, *AIChE J.* **30** (4) 637 (1984).
- Ramachandran, P. A. and M. H. Rashid and R. Hughes, A Model for Coke Oxidation from catalysts Pellets in the Initial Burning Period, *Chem. Eng. Sci.* **30**, 1391 (1975).
- Ramachandran, P. A., Analysis of Non - catalytic Reactions following Langmuir - Hinshelwood Kinetics, *Chem. Eng. J.* **23**, 223 (1982).
- Rao, Y. K., Dual - Reaction Model for Hydrogen reduction of Metallic Chlorides, *Trans. Instn. Min. Metall.* **90**, C47 (1981).
- Rao, Y. K., Mechanisms and Intrinsic Rates of reduction of Metallic Oxides, *Met. Trans.* **10B**, 243 (1979).
- Reid, R. C., and T. K. Sherwood, *The Properties of Gases and Liquids*, McGraw-Hill Comp., New York, (1977).
- Reid, R. C., J. M. Prausnitz and B. E. Poling, *The Properties of Gases and Liquids*, 4th ed., McGraw-Hill Comp., New York, (1987).
- Reyes, S. and K. F. Jensen, Estimation of Effective transport Coefficients in Porous Solids based on Percolation Concepts, *Chem. Eng. Sci.* **40**, 1723 (1985).

- Reyes, S. and K. F. Jensen, Percolation Concepts in Modeling of Gas - Solid Reactions - I. Application to Char Gasification in the Kinetic Regime, *Chem. Eng. Sci.* **41**,333 (1986a).
- Reyes, S. and K. F. Jensen, Percolation Concepts in Modeling of Gas - Solid Reactions - II. Application to Char Gasification in the Diffusion Regime, *Chem. Eng. Sci.* **41**, 345 (1986b).
- Reyes, S. and K. F. Jensen, Percolation Concepts in Modeling of Gas - Solid Reactions III. Application to Sulfation of Calcined Limestone, *Chem. Eng. Sci.* **42**(3), 565 (1987).
- Rowe, P. N. and K. T. Claxton, *Trans. Inst. Chem. Eng.* **43**, T231, (1965).
- Sampath, B. S., P. A. Ramachandran and R. Hughes, Modelling of Non - catalytic Gas- Solid Reactions - I. Transient Analysis of the Particle Pellet Model, *Chem. Eng. Sci.* **30**, 125 (1975a).
- Sampath, B. S., P. A. Ramachandran and R. Hughes, Modelling of Non - catalytic Gas- Solid Reactions - II. Transient Simulation of a Packed Bed Reactor, *Chem. Eng. Sci.* **30**, 135 (1975b).
- Satterfield, C. N., Heterogeneous Catalysis in Industrial Practice, 2nd ed., McGrawHill Inc., pg 421, New York, (1991).
- Simons, G. A., and W. T. Rawlins, Reaction of Sulfur dioxide and Hydrogen sulfide with Calcined Limestone, *Ind. Eng. Chem. Proc. Des. Dev.* **19**, 565 (1980).

- Simonsson, D., Reduction of Fluoride by Reaction with Limestone Particles in a Fixed Bed, *Ind. Eng. Chem. Proc. Des. Dev.* **18**, 228 (1979).
- Skelland, A. H. P., Diffusional Mass Transfer, Krieger Publishing Comp., Florida, (1985).
- Sohn, H. Y., The Law of Additive Reaction Times in Fluid - solid Reactions, *Met. Trans.* **9B**, 89 (1978).
- Sohn, H. Y. and H. J. Sohn, The Effect of Bulk Flow due to Volume Change in the Gas Phase on Gas - Solid Reactions: Initially Non - porous Solids, *Ind. Eng. Chem. Proc. Des. Dev.* **19**, 237 (1980).
- Sohn, H. Y. and J. Szekely, A Structural Model for Gas - Solid Reactions with Moving Boundary III. General Dimensionless Representation of Irreversible Reaction between a Porous Solid and a Reactant Gas, *Chem. Eng. Sci.* **27**, 763 (1972b).
- Sohn, H. Y. and J. Szekely, A Structural Model for Gas - Solid Reactions with Moving Boundary IV. Langmuir - Hinshelwood Kinetics, *Chem. Eng. Sci.* **28**, 1169 (1973b).
- Sohn, H. Y. and J. Szekely, Reactions between Solids through Gaseous Intermediates I. Reactions Controlled by Chemical Kinetics, *Chem. Eng. Sci.* **28**, 1789 (1973a).
- Sohn, H. Y. and J. Szekely, The Effect of Intragrain Diffusion on the Reaction between a Porous Solid and a Reactant Gas, *Chem. Eng. Sci.* **29**, 630 (1974).

- Sohn, H. Y. and J. Szekely, The Effect of Reaction Order in Non -catalytic Gas - Solid Reactions, *Can. J. Chem. Eng.* **50**, 679 (1972a).
- Sohn, H. Y., and R. L. Braun, Simultaneous Fluid - Solid Reactions in Porous Solids : Reactions between one Solid and two Fluid Reactants, *Chem. Eng. Sci.* **35**, 1625 (1980).
- Sohn, H. Y., and R. L. Braun, Simultaneous Fluid - Solid Reactions in Porous Solids : Reactions between one Fluid and two Solid Reactants, *Chem. Eng. Sci.* **39**(1), 21 (1984).
- Sotirchos, S. V., and H. C. Yu, Mathematical Modelling of Gas - Solid Reactions with Solid Product, *Chem. Eng. Sci.* **40**, 2039 (1985).
- Sotirchos, S. V. and N. R. Amundson, Dynamic Behavior of a Porous Char Particle Burning in an Oxygen Containing Environment, *AIChE J.* **30**(4), 537, (1984).
- Sotirchos, S. V. and Yu, H. C., Overlapping Grain Models for gas - Solid Reaction with Solid Products, *Ind. Eng. Chem. Res.* **27**, 836 (1988).
- Szekely, J. and A. Hastaoglu, Reduction of Nickel oxide / Hematite Mixture with Hydrogen, *Trans. Inst. Mining Met.* **C78**, 85 (1976).
- Szekely, J. and J. W. Evans, A Structural Model for Gas - Solid Reactions with Moving Boundary, *Chem. Eng. Sci.* **25**, 1091 (1970).

Szekely, J. and J. W. Evans, A Structural Model for Gas - Solid Reactions with Moving Boundary II. Effect of Grain Size, Porosity and Temperature on the Reaction of Porous Pellets, *Chem. Eng. Sci.* **26**, 1903 (1971c).

Szekely, J. and J. W. Evans, Studies in Gas - Solid Reactions: Part I. A Structural Model for Reaction of Porous Oxides with a Reducing Gas, *Met. Trans.* **2**, 1691 (1971a).

Szekely, J. and J. W. Evans, Studies in Gas - Solid Reactions: Part II. An Experimental Study of Nickel Oxide Reduction with hydrogen, *Met. Trans.* **2**, 1699 (1971b).

Szekely, J. and M. Propster, A Structural Model for Gas - Solid Reactions with Moving Boundary VI. Effect of Grain Size Distribution on the Conversion of Porous Solids, *Chem. Eng. Sci.* **30**, 1049 (1975).

Szekely, J., J. W. Evans, and H. Y. Sohn, Gas-Solid Reactions, Academic Press, New York (1976).

Tadafumi, A., K. Toshinori and F. Takahiko, Estimation of Dynamic Change in Gasification Rate of Chars-II. Overlapped Grain Model, *Chem. Eng. Sci.* **42**(6), 1319 (1987).

Treybal, R. E., Mass transfer Operations, 3rd ed., McGraw-Hill, New York, (1980).

Tsay, Q. T., W. H. Ray and J. Szekely, The Modeling of Hematite Reactions with Hydrogen plus Carbon monoxide Mixture, *AIChE J.*, 1064 (1976).

- Turkdogan, E. T., R. G. Olsson, H. A. Wriedt and L. S. Darken, Calcination of Limestone, *SME Trans. AIME*. **254**, 9 (1973).
- Ulrichson, D. L. and D. J. Mahoney, Pore Closure Model for Gas - Solid Reactions: The Effect of Bulk Flow and Reversibility, *Chem. Eng. Sci.* **35**, 567 (1980).
- Whitaker, S. Mass Transport and Reactions in Catalyst Pellets, *Transport in Porous Media* **2**, 269 (1987).
- Wu, P. C., The Kinetics of the Reaction of Carbon with Carbon Dioxide, D.Sc. Thesis, M.I.T., Cambridge, (1949).
- Yortsos, Y. C. and M. Sharma, Application of Percolation Theory to Non-catalytic Gas - Solid Reactions, *AIChE J.* **32**(1), 46 (1986).
- Yortsos, Y. C. and M. Sharma, Application of Percolation Theory to Non-catalytic Gas - Solid Reactions, *AIChE Ann. Meet. San Francisco* (Nov., 1984).
- Yu, H. C. and S. V. Sotirchos, A Generalized Pore Model for Gas - Solid Reactions Exhibiting Pore Closure, *AIChE J.* **33**(3), 382 (1987).
- Zygourakis, K., L. Ari, and N. R. Amundson, Studies on the Gasification of a Single Char Particle, *Ind. Eng. Chem. Fundam.* **21**, 1 (1982).

APPENDICES

APPENDIX A

MAIN COMPUTER CODING

```

C*****
C THIS PROGRAM IS WRITTEN TO SOLVE THE MODEL EQUATIONS DESCRIBING
C THE FOLLOWING MULTICOMPONENT, MULTIREACTION GAS SOLID SCHEME
C
C  $A_{11} * A_1 + A_{12} * A_2 + \dots + A_{1NG} * ANG + B_{11} * B_1 + B_{12} * B_2 + \dots + B_{1NS} * BNS = 0$ 
C  $A_{21} * A_1 + A_{22} * A_2 + \dots + A_{2NG} * ANG + B_{21} * B_1 + B_{22} * B_2 + \dots + B_{2NS} * BNS = 0$ 
C  $A_{31} * A_1 + A_{32} * A_2 + \dots + A_{3NG} * ANG + B_{31} * B_1 + B_{32} * B_2 + \dots + B_{3NS} * BNS = 0$ 
C .....
C .....
C  $ANR_1 * A_1 + ANR_2 * A_2 + \dots + ANR_{NG} * ANG + BNR_1 * B_1 + BNR_2 * B_2 + \dots + BNR_{NS} * BNS = 0$ 
C
C WHERE:
C ANG = GASEOUS COMP. NG
C BNS = SOLID COMP. NS
C ANRNG = COEFF OF GASEOUS COMP. ANG IN REACTION NR
C BNRNS = COEFF OF SOLID COMP. BNS IN REACTION NR
C
C ALLOWANCES ARE MADE FOR THE SPECIAL CASE OF GASIFICATION
C REACTIONS (I.E BNRNS=0, FOR BNRNS NOT > 0)
C
C THE MODEL EQUATIONS ARE BASED ON THE GRAIN MODEL OF SZEKELY
C
C UNSTEADY STATE NON-ISOTHERMAL BEHAVIOUR IS MODELLED BASED ON
C APPROPRIATE ENERGY AND MATERIAL BALANCE EQUATIONS
C
C DIFFUSION THROUGH THE POROUS PELLETT IS BASED ON THE " DUS
C GAS MODEL" OF EVANS ET AL. BOTH KNUDSEN AND MOLECULAR
C DIFFUSION MECHANISMS HAVE BEEN INCOPORATED.
C
C THE MODEL INCLUDES THE EFFECTS OF BULK FLOW, DIFFUSION THROUGH
C PRODUCT LAYER SURROUNDING THE INDIVIDUAL GRAINS, ANY TYPE
C REACTION KINETICS DESIRED. CHANGE IN PORE STRUCTURE DUE TO
C REACTION AND EXTERNAL HEAT AND MASS TRANSFER RESISTANCE.
C
C THE SOLUTION OF THE MODEL EQUATIONS IS ACHIEVED BY ESTABLISHING
C A GRID SYSTEM IN R (PELLET RADIUS). THE PELLETT RADIUS IS DIVIDED
C INTO N GRID SPACES (BLOCKS) AND M=N+1 GRID POINTS I, I=1 BEING
C THE PELLETT CENTRE AND I=M THE PELLETT SURFACE (R= RP)
C
C SOLUTION PROCEDURE
C
C THE TIME IS ADVANCED BY ONE TIME STEP (DELT) AND THE REACTION
C FRONT RADII AT THE NEW TIME (TIME+DELT) AT EACH POINT IN THE
C PELLETT I ARE DETERMINED.
C
C

```

C TO ACHIEVE THE ABOVE THE RUNGE-KUTTA ORDER 4 NUMERICAL ROUTINE
 C IS UTILIZED
 C
 C OVERALL CONVERSION (AND SUBSEQUENTLY PELLET WEIGHT) ARE THEN
 C DETERMINED USING A NUMERICAL INTEGRATION TECHNIQUE (SIMPSONS
 C COMPOSITE RULE)
 C
 C A SUBROUTINE IS CALLED TO DETERMINE THE NEW PHYSICAL PARAMETER
 C (POROSITY, GRAIN RADIUS, DIFFUSIVITIES)
 C
 C CONCENTRATION AND TEMPERATURE PROFILES ARE UPDATED
 C
 C THE PROGRAM HAS BEEN MODIFIED TO DESCRIBE REACTIONS
 C WHICH LEAD TO PARTICLE SHRINKAGE/SWELLING
 C
 C A SHRINKAGE/SWELLING FACTOR IS USED TO ACCOUNT FOR THE
 C LOSS OF PORE VOLUME WITH REACTION
 C
 C
 C

NOMENCLATURE

C A, B - STOICHOOMETRIC COEFFICIENTS, DIMENSIONLESS
 C CBULK(IG) - CONCENTRATION OF COMP. IG IN THE BULK GAS STREAM,
 C MOL/M²/MICRON
 C CINT(IG) - CONCENTRATION OF IG AT THE REACTION FRONT IN GRAINS,
 C MOL/M²/MICRON
 C CAN(IG) - CONCENTRATION OF IG IN THE PORE SPACES OF THE PELLET,
 C PREVIOUS TIME LEVEL, MOL/M²/MICRON
 C CNP1(IG) - CONCENTRATION OF IG IN THE PORE SPACES OF THE PELLET,
 C NEW (CURRENT) TIME LEVEL, MOL/M²/MICRON
 C CF - COLLISION FUNCTION ARGUMENT (KT/E), DIMENSIONLESS
 C CTBULK- TOTAL BULK CONCENTRATION, MOL/M²/MICRON
 C DELT - TIME STEP SIZE, S
 C DR - STEP SIZE OF GRID SYSTEM (DISTANCE BETWEEN GRID POINTS), M
 C DENS(IS) - TRUE DENSITY OF SOLID REACTANT OR PRODUCT IS, KG/M³
 C D(I,J) - MOLECULAR (BULK) DIFFUSION COEFFICIENT FOR BINARY SYSTEM
 C CONTAINING I,J, (M²/S)
 C DE(I,J) - EFFECTIVE MOLECULAR BULK DIFFUSIVITY, M²/S
 C DK(IG) - KNUDSEN DIFFUSIVITY FOR IG, M²/S
 C DKE(IG) - EFFECTIVE KNUDSEN DIFFUSIVITY FOR IG, M²/S
 C GRAINS, M²/S
 C DXX - INCREMENTS IN CONCENTRATIONS AND TEMPERATURE
 C EPSI - INITIAL PELLET POROSITY, DIMENSIONLESS
 C EPS - PELLET POROSITY AT ANY TIME, DIMENSIONLESS
 C EPSD- POROSITY OF PRODUCT LAYER SURROUNDING EACH GRAIN
 C , DIMENSIONLESS
 C EPD- EFFECTIVE PORE DIAMETER IN PELLET, MICRONS
 C EPDG- EFFECTIVE PORE DIAMETER IN PRODUCT LAYER SURROUNDING
 C MICRONS
 C EMA(IG) - ENERGY OF MOLECULAR ATTRACTION DIVIDED BY BOLTZMANN'S
 C CONSTANT, K (FOR COMP. IG)
 C NF(IG) - FLUX OF COMPONENT IG, GMOL/M/MICRON/S
 C FP - PELLET SHAPE FACTOR, DIMENSIONLESS

C FP=1 - FLAT PLATE
C FP=2 - CYLINDER
C FP=3 - SPHERE
C FG - GRAIN SHAPE FACTOR, DIMENSIONLESS
C FG=1 - FLAT PLATE
C FG=2 - CYLINDER
C FG=3 - SPHERE
C FCF- COLLISION FUNCTION F(KT/E), DIMENSIONLESS
C FLOW- FLOW RATE OF GAS STREAM, M3/S
C GAM - MOLAL VOLUME RATIO, DIMENSIONLESS
C GAM .LT. 1 - GRAINS SHRINK DURING RXN
C GAM .GT. 1 - GRAINS SWELL DURING RXN
C GAM .EQ. 1 - NO CHANGE IN GRAIN SIZE DURING RXN
C GX - GLOBAL(OR OVERALL) CONVERSION, DIMENSIONLESS
C HM - EXTERNAL HEAT TRANSFER COEFFICIENT, W/M2/K
C HMC- EXTERNAL HEAT TRANSFER COEFFICIENT CORRECTED FOR MASS TRANSFER
C R, W/M2/K
C ITC - ITERATION COUNTER
C IFLAG - INDICATOR THAT DIRECTS INITIALIZATION OF FLUXES IN
C SUBROUTINE FLUX
C IFLAG .EG. 0 - INITIALIZE (LINEAR APPROXIMATION)
C IFLAG .GT. 0 - USE OLD CALCULATED VALUES AS INITIAL GUESS
C IRATE-A COUNTER THAT INDICATES WHETHER CALL TO 'ROUTINE RATE IS IN
C 'ROUTINE TSTEP OR ELSEWHERE.
C IRATE=0: CALL TO 'ROUTINE RATE IS ELSEWHERE(NOT IN TSTEP)
C IRATE=1: CALL TO 'ROUTINE RATE IS IN 'ROUTINE TSTEP
C ISCHEME - A COUNTER THAT SPECIFIES THE PARTICULAR REACTION UNDER
C STUDY. IT IS USED IN THE RATE AND HEAT OF RXN CALCULATION
C ISCHEME = 1: CARBON GASIFICATION
C ISCHEME = 2: WOOD PYROLYSIS
C ISCHEME = 3: NICKEL OXIDE/HEMATITE REDUCTION
C IG - ITERATION COUNTER FOR GASEOUS COMPONENTS
C IS - ITERATION COUNTER FOR SOLID COMPONENTS
C IR - ITERATION COUNTER FOR REACTIONS
C KC - EXTERNAL MASS TRANSFER COEFFICIENT, M/S
C MAX - MAXIMUM NO OF ITERATION IN ROUTINE PROFILE
C N - NO OF SUBINTERVALS (GRID SPACINGS) IN PELLET, DIMENSIONLESS
C NR - NO OF REACTIONS
C NG - NO OF GASEOUS COMPONENTS (REACTANTS AND PRODUCTS)
C NS - NO OF SOLID COMPONENTS (REACTANTS AND PRODUCTS)
C NNUS - NUSSULT NUMBER
C PB - BULK GAS PRESSURE, ATM
C PC(IG) - CRITICAL PRESSURE OF IG, ATM
C PEL - PELLET LENGTH (IF CYLINDRICAL GEOMETRY)
C PWI - INITIAL PELLET WEIGHT, MG
C PW - PELLET WEIGHT AT ANY TIME, MG
C PIPEID - INTERNAL PIPE DIAMETER, M
C PRAN - PRANDTL NUMBER, DIMENSIONLESS
C PN - TOTAL PRESSURE AT ANY LOCATION, PREVIOUS TIME LEVEL (ATM)
C PNPI - TOTAL PRESSURE AT ANY LOCATION, NEW (CURRENT) TIME LEVEL,
C ATM
C PROFLAG- FLAG INDICATING WHETHER CONVERGENCE IS ACHIEVED OR NOT
C RP - PELLET RADIUS (ASSUMED CONSTANT), M
C RP= HALF THICKNESS OF FLAT PLATES

C RP= PELLET RADIUS FOR CYLINDERS AND SPHERES
 C R - RADIAL POSITION IN PELLET, M
 C RB - RADIAL POSITION OF BLOCK BOUNDARIES IN THE PELLET, M
 C RO - INITIAL GRAIN RADIUS, MICRONS
 C RG - GRAIN RADIUS AT ANY TIME, MICRONS
 C RC - REACTION FRONT RADIUS IN GRAIN, MICRONS
 C RCNEW - REACTION FRONT RADIUS AFTER TIME STEP (GIVEN BY RK),
 C MICRONS
 C RMS(IG) - MOLECULAR SEPARATION DISTANCE, A (AMSTRONG)
 C RX1, RX2, RX3 - REACTION RATE CONSTANTS, MOL/ATM/CM3/S, 1/ATM,
 C 1/ATM (FOR CARBON GASIFICATION)
 C REYNO - REYNOLDS NUMBER, DIMENSIONLESS
 C RGAS = GAS CONSTANT, ATM-CM3/GMOL/K=(ATM-M2-MICRON/GMOL/K)
 C SCHNO- SCHMIDT NUMBER, DIMENSIONLESS
 C SHERNO - SHERWOOD NUMBER, DIMENSIONLESS
 C TIME - TIME OF REACTION, S
 C TMAX - MAXIMUM ALLOWABLE TIME FOR REACTION TO OCCUR, S
 C TB - BULK GAS TEMPERATURE, K
 C TN - TEMPERATURE AT ANY LOCATION, PREVIOUS TIME (K)
 C TNP1 - TEMPERATURE AT ANY LOCATION, NEW (CURRENT) TIME, K
 C TC(IG) - CRITICAL TEMPERATURE OF IG, K
 C TOLER - THE TOLERANCE USED INSIDE THE GAUSSIAN SOLVER
 C TOLGAS - CRITERIA FOR CONVERGENCE FOR GASEOUS COMPONENTS
 C TOLTEMP - CRITERIA FOR CONVERGENCE FOR TEMPERATURE
 C TKB- BULK THERMAL CONDUCTIVITY OF GAS STREAM, W/MK
 C VA- RATE OF CONSUMPTION OF GASEOUS REACTANT A, MOL/M2/MICRON/S
 C VEL - VELOCITY OF GAS STREAM, M/S
 C VISB - BULK VISCOSITY OF GAS STREAM, KG/M/S (POISE)
 C WMI- MOLECULAR WEIGHT OF COMPONENT I, G/GMOL OR KG/KGMOL
 C X- LOCAL CONVERSION, DIMENSIONLESS
 C
 C
 C

MAIN PROGRAM

IMPLICIT DOUBLE PRECISION (A-H,O-Z)
 INTEGER N,NR,NS,NG,I,IS,IR,PROFLAG,MAX,ITC,IFLAG
 DOUBLE PRECISION NF
 REAL KC
 PARAMETER(KS=10,KG=10,KN=10,KR=10,LL=4)
 DIMENSION RC(KS,KN),RG(KS,KN),EPSS(KS,KN),EPS(KN), RO(KS)
 DIMENSION CAN(KG,KN), CA(KG.KN), VAS(KG.KN), TN(KN), XT(KN)
 DIMENSION CNP1(KG,KN), TNP1(KN)
 DIMENSION RCNEW(KS,KN) , TERM(KN), BETA(KS)
 DIMENSION RATES(KS,KN)
 DIMENSION R(KN), RB(KN)
 DIMENSION X(KS,KN), GX(KS), GN(KS)
 DIMENSION P(KN),RATE(KR,KN)
 DIMENSION NF(KG,KN+1)
 DIMENSION XA(KG,KN),CT(KN),EPD(KN),DE(KG,KG,KN)
 DIMENSION XAB(KG), DXX((KG+1)*KN), HR1(KR), TR1(KR)
 DIMENSION DKE(KG,KN)

DIMENSION VISM(KN), VIS(KG,KN),TKE(KN),CPE(KN),CP(KG,KN)
DIMENSION PA(KG,KN)
DIMENSION BO(KN),VFP(KN)
DIMENSION TIN(KN), HRX(KR,KN)
DIMENSION VPO(KN)
DIMENSION DENS(KS), DEN(KG),WMS(KS),WM(KG),WF(KS)
DIMENSION TC(KG), PC(KG)
DIMENSION RMS(KG), RMSS(KG,KG), EMA(KG), EMAA(KG,KG)
DIMENSION EPSD(KS)
DIMENSION TKM(KS), CPS(KS)
DIMENSION CPA(KG,LL)
DIMENSION CBULK(KG)
DIMENSION A(KR,KG), B(KR,KS)
DIMENSION XFP(KG,KN),XFPXT(KN)
COMMON /STOIC/A,B
COMMON /CONS1/DEN,DENS,WM,WMS
COMMON /CONS2/TC,PC
COMMON /CONS3/RMS,EMA
COMMON /CONS4/EPsi,EPsD,RO
COMMON /CONS6/RGAS
COMMON /CONS10/ MAX
COMMON /CONS5/RX1,RX2,RX3
COMMON /TOL/TOLGAS,TOLTEMP
COMMON /TOLSOLN/TOLER
COMMON /RAD/R
COMMON /RAD1/RB
COMMON /CONS7/DR
COMMON /CONS71/N,NG,NS,NR
COMMON /HEAT/ TKM,CPS
COMMON /CP1/ CPA
COMMON /CONS8/ CBULK,TB
COMMON /CONS9/ GAM,HM
COMMON /CONS11/KC
COMMON /CONS13/NT
COMMON /BLOCK1/ CAN,TN
COMMON /BLOCK3/ DXX
COMMON /BLOCK6/ TM
COMMON /BLOCK7/ NF
COMMON /RADIA/ EMI,SIGMA
COMMON /FLAG/ IFLAG
COMMON /R1/ AK10
COMMON /R11/ EA1
COMMON /R2/ AK20
COMMON /R21/ EA2
COMMON /R3/ AK30
COMMON /R31/ EA3
COMMON /R441/ AK40,EA4,AK50,EA5
COMMON /H1/ HR1,TR1
COMMON /S1/ BETA
COMMON /S2/PI.PEL
COMMON /S3/ FLOW,PIPEID,PB
COMMON /S4/PWI,PW
COMMON /VOL/ VPO
COMMON /WTFRCN/ WF

```

COMMON /XABULK/ XAB
COMMON /FPFG/ FP,FG
COMMON /SCHEME/ISHEME
OPEN (5,FILE='INERT.DAT')
OPEN (7,FILE='INERT.OUT')
OPEN (8,FILE='INERT.OT1')
OPEN (1,FILE='INERT.CON')
OPEN (2,FILE='INERT.TEM')
OPEN (3,FILE='INERT.PRE')

```

```

*****
***** INPUT CONSTANTS *****
*****
      NOUT=8

```

C...READ IN THE SOLUTION CONSTANTS

```

READ (5,*) N, NG, NS, NR, DELT, TMAX, MAX
READ (5,*) ((A(IR,IG),IR=1,NR),IG=1,NG)
READ (5,*) ((B(IR,IS),IR=1,NR),IS=1,NS)
READ (5,*) ((CPA(IG,L),L=1,4),IG=1,NG)
READ (5,*) ((CAN(IG,I),I=1,N),IG=1,NG)
READ (5,*) TB,PB
READ (5,*) AK10,EA1
READ (5,*) AK20,EA2
READ (5,*) AK30,EA3
READ (5,*) AK40,EA4
READ (5,*) AK50,EA5
READ (5,*) RP
READ (5,*) (RO(IS),IS=1,NS)
READ (5,*) EPSI,PWI,PEL,RGAS
READ (5,*) (WM(IG),IG=1,NG)
READ (5,*) (DENS(IS),WMS(IS),IS=1,NS)
READ (5,*) (XAB(IG),IG=1,NG)
READ (5,*) (RMS(IG),EMA(IG),IG=1,NG)
READ (5,*) (TC(IG),PC(IG),IG=1,NG)
READ (5,*) FLOW,PIPEID
READ (5,*) (HR1(IR),TR1(IR),IR=1,NR)
READ (5,*) PR
READ (5,*) (TKM(IS),CPS(IS),IS=1,NS)
READ (5,*) TOLGAS,TOLTEMP
      NN = (NG+1)*N
READ (5,*) (DXX(IX),IX=1,NN)
READ (5,*) EMI,SIGMA
READ (5,*) IFLAG
READ (5,*) (TIN(I),I=1,N)
READ (5,*) (BETA(IS), IS=1,NS)
READ (5,*) (EPSD(IS),IS=1,NS)
READ (5,*) (WF(IS),IS=1,NS)
READ (5,*) TOLER
READ (5,*) FP,FG,ISHEME

      IF(ISHEME.EQ.1) WRITE(6,*) 'THIS IS CARBON GASIFICATION RXN'

```

```
IF(ISCHEME.EQ.2) WRITE(6,*) 'THIS IS WOOD PYROLYSIS RXN'
IF(ISCHEME.EQ.3) WRITE(6,*) 'THIS IS NIO/HEMATITE REDUCTION'
```

```
*****
***** COMMENCE OPERATION *****
*****
```

```
TIME= 0.
NT = 1
PI= 4.*ATAN(1.)
DO 1 IS=1,NS
1 GX(IS)= 0.
KX = NN
```

C..CALCULATE INITIAL GRID SPACING

```
CALL GRID (RP,VPO)
DO 6 IG=1,NG
6 CBULK(IG) = XAB(IG)*PB/RGAS/TB
CTBULK= PB/RGAS/TB
```

C...CAL THE BULK PROPERTIES

```
CALL HMASS (RP)
```

C.. CALCULATE THE MOLAL VOLUME RATIO = GAM

```
VREACT = 0.0
VPRODT = 0.0
DO 7 IR=1,NR
DO 7 IS=1,NS
IF(B(IR,IS)) 8,7,99
99 VREACT = VREACT + B(IR,IS)*WMS(IS)/DENS(IS)
GOTO 7
8 VPRODT = VPRODT + ABS(B(IR,IS))*WMS(IS)/DENS(IS)/(1-EPSPD(IS))
7 CONTINUE
```

```
GAM = VPRODT/VREACT
```

C//

```
WRITE(6,*) 'GAM',GAM
```

C PRINT INPUT DATA AND CALCULATED PHYSICAL CONSTANTS

C...SET INITIAL CONDITIONS

```
DO 9 I=1,N
DO 10 IS=1,NS
RC(IS,I)= RO(IS)
10 RG(IS,I)= RO(IS)
EPS(I)= EPSI
9 TN(I)= TIN(I)
IDIRECT = 1
CALL PRINT(TIME,GX,CAN,TN,P.RC,TB,6,IDIRECT)
```

C//

```
WRITE(8,*) 'TIME, GX(1), GX(2), GX(4), GXT'
```

C//

C...INCREMENT TIME AND COMMENCE TRANSIENT OPERATION

```
150 TIME = TIME + DELT
```

```

IFLAG = 0
C...CALL SUBROUTINE TSTEP TO DETERMINE REACTION FRONT RADII OF
C...GRAINS AT EACH GRID POINT FOR THE NEW TIME.
  CALL TSTEP(RP,RC,RG,EPS,DELT,PROFLAG,RCNEW)
C...SET PROFLAG TO 1
  IF (PROFLAG.NE.1) GO TO 24
  DO 11 I=1,N
    DO 11 IS=1,NS
      RC(IS,I)=RCNEW(IS,I)
  11 IF(RC(IS,I).LT.0.) RC(IS,I)=0.
C DETERMINE THE CONVERSION AT THE NEW TIME
  CALL CONVER (RC,RP,PWI,X,GX,PW)
  DO 299 IS =1,NS
  299 IF(GX(IS).GE.1.) GX(IS)=1.0
C..PRINT THE TIME AND CALCULATED CONVERSION
  CALL PRINT(TIME,GX,CAN,TN,P,RC,TB,6,2)
  CALL PROPS1 (X,RC,RG,EPS)
C...BEGIN ITERATION FOR THE CONCENTRATION AND TEMPERATURE PROFILES
C...FOR THE NEW TIME LEVEL
  DO 12 I=1,N
    DO 13 IG=1,NG
  13  CNP1(IG,I)= CAN(IG,I)
  12  TNP1(I)= TN(I)
    CALL PROFILE (RC,RG,EPS,CNP1,TNP1,DELT,PROFLAG,ITC)
    IF (PROFLAG.NE.1) GO TO 24
    DO 14 I=1,N
      SUMCT=0.0
      DO 15 IG=1,NG
  15  SUMCT=SUMCT + CNP1(IG,I)
      CT(I)= SUMCT
      P(I)= CT(I)*RGAS*TNP1(I)
      DO 16 IG=1,NG
        XA(IG,I)= CNP1(IG,I)/CT(I)
  16  PA(IG,I)= XA(IG,I)*P(I)
  14  CONTINUE
C...CALL PROPS2 TO CALCULATE THE PROPERTIES AT THE NEW TIME STEP
  CALL PROPS2 (TNP1, P, XA ,CT, RC, RG, EPS, EPD,DE, DKE,
&      VISM, TKE, CPE, HRX, CP )
  DO 17 I=1,N
    DO 18 IG=1,NG
  18  CAN(IG,I)= CNP1(IG,I)
  17  TN(I)= TNP1(I)
      GXT = (PWI-PW)/PWI
      IF((GXT).GE.1.0) GOTO 25
C//
  WRITE(8,30) TIME,GX(1),GX(2),GX(4),GXT
  30  FORMAT(1X,F10.4,1X,4(1X,E12.4))
C...OUTPUT THE CONCNS.,TEMP.,PRESS. REACTION FRONT RADII AND CONVERSION
  CALL PRINT(TIME,GX,CAN,TN,P,RC,TB,7,3)
  WRITE(6,*)PW = 'PW
C...GO BACK TO THE "BEGINNING" OF THE PROCEDURE, ADVANCE TIME STEP AND
C...REPEAT THE ENTIRE PROCEDURE FOR THE NEW TIME LEVEL
  NT =NT+1

```

```

WRITE(1,1000) TIME, (CNP1(IG,3),IG=1,NG)
1000 FORMAT(F9.4,1X,5(1X,E10.4))
WRITE(2,2000) TIME, (TNP1(I),I=1,N)
2000 FORMAT(2X,F9.4,1X,5(1X,F10.4))
WRITE(3,3000) TIME, (P(I),I=1,N)
3000 FORMAT(2X,F9.4,1X,5(1X,F10.4))

```

```

DELT = DELT*1.5
IF(DELT.GT.1.) DELT = 50
IF(TIME.LT.TMAX) GOTO 150

```

```

C...PRINT MAXIMUM TIME IS EXCEEDED
CALL PRINT(TIME,GX,CAN,TN,P,RC,TB,6,4)
GO TO 28
C...PRINT CONVERSION IS COMPLETE
25 CALL PRINT(TIME,GX,CAN,TN,P,RC,TB,6,5)
GO TO 28
24 CONTINUE
28 STOP
END

```

```

***** END OF MAIN PROGRAM *****

```

LIST OF SUBROUTINES USED IN THE OVERALL CODING

1. SUBROUTINE CONVER:

```

*****
* THIS SUBROUTINE IS CALLED TO DETERMINE THE CONVERSION OF THE SOLID
* REACTANT(S) AFTER EACH ADVANCEMENT OF THE TIME STEP. THE LOCAL CON-
* VERSION (IE. THE CONVERSION AT EACH GRID POINT IN THE PELLET) IS
* COMPUTED BY FINDING THE RATIO OF THE VOLUMES OF THE UNREACTED CORE IN
* THE GRAIN AND INITIAL GRAIN SIZE. THE GLOBAL OR OVERALL CONVERSION
* IS DETERMINED FROM THE INTEGRAL WITH INTEGRAND  $(R^{**}(FP-1))*X$ , WHERE X
* IS THE LOCAL CONVERSION. THIS IS INTEGRATED NUMERICALLY USING SIMP-
* SON'S COMPOSITE RULE. FINALLY, A PELLET WEIGHT AT THE GIVEN TIME IS
* DETERMINED FROM THE OVERALL CONVERSION AND A RATIO OF PRODUCT
* AND REACTANT SOLID MOLECULAR WEIGHTS.
*****

```

2. SUBROUTINE PROPS1:

```

*****
* SUBROUTINE PROPS1 IS CALLED TO RECALCULATE THOSE PHYSICAL PARAMETERS
* WHICH CHANGE WITH ONGOING REACTION:- GRAIN RADIUS AND POROSITY.
* THESE WILL HAVE, AT A GIVEN TIME, DIFFERENT VALUES AT EACH GRID
* POINT IN THE PELLET.
*****

```

3. *SUBROUTINE PROPS2:*

```
*****
* SUBROUTINE PROPS2 CALCULATES PATAMETERS DEPENDENT ON PHYSICAL
* PROPERTIES OF MATRIX, TEMPERATURE, AND PRESSURE. THESE
* INCLUDE EFFECTIVE MOLECULAR, KNUDSEN, PRODUCT DIFFUSIVITIES,
* VISCOSITY, EFFECTIVE PELLET THERMAL CONDUCTIVITIES AND HEAT
* CAPACITIES.
*****
```

4. *SUBROUTINE PROFILE:*

```
*****
*** -THIS SUBROUTINE SETS UP THE JACOBIANS OF THE PRINCIPAL ****
*** MODEL EQUATIONS RETURNED BY SUBROUTINES FNG AND FTEMP AS THE
*** RIGHT HAND SIDE VECTORS
*** -THE DOUBLE SUBSCRIPTED VARIABLES ARE REDUCED TO SINGLE SUBS- *
*** CRIPTED ONES FROM WHICH THE JACOBIANS ARE SET UP.
*** -SUBROUTINE SOLN1 IS CALLED TO SOLVE THE SET OF LINEAR EQUATIONS
*** GENERATED AND THE INCREMENTS IN THE CONCENTRATIONS AND TEMP.
*** ARE RETURNED.
*** -THE ROUTINE CHECKS AND SETS ALL CONCNS AND TEMP TO ZERO
*** IF THERE IS NO CONVERGENCE AND HALTS IF THE DETERMINANTS OF
*** THE LINEAR EQUATIONS RETURNED ARE EQUAL TO ZERO (I.E IF THE
*** MATRIX IS ILL-CONDITIONED OR SINGULAR)
*****
```

5. *SUBROUTINE TSTEP:*

```
*****
* SUBROUTINE TSTEP IS CALLED TO ADVANCE THE TIME STEP BY DELT
* (THE TIME STEP SIZE). THIS IS ACHIEVED BY SOLVING THE MODEL
* EQUATION FOR THE CHANGE IN REACTION FRONT RADIUS(RC) WITH TIME(T)
* USING A RUNGE-KUTTA METHOD OF ORDER 4.
*****
```

6. *SUBROUTINE FNG:*

```
*****
* SUBROUTINE FNG CALCULATES THE RIGHT HAND SIDE VECTOR (CONTINUITY
* EQUATION FOR ALL THE GASEOUS COMPONETNS-REACTANTS AND PRODUCTS
* FOR INPUT TO LINEAR SOLVER
*****
```

7. *SUBROUTINE FTEMP:*

```
*****
* SUBROUTINE FTEMP CALCULATES RHS VECTOR ( TEMPERATURE EQUATION
* FOR INPUT TO THE LINEAR SOLVER
*****
```

8. *SUBROUTINE FLUX:*

* THIS ROUTINE RETURNS THE FLUX FOR ALL THE GASEOUS COMPONENTS.
* THIS IS DONE BY EMPLOYING THE GENERALISED "DUSTY GAS MODEL"

9. *SUBROUTINE GRID:*

* SUBROUTINE COMPUTES GRID SPACING GIVEN CHARACTERISTIC
* PELLET DIMENSION AND THE NUMBER OF GRID POINTS

10. *SUBROUTINE VOLUME:*

* SUBROUTINE CALCULATES PELLET SIZE GIVEN OVERALL
* CONVERSION AND SHRINKAGE/SWELLING FACTOR

11. *SUBROUTINE HMASS:*

* SUBROUTINE CALCULATES HEAT AND MASS TRANSFER COEFFICIENTS AND ALL
* BULK PROPERTIES

12. *SUBROUTINE HRXN:*

* THIS SUBROUTINE RETURNS THE HEAT OF REACTION OF THE SPECIFIC
* REACTION SCHEME CONSIDERED.

13. *SUBROUTINE RATE1:*

* THE REACTION RATE EXPRESSION FOR THE PARTICULAR SCHEME UNDER
CONSIDERATION IS RETURNED VIA THIS SUBROUTINE.

14 *SUBROUTINE SUMMATN:*

*** -THIS SUBROUTINE RETURNS THE AVERAGED VALUES OF THE FOLL. PARAMETERS
*** - THE DENSITY OF THE SOLID REACTANTS (DENN)
*** - THE SP. HEAT. CAP. OF THE SOLID REACTANTS (CPSS) &
*** - THE THERMAL COND. OF THE SOLID REACTANTS (TKMM)

15 *SUBROUTINE CONVERT1:*

```
*****
* THIS SUBROUTINE CONVERTS THE DOUBLE SUBSCRIPTED VARIABLES TO SINGLE
* SUBSCRIPTED ONES.
*****
```

16. *SUBROUTINE CONVERT2:*

```
*****
* THIS SUBROUTINE CONVERTS THE SINGLE SUBSCRIPTED VARIABLES TO DOUB
* SUBSCRIPTED ONES.
*****
```

17. *SUBROUTINE COLLFCN:*

```
*****
*** -THIS SUBROUTINE RETURNS THE VALUE OF THE COLLISION FUNCTION
*** DEPENDING ON THE MAGNITUDE OF THE COLLISION FUNCTION EQN.
*****
```

18. *SUBROUTINE SOLN1:*

```
*****
*** -THIS SUBROUTINE SOLVES THE SYSTEM OF THE NON LINEAR EQNS
*** BY EMPLOYING THE GAUSS-JORDAN COMPLETE ELIMINATION WITH
*** THE MAXIMUM PIVOT STRATEGY. THE VALUE OF THE DETERMINANT,
*** DET IS RETURNED AS THE VALUE OF THE SUBROUTINE.
*** -SHOULD THE POTENTIAL PIVOT OF LARGEST MAGNITUDE BE SMALLER IN
*** MAGNITUDE THAN EPS, THE MATRIX IS CONSIDERED TO BE SINGULAR
*** AND A TRUE ZERO IS RETURNED AS THE VALUE OF THE SUBROUTINE.
*****
```

19. *SUBROUTINE PRINT:*

```
*****
*** -THIS SUBROUTINE IS CALLED UPON TO PRINT THE RESULTS
*** OF THE MODEL EQUATIONS. THE COUNTER IDIRECT DIRECTS THE
*** PARTICULAR OUTPUT OF INTEREST TO BE PRINTED
*****
```


APPENDIX B

COMPLETE DATA FILES

Table B1. Input data to the main computer coding for the carbon gasification reaction.

```

5, 2, 1, 1, 1.0, 10800., 300
1, -2
1
4.728,1.754E-2,-1.338E-5,4.097E-9, 7.373,-0.307E-2,6.662E-6,-3.037E-9
0.0E-6,0.0E-6,0.0E-6,0.0E-6,0.0E-6, 4.0E-6,4.0E-6,4.0E-6,4.0E-6,4.0E-6
1173.0, 1.0
627., 52.317
3.3E-9, 60.44
0.176, 6.7
0.00128
0.0375
0.566, 800., 0.015, 82.05
44.0, 28.0
1800.0, 12.
1.0, 0.
3.941, 195.2, 3.69, 91.7
304.1, 73.8, 132.9, 35
8.33E-5, 0.027
1.74E5, 1000.
1.
1.890, 1.46
1.0E-8,1.E-2
1E-8,1E-8,1E-8,1E-8,1E-8,1E-8,1E-8,1E-8,1E-8,1E-8,1.0,1.0,1.0,1.0,1.0
0.8,5.676E-8
1
300.,300.,300.,300.,300.
0.
0.0
1.00
1.0E-15
1.0,3.0,1,0

```

```

*****
***** DATA FOR CARBON GASIFICATION REACTION *****
***** ORDER IN WHICH THE ABOVE DATA IS READ IN *****
*****
C...READ IN THE SOLUTION CONSTANTS

```

```

N, NG, NS, NR, DELT, TMAX, MAX
((A(IR,IG),IR=1,NR),IG=1,NG)
((B(IR,IS),IR=1,NR),IS=1,NS)
((CPA(IG,L),L=1,4),IG=1,NG)

```

((CAN(IG,I),I=1,N),IG=1,NG)
TB,PB
AK10,EA1
AK20,EA2
AK30,EA3
RP
(RO(IS),IS=1,NS)
EPSI,PWI,PEL,RGAS
(WM(IG),IG=1,NG)
(DENS(IS),WMS(IS),IS=1,NS)
(XAB(IG),IG=1,NG)
(RMS(IG),EMA(IG),IG=1,NG)
(TC(IG),PC(IG),IG=1,NG)
FLOW,PIPEID
(HR1(IR),TR1(IR),IR=1,NR)
PR
(TKM(IS),CPS(IS),IS=1,NS)
TOLGAS,TOLTEMP
NOTE: NN=(NG+1)*N AND DXX IS THE CONC N AND TEMP. INCREMENTS
(DXX(IX),IX=1,NN)
EMI,SIGMA
NFLAG
(TIN(I),I=1,N)
(BETA(IS), IS=1,NS)
(EPSD(IS),IS=1,NS)
(WF(IS), IS=1,NS)
TOLER
FP,FG,ISCHEME

Table B2. Input data to the main computer coding for the reduction of NiO / Fe₂O₃ mixture

```

5, 2, 4, 2, 5.E-2, 840., 100
1,3, -1,-3
1,0, -1,0, 0,1, 0,-2
6.477,2.213E-3,-0.3296E-5,1.825E-9, 7.694,4.592E-4,2.517E-6,-0.858E-9
0.0E-6,0.0E-6,0.0E-6,0.0E-6,0.0E-6, 2.0E-5,2.0E-5,2.0E-5,2.0E-5,2.0E-5
581.0, 1.0
4.0737E-1, 12.78
5.956E-1, 18.837
0, 0
0.0004450
0.09, 0.09, 0.1, 0.1
0.500, 800., 0.015, 82.05
2.0, 18.0
7500.,74.7,8900,58.7,5210.,159.7,7860.,55.8
1.0, 0.
2.827, 59.7, 2.64, 809.1
33.2, 13., 647.1,221.2
8.33E-5, 0.027
0.02598E5, 300.,1.0542E5, 300.
1.
5.9, 0.673, 91., 0.428, 18., 0.638, 80., 0.452
1.0E-7,1.E-1
1E-8,1E-8,1E-8,1E-8,1E-8,1E-8,1E-8,1E-8,1E-8,1E-8,0.1,0.1,0.1,0.1,0.1
0.80,5.676E-8
1
500.,500.,500.,500.,500.
0, 0, 0, 0
0,0.35,0,0.35
0.50, 0, 0.50, 0
1.0E-15
1.0, 3.0, 3

```

```

*****
***** DATA FOR REDUCTION OF NiO / Fe2O3 MIXTURE*****
***** ORDER IN WHICH THE ABOVE DATA IS READ IN *****
*****

```

C...READ IN THE SOLUTION CONSTANTS

```

N, NG, NS, NR, DELT, TMAX, MAX
((A(IR,IG),IR=1,NR),IG=1,NG)
((B(IR,IS),IR=1,NR),IS=1,NS)
((CPA(IG,L),L=1,4),IG=1,NG)
((CAN(IG,I),I=1,N),IG=1,NG)
TB,PB      (for tb= 608.0 K, Pb = 1.0 )
AK10,EA1   (7.0737E-1, 12.78
AK20,EA2   (4.956E-1, 18.837
AK30,EA3

```

RP

(RO(IS),IS=1,NS)

EPSI,PWI,PEL,RGAS

(WM(IG),IG=1,NG)

(DENS(IS),WMS(IS),IS=1,NS)

(XAB(IG),IG=1,NG)

(RMS(IG),EMA(IG),IG=1,NG)

(TC(IG),PC(IG),IG=1,NG)

FLOW,PIPED

(HR1(IR),TR1(IR),IR=1,NR)

PR

(TKM(IS),CPS(IS),IS=1,NS)

TOLGAS,TOLTEMP

NOTE: NN=(NG+1)*N AND DXX IS THE CONCEN AND TEMP. INCREMENTS

(DXX(IX),IX=1,NN)

EMI,SIGMA

NFLAG

(TIN(I),I=1,N)

(BETA(IS),IS=1,NS)

(EPSD(IS),IS=1,NS)

(WF(IS),IS=1,NS)

TOLER

FP,FG,ISCHEME

Table B3. Input data to the main computer coding for the multiple reaction (carbon gasification, NiO / Fe₂O₃ reduction and water gas shift reaction) with inert gas in the bulk stream.

5, 5, 5, 4, 5.E-2, 500., 300
 1,0,0,-1, -2,0,0,1, 0,1,3,-1, 0,-1,-3,1, 0,0,0,0
 1,0,0,0, 0,1,0,0, 0,-1,0,0, 0,0,1,0, 0,0,-2,0
 4.728,1.754E-2,-1.338E-5,4.097E-9, 7.373,-0.307E-2,6.662E-6,-3.037E-9,
 6.477,2.213E-3,-0.3296E-5,1.825E-9, 7.694,4.592E-4,2.517E-6,-0.858E-9,
 7.434,-3.24E-3,0.6396E-5,-2.787E-9
 0.0E-5,0.0E-5,0.0E-5,0.0E-5,0.0E-5, 0.0E-5,0.0E-5,0.0E-5,0.0E-5,0.0E-5,
 0.0E-5,0.0E-5,0.0E-5,0.0E-5,0.0E-5, 0.0E-7,0.0E-7,0.0E-7,0.0E-7,0.0E-7,
 3.0E-5,3.0E-5,3.0E-5,3.0E-5,3.0E-5
 1173.0, 1.0
 1094.E0, 52.317
 3.3E-9, 60.44
 0.176, 6.7
 1.0737E-4, 12.78
 1.956E-6, 18.837
 0.000328
 0.00375, 0.009, 0.009, 0.001, 0.001
 0.556, 800., 0.015, 82.05
 44.0, 28.0, 2.0, 18.0, 28.
 1800.0, 12., 7500.,74.7,8900,58.7,5210.,159.7,7860.,55.8
 0.5, 0., 0.5, 0., 0.
 3.941, 195.2, 3.69, 91.7, 2.827, 59.7, 2.64, 809.1, 3.798, 71.4
 304.1, 73.8, 132.9, 35., 33.2, 13., 647.1,221.2, 126.2, 33.9
 8.33E-5, 0.027
 1.74E5, 1000., 0.02598E5, 300.,1.0542E5, 300., 2.05E5, 300.
 1.
 1.890, 1.46, 5.9, 0.673, 91., 0.428, 18., 0.638, 80., 0.452
 1.0E-5,1.E-1
 1E-8,1E-8,1E-8,1E-8,1E-8,1E-8,1E-8,1E-8,1E-8,1E-8,
 1E-8,1E-8,1E-8,1E-8,1E-8,1E-8,1E-8,1E-8,1E-8,1E-8,
 1E-8,1E-8,1E-8,1E-8,1.0,1.0,1.0,1.0,1.0
 0.8,5.676E-8
 1
 400.,400.,400.,400.,400.
 0, 0, 0, 0, 0
 0.0, 0,0.35,0,0.35
 0.12, 0.28, 0, 0.60, 0
 1.0E-15
 1.0,3.0,5

 ***** DATA FOR MULTIPLE REACTION *****
 ***** ORDER IN WHICH THE ABOVE DATA IS READ IN *****

 C...READ IN THE SOLUTION CONSTANTS

N, NG, NS, NR, DELT, TMAX, MAX

((A(IR,IG),IR=1,NR),IG=1,NG)

((B(IR,IS),IR=1,NR),IS=1,NS)

((CPA(IG,L),L=1,4),IG=1,NG)

((CAN(IG,I),I=1,N),IG=1,NG)

TB,PB

AK10,EA1

AK20,EA2

AK30,EA3

AK40,EA4

AK50,EA5

RP

(RO(IS),IS=1,NS)

EPSI,PWI,PEL,RGAS

(WM(IG),IG=1,NG)

(DENS(IS),WMS(IS),IS=1,NS)

(XAB(IG),IG=1,NG)

(RMS(IG),EMA(IG),IG=1,NG)

(TC(IG),PC(IG),IG=1,NG)

FLOW,PIPEID

(HR1(IR),TR1(IR),IR=1,NR)

PR

(TKM(IS),CPS(IS),IS=1,NS)

TOLGAS,TOLTEMP

NOTE: NN=(NG+1)*N AND DXX IS THE CONC N AND TEMP. INCREMENTS

(DXX(LX),LX=1,NN)

EMI,SIGMA

NFLAG

(TIN(I),I=1,N)

(BETA(IS),IS=1,NS)

(EPSD(IS),IS=1,NS)

(WF(IS),IS=1,NS)

TOLER

FP,FG,ISCHEME